THE PROTEIN AND PEPTIDE MEDIATED SYNTHESES OF NON-BIOLOGICALLY-PRODUCED OXIDE MATERIALS

A Dissertation
Presented to
The Academic Faculty

By

Matthew B. Dickerson

In Partial Fulfillment
Of the Requirements for the Degree
Doctor of Philosophy in the
School Materials Science and Engineering

Georgia Institute of Technology

August 2007

THE PROTEIN AND PEPTIDE MEDIATED SYNTHESES OF NON-BIOLOGICALLY-PRODUCED OXIDE MATERIALS

Approved by:

Dr. Kenneth H. Sandhage, Advisor
School of Materials Science & Engineering
Georgia Institute of Technology

Dr. Seth R. Marder
School of Chemistry & Biochemistry
Georgia Institute of Technology

Dr. Nils Kröger, Co-Advisor
School of Materials Science & Engineering
School of Chemistry & Biochemistry
Georgia Institute of Technology

Dr. Nicholas V. Hud
School of Chemistry & Biochemistry
Georgia Institute of Technology

Dr. Rajesh R. Naik, Co-Advisor
Materials and Manufacturing Directorate
Air Force Research Laboratory

Date Approved: July 6, 2007

ACKNOWLEDGMENTS

Completion of this work would not have been possible without the expert guidance of my advisors, Professor Kenneth H. Sandhage, Professor Nils Kröger, and Dr. Rajesh R. Naik. I would like to thank Professor Sandhage for facilitating my expedition both to a new university (Georgia Institute of Technology) and into a new area of study (the bio-enabled synthesis of materials). Professor Sandhage has been a great source of optimism and his extensive knowledge of ceramic engineering was a considerable asset during my research. It has been a privilege to work with Professor Nils Kröger, whose work initially inspired me to enter this area of research. Professor Kröger's guidance and insight have been invaluable in completing my research and my development as a scientist. Dr. Rajesh Naik played a critical role in the success of my research by initially training me in basic molecular biology procedures, including the biopanning technique, as well as introducing me to the literature of the field. Beyond my initial training, Dr. Naik remained a constant source of inspired and often critical ideas throughout my doctoral education.

I would like to thank Professor Seth Marder and Professor Nicholas Hud for their support of my work as members of my dissertation committee. I would additionally like to thank Professor Marder for his contributions to my work on immobilized biomolecules. I am also grateful for the assistance and knowledge provided by several members of the Professor Marder's research group including Dr. Simon C. Jones and Dr. Guojie Wang.

It has been a distinct pleasure working side-by-side with talented, intelligent, and friendly individuals here at the North Avenue Trade School. My group mates, Dr. Gul Ahmad, Micheal Weatherspoon, Eric Ernest, Shawn Allan, Dr. Benjamin Church, Dr. Micheal Haluska, Phillip Graham, David Lipke, Samuel Shian, Dr. Ye Cai, and Zhao Bao have all been good friends and colleagues who always willing to lend a hand, tip a pint glass or a coffee cup, and discuss an idea.

I would like to thank Dr. Morley Stone for inviting me into his group at the Air Force Research Laboratory and for providing an outstanding example personal and scientific leadership. I thoroughly enjoyed working with the members of the biotechnology group during my year at AFRL. I would like to express my gratitude to Sharon Jones for her assistance in my early training and her collaboration in my biopanning research through the sequencing of phage DNA.

I would also like to express my gratitude to my family for their years of support and encouragement. I would like to thank my parents, Ronald and Connie, for both the "nature and the nurture" that have carried me to this point. My brother Christopher has been a lifelong friend and perhaps has the best understanding of the unique humor and ideas produced by my mind. I would like to thank my wife, Miranda, for her constant support, love, and encouragement. I would additionally like to thank Miranda for her non-technical editing of my various publications and this dissertation, I'm sure she now knows more about proteins, phage, and technical ceramics than she ever thought she wanted to. I am additionally indebted to Miranda and Hooligan Dickerson for dragging me out of the lab and onto the wooded trails of Georgia for much needed respites from the often slow and frustrating world of research.

This research was supported by the Air Force Office of Scientific Research (Dr. J. Fuller, Dr. H. C. De Long, program managers) and the Office of Naval Research (Dr. M. Spector).

TABLE OF CONTENTS

LIST OF TABLES

LIST OF FIGURES

SUMMARY

Numerous examples exist in nature of organisms which have evolved the ability to produce sophisticated structures composed of inorganic minerals. Studies of such biomineralizing organisms have suggested that specialized biomolecules are, in part, responsible for the controlled formation of these structures. The research detailed in this dissertation is focused on the use of biomolecules (i.e., peptides and proteins) to form non-biologically produced materials under mild reaction conditions (i.e, neutral pH, aqueous solutions, and room temperature).

The peptides utilized in the studies detailed in this dissertation were identified through the screening of single crystal rutile TiO_2 substrates or Ge powder with a phage-displayed peptide library. Twenty-one peptides were identified which possessed an affinity for Ge. Three of these twenty one peptides were tested for germania precipitation activity. Those peptides possessing a basic isoelectric point as well as hydroxyl- and imidazole-containing amino acid residues were found to be the most effective in precipitating amorphous germania from an alkoxide precursor.

The phage-displayed peptide library screening of TiO_2 substrates yielded twenty peptides. Four of these peptides, which were heavily enriched in histidine and/or basic amino acid residues, were found to possess signficant titania precipitation activity. The activity of these peptides was found to correlate with the number of positive charges they carried. The sequence of the most active of the library-identified peptides was modified to yield two additional peptides. The titania precipitation activity of these designed peptides was higher than the parent peptide, with reduced pH dependence. The titania

materials generated by the library-identified and designed peptides were found to be composed of amorphous titania as well as <10 nm anatase and/or monoclinic TiO_2 crystallites.

The production of titania and zirconia resulting from the interaction of the cationic enzyme, hen egg white lysozyme, with Ti- or Zr-lactate precursors is also presented in this dissertation. Lysozyme was found to entrap itself in an active form within the nanoparticles of amorphous titania or zirconia precipitated by this protein under ambient conditions. The lysozyme synthesized titania was observed to be superior to the lysozyme-zirconia materials in preserving the activity of the enzyme under denaturing conditions.

Four recombinant proteins, derived from the amino acid sequences of proteins (silaffins) associated with biosilicification in diatoms, were also investigated for titania precipitation activity. The two most basic of these recombinant silaffins, rSil1L and rSilC, were able to induce the formation of titania. The titania precipitates generated by rSil1L were found to be similar to those produced by the phage-displayed library identified peptides. The second recombinant silaffin, rSilC, was found to produce hollow spheres of titania, which, following dehydration, were observed to transform into larger, solid spheres composed of radially aligned columns of rutile TiO_2. The highly repetitive nature of the rSilC's amino acid sequence is believed to be responsible for the differences in TiO_2 polymorph generated by the different recombinant silaffins and peptides.

This dissertation also details research conducted on the formation of titania utilizing rSilC conjugated to synthetic and biogenic silica surfaces. These silica surfaces were functionalized with a newly developed drendritic growth technique. The dendritic

functional-group amplification process was demonstrated to increase the loading of hexahisitidine tagged proteins on silica surfaces by more than 40%, as compared to traditional immobilization procedures. The higher loadings of rSilC provided by this dendritic growth method were observed to have a positive impact on the extent of surface mineralization. The titania formed by immobilized rSilC was observed to be composed of amorphous and crystalline TiO_2.

CHAPTER 1: INTRODUCTION

1.1 Research Motivation

During the last 550 million years, certain organisms have evolved the capability to produce complex structures from simple inorganic materials[1-5]. A specific example of such a precisely engineered structure is the calcium carbonate lenses of the brittlestar primitive eye[5]. These lenses are composed of a single crystal of $CaCO_3$ exactly grown and aligned in an orientation which avoids the image doubling affect (birefringence) common to other crystallographic orientations of this mineral[5]. Other organisms, including some marine sponges, produce light guiding structures composed of SiO_2 instead of $CaCO_3$[3,4]. From the perspective of a materials engineer, the frustules (microshells) of diatoms are particularly interesting as they possess intricately detailed features such as ribs, pores and ridges that are formed with nanometer scale precision[6].

The seemingly limitless ability of brittlestars, diatoms, sponges and other organisms to control the polymorph, size, texture and morphology of the inorganic materials they form appears to be derived, in part, from the action of specific biomolecules[1]. The biologically mediated formation of these materials, especially SiO_2, under physiological conditions of pH and temperature, is in sharp contrast to the anthropogenic or geologic synthesis of such inorganic materials, which typically occurs at very high temperatures and/or under extremely caustic conditions[7,8].

The synthesis of materials under the gentle conditions in which they are biologically formed would be immensely beneficial in the fabrication of advanced devices or composites, especially those containing sensitive materials such as polymers

or drugs. For example, photonic crystals may contain polymeric phases that are incompatible with the high temperature formation of the inorganic materials needed to facilitate their operation. Unfortunately, the calcium carbonate and silicon dioxide materials produced by sponges and diatoms do not possess the most attractive properties for many advanced devices and applications[9]. The motivation of this research is to couple the attractive features of protein mediated inorganic materials biosynthesis with the highly functional properties of advanced inorganic oxides not natively produced in the biological world[10].

1.2 Terminology of the Field

It is appropriate to begin this dissertation by defining a few terms that have pervaded this field of research in recent years. *Biomineralization* is the process of inorganic material formation in biological sytems[1]. Although some organisms synthesize inorganic minerals as byproducts of their physiology, the study of biomineralization is predominantly concerned with the materials intentionally generated by organisms. Familiar examples of biomineralized structures include the sand dollars and shells commonly found on beaches, as well as the human skeleton and teeth[1].

As described briefly above in section 1.1, the materials science community has found interest in replicating or mimicking the methods by which biology creates inorganic materials. The application of biological principals to materials processing is known as *biomimetics*[1,2]. Biomimetics may also encompass materials that in some way resemble the structure or properties of materials produced by biology[1,2]. Biomimetics is used interchangeably with the term *bio-inspired*. The research summarized in this dissertation has concentrated on a type of biomimetic processing designated *bio-enabled*

materials synthesis. This term specifically refers herein, to the use of biomolecules, typically peptides or proteins, to initiate or mediate the formation of a material (e.g., germania, titania, or zirconia). While bio-enabled materials synthesis may be considered a synthetic analogue to biomineralization, these two terms are distinct and should not be used interchangeably.

1.3 Introduction to Biomineralization

Organisms that produce hard biominerals composed of silica have been the main inspiration of, and are most relevant to the research presented in this dissertation. Examples of such silica bioarchitectures include the cell walls (i.e., frustules) of diatoms and the spicules of select sponges[1,3,4,6]. While SiO_2 may assume eight distinct crystalline structures, biologically produced silica is formed exclusively in an amorphous state (glass)[1]. Although lacking long range order at the molecular level, the incredible ultrastructure of diatom frustules and sponge spicules have fostered extensive research efforts aimed at identifying the proteins and biomolecules involved in the formation of such structures[11-20].

1.3.1 Silica Associated Proteins in Demosponges

Recent investigations into the nature of the proteins contained within, and possibly playing a role in the formation of, silica sponge spicules have been conducted by Morse and co-workers[11,12]. These researchers found that dissolution of the silicaceous portion of *Tethya aurantia* spicules in a buffered HF solution yielded a proteinaceous inner filament composed of three proteins: silicatein α, β, and γ[11]. The naming of these proteins, silicateins, stems from their occlusion within silica and the observed ability of

the proteins to initiate silica condensation from silicon alkoxide precursors[11,12]. The silica condensation activity of these proteins is believed to lie in a catalytic histidine-serine pair (His165-Ser26) that serves as a general acid/base catalyst in the hydrolysis of silicon alkoxides[12,22]. While the reputed role of this histidine-serine active site has not been explicitly determined, the silica condensation activity of silicatein α (the most abundant silicatein) was nearly abolished in structural variants in which alanine was substituted for either histidine-165 or serine-26[22]. While these experiments specifically addressed the amino acid composition of the silicateins' active site, denaturing experiments have proven the fold of this protein to be equally critical for silica formation activity, as denatured silicatein α possesses ~1% of the activity of native silicatein α[12]. Although structurally related to proteolytic enzymes (i.e., silicatein α possesses 52% sequence identity and 75% sequence homology to human cathepsin L), the histidine-serine pairings native to the active sites of the proteases trypsin and papain are insufficient to instill these proteins with significant silica condensation activity[12].

Working with the sponge *Suberites domuncula*, Müller and colleagues have identified silicateins possessing high homology (i.e., 70% sequence identity and 79% sequence homology) and *in vitro* silica formation activity similar to the silicateins isolated from *T. aurantia*[13,14].

1.3.2 Silica Associated Biomolecules in Diatoms

Given the vast phylogenetic divide between demosponges and diatoms (i.e., these organisms are members of the kingdoms Animalia and Protista, respectively), it is not surprising that the diatoms have developed biosilicification mechanisms distinct from those believed to occur in sponges. Instead of relying on the reputed histidine-serine

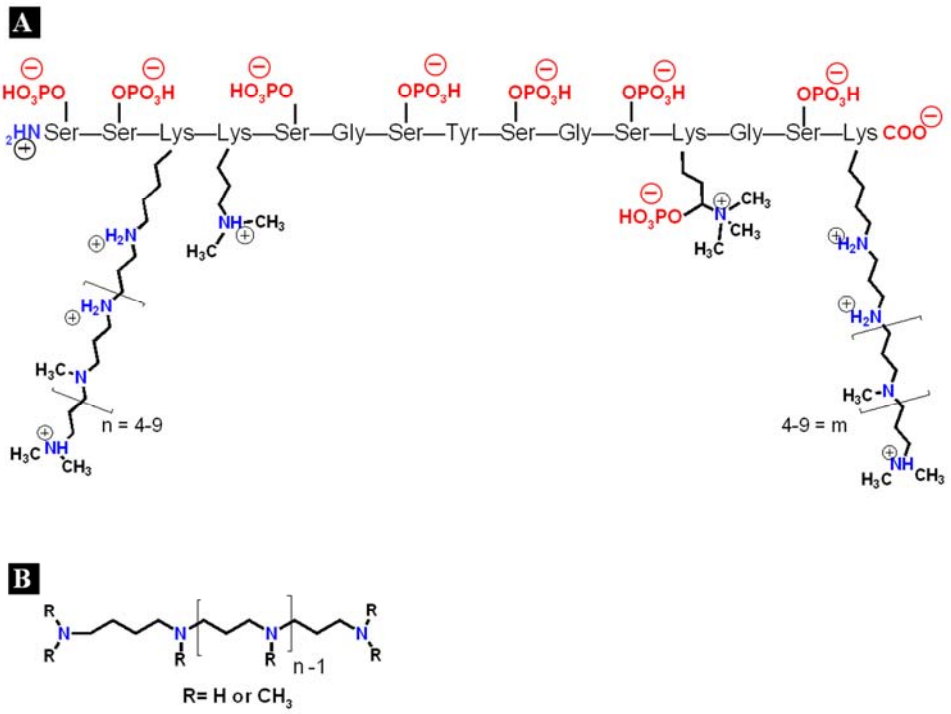

Figure 1.1: Schematic structures of A) natsil-1a$_1$ and B) long-chain polyamines. Figure modeled from those contained within references 21 and 23.

based catalysis mechanism native to sponge silicateins, silica formation in diatoms is believed to be mediated by specialized proteins and long chain polyamines (LCPAs)[15-20,22-24]. In fact, the proteins isolated from diatoms (termed silaffins for their affinity to silica) share no sequence homology with silicateins, or any other known protein[15,19].

The first silaffins to be described by Kröger and colleagues, silaffins-1A$_1$,-1A$_2$,-1B and 2, were isolated through the anhydrous HF dissolution of the silicaceous portion of *Cylindrotheca fusiformis* diatom frustules[15]. Analyses of the closely related peptides, silaffins 1A and 1B, indicated that these peptides were enriched in serine, tyrosine and highly modified lysine residues (Figure 1.1)[15]. Lysine modifications were found to include the covalent addition of 6 to 11 repeats of a N-methyl-propylamine unit and ε-amine dimethylation (i.e., ε-N,N-dimethyl-lysine)[15]. In a subsequent study, additional

residue modifications were identified in silaffins extracted in their native form (termed natSils) from *C. fusiformis* frustules[23]. Modified residues in natSil-1A and -1B included phosphorylated serine and trimethylhydroxylysine phosphate (Figure 1.1)[23].

The extensive post-translational modifications of natSil-1A and -1B are believed to have a significant impact on the ability of these peptides to induce silica formation[15,23]. The formation of the diatom cell wall occurs within a specialized membrane-bound compartment termed the silica deposition vesicle (SDV)[17,21]. Under *in vitro* conditions thought to reflect the acidic internal environment of the SDV, silaffin-1A possesses significant silica precipitation activity. Under similar acidic conditions (i.e., < pH 6) a synthetic analog to silaffin-1A, peptide R5 (which does not carry post-translational modifications), is unable to induce the condensation of silicic acid into silica[15,17]. This indicated that the numerous lysine residue modifications of silaffin-1A and -1B are required for silica precipitation activity within the proposed environment of the SDV[15]. Similarly, the phosphorylation of native silaffins' serine residues was found to play a significant role in the ability of these peptides to induce silica condensation[23]. Silaffins lacking these native phosphate groups displayed no silica precipitation activity under sodium acetate buffered conditions[23]. The ability of silaffin-1A (the dephosphorylated version of the natSil-1A) to induce silica condensation was restored when phosphate ions were added to the reaction solution[23]. Kröger and Sumper hypothesized that silicic acid species are absorbed in and/or onto the silaffins aggregates, forming a "liquid precipitate" which may then polymerize into silica[17]. In an additional role, silaffins may precipitate silica by serving as flocculating agents[15,17]. The cationic silaffin-1 proteins may counteract the negative surface charges which repel polysilicic acid particles in

solution[15,17]. This allows silica embryos to form larger nuclei and, eventually, precipitate from solution as silica particles[15,17].

The *C. fusiformis* protein, silaffin-2, is more enigmatic than its silaffin-1 counterparts, as its primary structure has not as of yet been sequenced, despite significant efforts on the part of Kröger and colleagues[15,18,23]. Although the exact structure of natSil-2 remains unknown, the amino-acid composition of the protein has been characterized[18]. Much like the natSil-1 proteins, natSil-2 carries methylated and polyamine-modified lysine residues[18,23]. Unlike natSil-1A and B, however, natSil-2 is anionic in nature and possesses no intrinsic silica precipitation activity[18,23]. Beyond phosphoserine modifications, natSil-2 was found to carry the additional negatively charged modified residues phosphothreonine and phosphorylated hydroxyproline[18,23]. natSil-2 was additionally found to be heavily glycosylated, with carbohydrate moieties including glucuronic acid, a molecule which also contributes to the protein's negative charge density[18]. The anionic character introduced to natSil-2 through these numerous amino acid modifications is believed to enable the protein to influence the silica formation behavior of silaffins 1A and 1B (as well as LCPAs, discussed below)[18]. natSil-2 was shown to be a regulator of both the morphologies of the material precipitated by other biomacromolecules, as well as the amount of silica formed[18]. It was speculated by these authors that the organic matrix assembled from the diatom's cationic (i.e., natsil-1A, -1B and LCPAs) and anionic (i.e., natSil-2) components may guide the formation of the porous silica observed in certain species of diatoms[18].

The development of silaffins that act as regulators or modifiers of diatom silica formation do not appear to be unique to *C. fusiformis*[18,19]. In a recent study, Poulsen and

Kröger isolated and characterized five natSil-2-like silaffins from the diatom *Thalassiosira pseudonana*[19]. These *T. pseudonana* silaffins, tpSil-(1H, 1L, 2H, 2L, and 3), were found to share no sequence homology to the *C. fusiformis* silaffins, but do possess substantial post-translational modifications similar to those of natSil-2[15,18,19,23]. Mirroring the regulatory role of natSil-2, addition of the *T. pseudonana* silaffins to reaction solutions containing LCPAs enables the formation silica[18,19]. Silica formed in the presence of *T. pseudonana* silaffins also possessed a morphology differing from the microspheres typically produced by LCPAs in phosphate buffers[19,20].

As mentioned briefly above, silica and frustule formation in diatoms is not conducted exclusively by proteins[19,20,24]. The polyamine chains post-translationally modified onto the lysine residues of natSil-1A, -1B, and -2 may also be appended to non-peptide-based amines, such as putrescine or ornithine (Figure 1.1)[19,20]. Investigating 6 species of diatoms, Kröger and colleagues found that these algae possessed species specific mixtures of LCPAs that varied in length (i.e., number of propylamine repeat units) and degree of amine methylation[20]. As detailed above, these LCPAs are able to precipitate silica spheres from silicic acid solutions containing multivalent anionic species (e.g., phosphate or tpSil-1L)[19,20]. In his 2002 manuscript, Sumper theorized that the honeycomb-like patterns of silica present on the diatom valve may be generated by silicic acid condensation around the periphery of close packed arrays of LCPA droplets[24].

A significant amount of information regarding silica biogenesis may be obtained in the future through continued efforts to purify and characterize biomolecules occluded within the silica of both diatoms and sponges. The isolation of the SDV and characterization of proteins contained within this specialized compartment/organelle

could yield extensive insights into diatom frustule formation. Although the processes involved in biosilicification are not completely understood at this time, the biomolecules isolated and ideas generated by the research outlined above has provided considerable inspiration for the bio-enabled and biomimetic formation of materials.

1.4 Forging Beyond Biological Chemistries

1.4.1 Extended Applications of Silicateins

Very recently, several notable advances have been made in the silicatein mediated formation of inorganic compositions other than silica[25-27]. Silicatein filaments have been utilized by Morse and colleagues to produce titania and Ga_2O_3 from titanium-bis-ammonium-lactato-dihydroxide (TiBALDH) and gallium nitrate aqueous precursor solutions, respectively[25,26]. In these studies, nanocrystallites of anatase TiO_2 or γ-Ga_2O_3 were observed to be formed on the surface of the silicatein filaments which were then covered by an over layer of amorphous material[25,26]. Although these crystallites were distinguishable in transmission electron microscopy, they were not produced in sufficient quantities to be observed by x-ray diffraction characterization[25,26]. In a 2006 manuscript, Brutchey et. al, detailed the use of silicatein filaments to partially hydrolyze an acidic solution of $BaTiF_6$ to $BaTiOF_4$[27]. Much like the results obtained in the TiO_2 and Ga_2O_3 systems, small nanocrystallites of $BaTiOF_4$ were observed to form on the surface of silicatein filaments isolated from *T. aurantia*[27]. The synthesis of anatase-TiO_2 and γ-Ga_2O_3 at room temperature and neutral pH represent important steps forward in the bio-enabled formation of "synthetic" materials. However, the long reaction times required

(typically 24 hours) and poor yields of the silicateins leave considerable room for further improvements.

The enzymatically-induced formation of titania was also pursued by Morse and co-workers with recombinant silicateins[28]. In their 2005 manuscript, these authors detail the expression of silicatein-α fused to the outer membrane protein A (ompA) in *Escherichia coli*[28]. The construction of this ompA fusion was driven by the poor activity of soluble silicatein-α conjugates (i.e., maltose binding protein/silicatein-α fusion protein) and the desire to display silicatein-α on the *E. coli* cell surface[28]. Although titanium phosphate and sodium titanium phosphate phases could be generated by heating ompA-silicatein expressing bacteria in excess of 600° C, these bacteria were not shown to accumulate levels of Ti to a greater extent than ompA expressing control cells[28]. This evidently stems from the low activity of silicatein-α, which may be masked by the various proteases native to *E. coli*[28].

1.4.2 Bio-Inspired Syntheses of Non-Biologically Native Chemistries

The ability of the biomolecules outlined above to guide the formation of inorganic materials has led to an entire field of study dedicated to identifying chemical species which might mimic the activities of these proteins. Specific examples from this field of work include the use of poly-l-lysine, block copolymer cysteine-lysine poly-peptides, or poly-ethyleneimine to guide silica formation in the place of silaffins or silicateins[35-37]. The modulation of $CaCO_3$ growth by aspartate, glutamate, poly-aspartic acid, poly-glutamic acid and various synthetic compounds has also been thoroughly detailed in the literature[32,33].

The limitations of these types of bio-inspired studies are that they merely mimic the activity of a known biomineralizing protein and do not offer inorganic chemistries beyond those capable of being produced by the natural protein. Although the *de novo* design of proteins which might control the formation of inorganic materials beyond those currently produced under biological control is possible, such studies are rarely undertaken. Unfortunately, the *de novo* design method often suffers from the difficulties associated with anticipating the dramatic impacts which minor protein sequence or structure changes might impose upon protein activity[34,35].

1.4.3.1 Overview of the Screening of Peptide Libraries, the Biopanning Process

One possible alternative to the rational design approach is to screen peptide libraries for candidates that might guide the synthesis of materials. Peptide libraries exist in two main categories, those composed of chemically synthesized peptides, and those that are produced and displayed by biological systems (e.g., viruses or bacteria)[35,36]. The former of these types of libraries is certainly the most problematic, as synthetic peptide collections are expensive to construct and due to low numbers of peptide copies, the results obtained in screening these libraries are often challenging to interpret[36]. The more advantageous of the peptide libraries, those produced and displayed by biological systems, were pioneered in the laboratory of G. P. Smith in the late 1980's and early 1990s[37,38].

The peptide libraries created by Smith and collaborators were constructed through the genetic manipulation of filamentous *E. coli* infecting viruses (i.e, bacteriophages or phage)[38]. Specifically, these researchers ligated approximately 10^9 different small DNA fragments into the pIII capsid protein-encoding phage gene[38]. Phage DNA carrying the

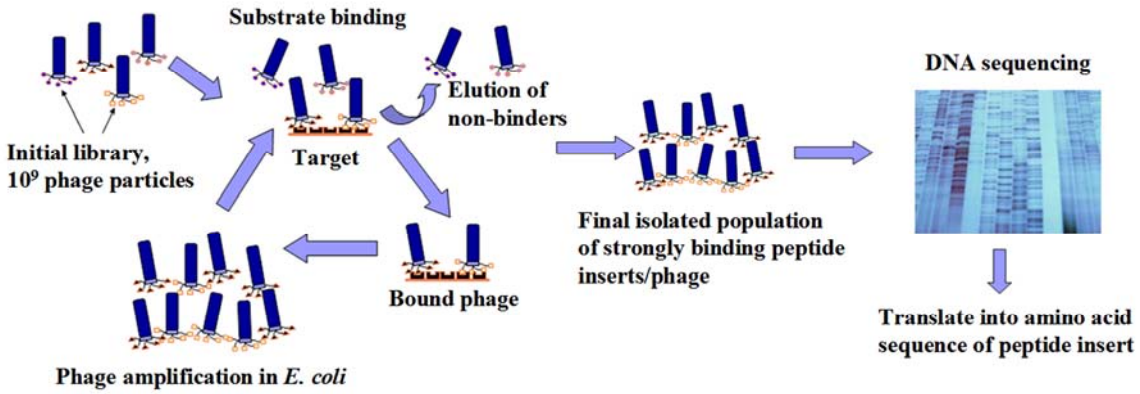

Figure 1.2: Procedure for the isolation of peptides possessing a high affinity for an inorganic material from a phage-displayed library. Several (3-8) rounds of stringent washing and elution are used to remove weakly binding peptides from the final phage population. The amino acid sequence of the displayed peptide is determined through the DNA sequencing of this final phage pool.

modified pIII gene were transfection into *E. coli* cells by electroporation[38]. These transformed *E. coli* then produce phages carrying only one copy of the modified pIII gene[38]. These filamentous phages carry functional pIII proteins with a short peptide fused at their N-terminus[38]. The amino acid sequence of this pIII fused peptide is encoded by the DNA insert sequence, thereby generating a pool of phage displaying approximately 10^9 different short peptides (i.e., a peptide library)[38]. This phage-displayed peptide library represents an infectious analog of synthetic peptide libraries, with the key advantages of replicability and clonability[38]. Due to the connection of the genotype and phenotype of these genetically engineered phage, the amino acid sequence of a given peptide may easily be determined through the sequencing of the corresponding DNA insert sequence[38].

Following construction, Scott and Smith utilized the first phage-displayed peptide library to identify peptide ligands to antibodies[38]. The general procedure utilized for the

screening of phage-displayed peptide libraries is presented in Figure 1.2. As depicted in Figure 1.2, the phage library is incubated with a target (e.g., antibodies in the case of Scott and Smith)[36,38]. This is typically done in a multi-welled plate or plastic centrifuge tube. During this incubation period, the target will be bound by phage-displayed peptides having an affinity for this material[36]. Following incubation, the unbound phages are removed from the target by extensive washing[36,38]. The target binding phage-displayed peptides are removed from the target through the disruption of the target-peptide interaction[36,38]. This is commonly accomplished by subjecting the target-peptide/phage pairing to a low pH buffer which disrupts ionic interactions and may partially denature proteins[36]. The elutant, containing the target specific phage-displayed peptides, is then pH neutralized. These selected viruses are then introduced into *E. coli* culture (i.e., liquid or plate) where they replicate in their infected host cells[36,38]. The replicated phages carry the same peptide and corresponding insert as the target eluted phage[36,38]. The replication of the selected phages represents the end of the first round of the screening or biopanning procedure[36,38]. Additional rounds of screening (i.e., typically 2-4) are conducted by re-incubating these replicated phages with the target[36,38]. These additional biopanning rounds are typically conducted with increasing stringency (e.g., increased levels of detergent, decreased surface area of the target) in order to exclude marginal target binders[36,38]. While Scott and Smith utilized this first phage-displayed peptide library to identify peptide epitopes, the screening of such libraries has been extended to the identification of peptides which bind, and, in some cases, initiate or modulate the formation of inorganic materials[39-51].

1.4.3.2 Application of the Biopanning Method to Materials Science

The first application of the biopanning method to identify peptides which bind to inorganic materials rather than to proteins was conducted by Brown in 1992. In this first study, Brown isolated peptides which selectively adhered to Fe_2O_3 surfaces[39]. In this case, selectivity refers to the preference of the peptides to bind to Fe_2O_3 but not the related compounds Cr_2O_3 or Fe_3O_4[39]. Diverging from the work of Smith, the libraries employed in this first study were expressed on the surfaces of genetically modified *E. coli* cells[39]. A specific weakness of this library, as compared to the commonly used phage-displayed library, is that multiple copies of DNA inserts were transformed into the *E. coli* cells[39]. This multiple insertion of genes is then translated into multimers of peptides being displayed on the cell surface[39]. Multiple copies of a displayed peptide actually decrease the specificity of peptides selected through the screening process, as the contributions of several weakly binding peptides taken together may have the same level of specificity as a high affinity monomeric peptide[36,39]. This problem is more pronounced in Brown's later works when libraries were constructed containing repetitive peptides (i.e., multimers of the same peptide)[40]. Despite the relative shortcomings in his library constructs, Brown's work was pioneering and has served as the stepping stone for all later investigations in this field.

Expanding on the prior work of Brown, Belcher and co-workers utilized a phage-displayed library to identify peptides that specifically recognized GaAs, InP, and Si semiconductor surfaces[39-41]. Utilizing the biopanning technique, Naik and colleagues identified peptides which possessed an affinity for the surface of silica[42]. Of the peptides that were found to bind to an amorphous silica substrate, a sub-population was identified

that exhibited significant silica condensation activity[42]. This finding, that peptides which specifically bind to an inorganic material may, in turn, initiate or control the formation of the same material, has significantly advanced the bio-enabled synthesis of materials[43].

Several additional examples of the ability of library identified peptides to direct the *in vitro* formation of inorganic materials natively produced in biology followed Naik's initial 2002 silica study[42,44-47]. These later studies included the precipitation of noble metals (Au and Ag) under the influence of library-identified peptides[44,45]. Kaplan and colleagues utilized the biopanning process to identify peptides able to modulate the crystallization behavior of $CaCO_3$ (a widely distributed biomineral)[46]. Flynn et. al., have also utilized this method to identify peptides which mimic the observed propensity of certain yeast cells to produce CdS nanoparticles when challenged with high levels of cadmium[47].

While these observations on the formation of CdS were of merit, the authors' concurrent study of the peptide induced synthesis of ZnS is of considerably greater consequence. This ZnS work represents the first time that phage-displayed peptides were utilized to both bind to and induce the precipitation of a non-biologically produced inorganic material[47]. Since this 2003 ZnS study, the biopanning procedure has been successfully utilized to identify magnetic CoPt and FePt alloy nanoparticle forming peptides[48,49]. The directed syntheses of ZnO and $CaMoO_4$ by biopanning isolated peptides have also been recently reported[50,51]. This work on $CaMoO_4$ (by Ahmad, Dickerson, et al.) represents the first report of the synthesis of a binary ceramic compound by peptides identified through the biopanning process[51]. In this study, peptides identified by biopanning were found to induce the precipitation of $CaMoO_4$ from

an aqueous precursor solution[51]. Small changes in the sequence or even ordering of the amino acids in these peptides were observed to have an impact on the yield of precipitated $CaMoO_4$[51]. Chapters 2 and 3 of this dissertation cover the use of the biopanning method to identify peptides possessing germania and titania precipitation activities[52,53].

One can imagine a scenario where peptides in the library possess such an affinity to the target that they are not removed by the typical low pH elution protocol. Addressing this issue, Naik and colleagues recently introduced a new biopanning method based upon the polymerase chain reaction (PCR)[49]. In the "PCR-driven biopanning method," the capsids of the target-bound phages are disassembled in a boiling detergent solution[49]. This solution was collected and the DNA released by the breakup of the phage was amplified by the PCR process[49]. The PCR-amplified phage DNA was transformed into *E. coli* to generate individual clones[49]. The phage DNA was extracted from these clones and sequenced in order to obtain the identity of the phage's high affinity peptide[49]. In their initial study, Naik et. al., utilized the PCR-driven biopanning method to identify peptides which possessed Ag-nanoparticle synthesis activity superior to those identified through traditional biopanning. In this same work, the PCR-driven biopanning method was exploited to identify CoPt specific peptides which were not uncovered during the initial screening of this material with the traditional biopanning method. Given this demonstration of the utility of the PCR-driven biopanning technique, it has been surprising that this method has not been more widely adopted by other "bio-prospectors".

1.5 Immobilization of Proteins for the Growth of Inorganic Materials on Surfaces

Although the protein- or peptide-mediated synthesis of inorganic materials has produced interesting results, the full potential of bioenabled synthesis will not be realized until these materials can be produced in a manner conducive to their integration into devices. The most direct route to the organization of such materials is likely through the immobilization of the precipitating biomolecule on a surface prior to exposure to mineralizing conditions.

Two of the four studies addressing this important topic have been undertaken by Stone and colleagues[44,54]. In the first of these studies, hybrid silica/polymer diffraction gratings were created through the 2-photon initiated holographic patterning of an acrylate-based monomer solution containing the R5 peptide[54]. It was suggested by these authors that the R5 peptide was displaced from those areas of the sample where high photon intensity had initiated the cross-linking of the acrylate polymer[54]. Following patterning, the sample was washed to remove excess polymer and peptide, and then incubated in a silicic acid solution[54]. Silica nanospheres were observed to have formed in the furrows of the patterned polymer (i.e., the areas suspected of containing the R5 peptide)[54]. The micropatterned silica spheres were observed to increase the first-order diffraction efficiency of the treated hologram by nearly 50-fold over patterns composed of solely the cross-linked monomer solution[54].

In their second study of this type, Stone and co-workers utilized surface immobilized peptides (i.e., peptide Ag4) to create spatially defined rows of silver nano-particles[44]. In place of their former holographic patterning approach, Stone and colleagues utilized microchannels, created by the placement of elastomeric moulds on a

substrate, to organize the Ag precipitating peptides prior to precursor exposure[44]. The immobilization of these peptides was accomplished electrostatically, through the interaction of the carboxylic acid groups of the Ag4 peptide and a layer of poly-lysine coating the glass substrates[44]. Incubation of these substrates with a solution of $AgNO_3$ resulted in the nucleation and growth of Ag particles only in those regions containing the adsorbed peptides[44].

The research team headed by Tremel has also made several contributions to the body of literature concerning the mineralization of surface immobilized biomolecules[55,56]. These researchers have focused their efforts on the synthesis of silica, titania, and zirconia utilizing sequestered silicateins[55,56]. In their 2004 study, recombinant silicateins were immobilized on gold substrates functionalized with a self-assembled layer of thiolated nitrilotriacetic acid (NTA)[55]. In their 2005 contribution, these authors have expanded upon their previous work through the generation of gold substrates functionalized with NTA displaying reactive ester polymer[56]. This poly(acetoxime methacylate) polymer was bonded to the gold substrate by reaction with a self-assembled cysteamine film present on the substrate surface[56]. This same amine based reaction was utilized to anchor amine terminated NTA ligands to the polymer surface, following its deposition onto gold[56]. The immobilization of silicatein was facilitated in these studies by the interaction of a hexahistidine tag engineered into the protein with a nickel ion chelated by the NTA ligand[56]. The silica deposits catalyzed by the conjugated silicateins from a silicon-alkoxide solution were observed to cover approximately 70% of the functionalized gold surfaces (as determined by Tremel and co-authors)[56]. The titania and zirconia synthesized from aqueous precursors by the Au-cysteamine-polymer-NTA-Ni^{2+}

conjugated silicateins are noted to cover far less surface area than their silica counterpart[55,56].

1.6 References

1. Mann, S. *Biomineralization: Principals and Concepts in Bioinorganic Materials Chemistry*, Oxford University Press, **2001**, 2-23.
2. Mann, S. *Biomimetic Materials Chemistry*, VCH Press, **1996**, 1-37.
3. Sundar, V.C.; Yablon, A. D.; Grazul, J. L.; Ilan, M.; Aizenberg, J. *Nature,* **2003** *424*, 899.
4. Cattaneo-Vletti, R.; Bavestrello, G.; Cerrano, C.; Sara, M.; Benatti, U.; Glovine, M.; Gaino, E. *Nature*, **1996,***383,*397.
5. Aizenberg, J.; Tkachenko, A.; Weiner, S.; Addadi, L.; Hendler, G., *Nature,* **2001**, *412*, 819.
6. Round, F. E.; Crawford, R. M.; Mann, D.G. *The Diatoms: Biology and Morphology of the Genera*, Cambridge University Press, **1990**.
7. Sigurdsson, H. *Encyclopedia of volcanoes*, Academic Press, **2000**, 55-69, 115-149.
8. Flachsbart, H.; Stöber, W.; *J. Colloid Interf. Sci.,* **1969,** *30,* 568.
9. Lide, D. *CRC Handbook of chemistry and physics 77th Edition*, CRC press, **1996**, 4-130-4-136.
10. Weiner, S.; Addadi, L. *Science*, **2002**, *298*, 375.
11. Shimizu, K.; Cha, J.; Stucky, G.; Morse, D. *Proc. Natl. Acad. Sci. USA,* **1998**, *95*, 6234.
12. Cha, J.; Shimizu, K.; Zhou, Y.; Christiansen, S. C.; Chmelka, B. F.; Stucky, G. D.; Morse, D. E. *Proc. Natl. Acad. Sci. USA*, **1999**, *96*, 361.
13. Krasko, A.; Lorenz, B.; Batel, R.; Schröder, H-C.; Müller, I. M.; Müller, W. E. G *Euro. J. Biochem.*, **2000**, *267*, 4878.
14. Müller, W. E. G.; Belikov, S. I.; Wolfgang, T.; Perry, C. C.; Gieskes, W. W. C.; Boreiko, A.; Schröder, H. C. *Prog. Mol. Subcell. Biol.*, **2003**, *33*, 195.
15. Kröger, N.; Deutzmann, R.; Sumper, M. *Science*, **1999**, *286*, 1129.
16. Kröger, N.; Deutzmann, R.; Sumper, M. *J. Biol. Chem.*, **2001**, *276*, 26066.

17. Kröger, N; Sumper, M. in *Biomineralization: Progress in Biology, Molecular Biology, and Application, 2nd Ed.*, (Baeuerlein, E., editor), **2004**, Wiley-VCH, Weinheim, Germany, 137.

18. Poulsen, N.; Sumper, M.; Kröger, N. *Proc. Natl. Acad. Sci. USA*, **2003**, *100*, 12075.

19. Poulsen, N.; Kröger, N. *J. Biol. Chem.*,**2004**, *279*, 42993.

20. Kröger, N.; Deutzmann, R.; Bergsdor, C.; Sumper, M. *Proc. Natl. Acad. Sci. USA*, **2000**, *97*, 14133.

21. Drum, R. W.; Pankratz, H. S. *J. Ultrastruct. Res.*, **1964**, *10*, 217.

22. Zhou, Y.; Shimizu, K.; Cha, J.; Stucky, G. D.; Morse, D. E. *Angew. Chem., Int. Ed.*, **1999**,*38*, 780.

23. Kröger, N.; Lorenz, S.; Brunner, E.; Sumper, M. *Science*, **2002**, *298*, 584.

24. Sumper, M. *Science*, **2002**, *295*, 2430.

25. Sumerel, J. L.; Yang, W.; Kisailus, D.; Weaver, J. C.; Choi J. H.; Morse D. E.; *Chem. Mater*. **2003**, *15*, 4804.

26. Kisailus, D.; Najarian, M.; Weaver, J. C.; Morse, D. E. *Adv. Mater*. **2005**, *17*, 1234.

27. Brutchey, R. L.; Yoo, E. S; Morse, D. E. *J. Am. Chem. Soc.* **2006**, *128*, 10288.

28. Crunow, P.; Bessette, P. H.; Kisailus, D.; Murr, M.; Daughert, P. S.; Morse, D. E. *J. Am. Chem. Soc.* **2005,** *27,*15749.

29. Patwardhan, S.; Maheshwari, R.; Mukherjee, N.; Kiick, K. L.; Clarson, S. J. *Biomacromolecules*, **2006**, *7*, 491.

30. Cha, J.; Stucky, G.; Morse, D.; Deming, T. *Nature*, **2000**, *403*, 289.

31. Yuan, J.; Jin, R. *Adv. Mater.*, **2005**, *17*, 885.

32. De Yoreo, J.; Dove, P. *Science*, **2004**, *306*, 1301.

33. Malkaj, P.; Dalas, E. *Cryst. Growth Design*, **2004**, *4*, 721.

34. Rodi, D.; Makowski, L. *Curr. Opin. Biotech*., **1999**, *10*, 87.

35. Marrs, B.; Delagrave, S.; Murphy, D. *Curr. Opin. Microbiol.,* **1999**, *2*, 241.

36. Scott, J. K. in *Phage Display: A Laboratory Manuel*, Cold Spring Harbor Laboratory Press, New York, **2001**, 4.1.

37. Smith, G. P.; Petrenko, V. A. *Chem. Rev.,* **1997**, *97*, 391.

38. Scott, J. K.; Smith, G. P. *Science*, **1990**, *249*, 386.

39. Brown, S. *Proc. Natl. Acad. Sci. USA,* **1992**, *89*, 8651.

40. Brown, S. *Nat. Biotechnol.*, **1997**, *15*, 269.

41. Whaley, S.; English, D.; Hu, E.; Barbara, P.; Belcher, A. *Nature,* **2000**,*405*, 665.

42. Naik, R. R.; Brott, L. L.; Clarson, S.; Stone, M. O., *J. Nanosci. Nanotech.,* **2002**, *2*, 95.

43. Baeuerlein, E. in *Biomineralization: Progress in Biology, Molecular Biology, and Application, 2nd Ed.*, (Baeuerlein, E., editor), **2004**, Wiley-VCH, Weinheim, Germany, 1.

44. Naik, R. R.; Stringer, S.; Agarwal, G.; Jones, S. E.; Stone, M. O. *Nat. Mater.,* **2002**, *1*, 169.

45. Brown, S.; Sarikaya, M.; Johnson, E. *J. Mol. Biol.*, **2000**, *299*, 725.

46. Lei, C.; Botsaris, G. D.; Kaplan, D. L. *Cryst. Growth Design*, **2002**, *2*, 387.

47. Flynn, C. ; Mao, C. ; Hayhurst, A. ; Williams, J. L. ; Georgiou, G. ; Iverson, B. ; Belcher, A. M. *J. Mater. Chem,.* **2003**, *13*, 2414.

48. Reiss, B.; Mao, C.; Solis, D.; Ryan, K.; Thomson, T.; Belcher, A.; *Nano Lett.*, **2004**, *4*, 1127.

49. Naik, R. R.; Jones, S. E.; Murray, C. J.; McAuliffe, J. C.; Vaia, R. A.; Stone, M. O. *Adv. Funct. Mater.,* **2004**, *14*, 25.

50. Umetsu, M.; Mizuta, M.; Tsumoto, K.; Ohara, S.; Takami, S.; Watanabe, H.; Kumagai, I.; Adschiri, T. *Adv. Mater.*, **2005**, *17*, 2571.

51. Ahmad, G.; Dickerson, M. B.; Church, B. C.; Cai, Y.; Jones, S. E.; Naik, R. R.; King, J. S.; Summers, C. J.; Kroger, N., Sandhage, K. H. *Adv. Mater*., **2006**, *18*, 1759.

52. Dickerson, M. B.; Naik, R. R.; Stone, M. O.; Jones, S. E.; Cai, Y.; Sandhage, K. H. *Chem. Commun.*, **2004**, 1776.

53. Dickerson, M. B.; Jones, S. E.; Cai, Y.; Ahmad, G.; Naik, R. R.; Sandhage, K. H. *Chem. Mater.,* (submitted).

54. Brott, L. L.; Naik, R. R.; Pikas, D. J.; Kirkpatrick, S. M.; Tomlin, D. W.; Whitlock, P. W.; Clarson, S. J.; Stone, M. O. *Nature,* **2001**, *413*, 291.

55. Tahir, M. N.; Théato, P.; Müller, W. E. G., Schröder, H. C.; Janshoff, A.; Zhang, J.; Huthe, J.; Tremel, W. *Chem. Commun.,* **2004**, 2848.

56. Tahir, M. N.; Théato, P.; Müller, W. E. G., Schröder, H. C.; Borejko, A.; Faiß, S.; Janshoff, A.; Huthe, J.; Tremel, W. *Chem. Commun.,* **2005**, 5533.

CHAPTER 2: IDENTIFICATION OF PEPTIDES THAT PROMOTE THE RAPID PRECIPITATION OF GERMANIA NANOPARTICLE NETWORKS VIA USE OF A PEPTIDE DISPLAY LIBRARY

The research in this chapter is distinct from, though represents a summary of the studies presented in the following publications:

i. Dickerson, M. B.; Naik, R. R.; Stone, M. O.; Cai, Y.; Sandhage, K. H.; *Chem. Commun.*, **2004**, 1776.

ii. Dickerson, M. B.; Cai, Y.; Sandhage, K. H.; Naik, R. R.; Stone, M. O. *Cer. Eng. Sci. Proc.,* **2005**, *26*, 25.

2.1 Introduction

The lands and waters of our planet are colonized by approximately 10^4 to 10^5 species of diatoms[1-4]. Each of these diatom species assembles a cell wall (termed the frustule) with a unique shape and species-specific patterns of submicron features (e.g., pores, spines, supporting ribs, channels)[1-4]. The ability of diatoms to produce such intricately detailed silica structures under cellular conditions and with precise genetic control has served as a source of inspiration for materials scientists[5]. While many investigations have been conducted into the bio-inspired or biomimetic synthesis of silica, few studies have focused upon the use of biomolecules to produce materials not natively produced by biology[5].

Given the relative chemical similarity of germanium and silicon, an examination of the bio-enabled formation of germanium oxide (germania) represents a logical first step in extending the use of biomolecules to produce "synthetic" compounds[6]. Investigating the biomimetic synthesis of germania is particularly important as germania-bearing glasses possess enhanced transmission at infrared wavelengths relative to silica-

rich glasses[7-10]. The biomimetic fabrication of germanium oxide-bearing glasses could be a key technology in the development of integrated optical lasers, sensors, display devices, and amplifiers[7-10].

While germania is known to be incorporated, in trace quantities, into the silicaceous structures of diatoms and sponges, these organisms do not specifically mineralize germania[11,12]. Indeed, diatoms and sponges are poisoned by elevated levels of germanic acid (i.e., the soluble form of germania), leading to cell death and gross distortions in silica architecture[11,12]. Although silica-forming biomolecules have been identified by several authors, proteins specific for the formation of germania have yet to be found in nature[13-15]. The objective of the research summarized in this chapter was to identify peptides, from a phage-displayed peptide library, that promote germania precipitation.

2.2 Experimental Procedure

2.2.1 Screening of a Phage-Displayed Peptide Library Against Ge Powder

Germania-binding peptides were isolated using the Ph.D.-12™ phage display library kit obtained from New England Biolabs (Beverly, MA). The target binding, elution, and amplification were carried out in accordance with the manufacturer's (New England Biolabs) instructions. The target powder (-100 Mesh, 99.999% germanium purity metals basis, Alfa Aesar, Ward Hill, MA) was first triple washed in 50 mM tris-(hydroxymethyl)-aminomethane buffered-saline (150 mM NaCl), pH 7.5 containing 0.2% Tween-20 detergent (referred to herein as 0.2% TBST). The powder was then exposed to the Ph.D.-12™ library for one hour, after which the powder was washed

repeatedly (10 times) with 0.2% TBST to remove any free phage particles. The bound phages were then eluted by incubation for 10 minutes with 0.2 M glycine-HCl pH 2.2. The supernatant was removed from the target powder and then neutralized with 1 M Tris-HCl pH 9.1. The eluted bacteriophages were amplified through infection into *Escherichia coli* strain ER2738. The phage population was further enriched with respect to germania-binding affinity by two subsequent panning rounds utilizing 0.2% TBST washing conditions followed by two rounds utilizing 0.5% TBST washing conditions. After the final panning procedure, ER2738 cells were infected with the eluted phages and plated on Luria Broth (LB) plates containing 5-bromo-4-chloro-3-indolyl-β-D-glactoside (X-gal, Invitrogen, Carlsbad, Ca) and isopropyl β-D-thioglactoside (IPTG, Invitrogen, Carlsbad, Ca). DNA was isolated from 30 independent blue plaques and sequenced by Sharon E. Jones (Air Force Research Laboratory) using an ABI 310 (PE Applied Biosystems, Ca) automated sequencer.

2.2.2 Germanium Oxide Precipitation Assay

Peptides Ge34, Ge8, and Ge2 of desalted grade, were purchased from New England peptide (Gardner, MA). Poly-amino acids (Sigma Aldrich, St. Louis, MO) were used as purchased without further purification or characterization. 5 mM stock solutions (based upon the molecular weight of their constituent amino acid) of the various poly-amino acids were prepared by adding the appropriate mass of powdered poly-amino acid to 500 µl of high purity (0.2 µm-filtered 18.2 MΩ·cm water). Stock solutions of the phage-displayed library isolated peptides were created at 10 mg/ml. Germanium oxide precipitation was conducted by diluting 10 µl of peptide stock solution into 40 µl of anhydrous methanol (99.9%, Alfa Aesar, Ward Hill, Ma). 50 µl of 270 mM

tetramethoxygermanium (TMOG) (99.999%, Alfa Aesar, Ward Hill, Ma) in anhydrous methanol was added to the diluted peptide solution and mixed by inversion several times. This precipitation reaction was conducted for 30 minutes with continual rotation being provided by a RKVSD rotamixer at 30 rpm (Appropriate Technical Resources Inc., Laural, MD). The resulting precipitates were concentrated by centrifugation and repeatedly washed with anhydrous methanol.

2.2.3 Molybdenum Blue Assay for the Determination of Germanium Concentration

The amount of germania precipitated from the alkoxide solution within 30 minutes in the presence of a given peptide (i.e., the germania precipitation activity) was determined by adapting the β-silicomolybdate method described by Iler[16]. Three precipitation reactions were conducted and measured in triplicate for each data point. Error bars represent one standard deviation. The germanium oxide precipitate was first dissolved in boiling 1 M NaOH for 20 minutes. The reaction of the molybdic acid with hydrolyzed germania gave a yellow product with an absorption maximum at 410 nm. The absorption value of the sample measured at 410 nm was found to be linearly related to the concentration of germania in the sample.

2.2.4 Precipitation Activity Versus Peptide Concentration

The germanium oxide precipitation assay described above was conducted with 10 μl of peptide solution drawn from stocks ranging from 1 to 50 mg of peptide Ge8 per ml of high purity H_2O. The amount of germania precipitated by the peptide was then quantified as described above, through the use of the molybdenum blue assay.

2.3 Results and Discussion

2.3.1 Phage-Displayed Peptide Library Screening

An effective technique for the identification of proteins specific to a target surface or molecule is the phage-displayed peptide screening method. This technique has been used to isolate peptides that possess an affinity to a variety of inorganic material surfaces, including III-V semiconductors, noble metals, and oxide ceramics[18-22]. Several of these studies have also identified peptides of unique sequence which proved effective in controlling the morphology or crystal structure of the materials prepared under their influence[19,21,23].

A commercially-available combinatorial peptide display library (Ph.D.-12^{TM}) was used to identify peptides that exhibit strong binding to germania. This library contained approximately 3×10^9 different 12-mer peptides displayed on the pIII minor coat proteins of the M13 phage[24]. *E. coli* cells infected by the phages selected by five rounds of selective biopanning against Ge were plated onto X-gal/IPTG plates. From these plates, 30 individual phage clones were selected and the DNA inserts encoding their displayed peptide was sequenced. The sequencing of the phage DNA was conducted by Sharon E. Jones of the Air Force Research Laboratory. The sequences provided by Jones yielded 21 unique peptides, primary structures of which are presented in Table 2.1. The theoretical isoelectric points (pI) of these peptides are observed to span a wide range of values, from acidic (4.1) to basic (11.0), and displayed no significant enrichment of amino acid residues beyond that reported for the starting Ph.D.-12^{TM} library. Preliminary experiments using a previously described polymerase chain reaction (PCR) method failed

Table 2.1: The characteristics and sequences of peptides identified by biopanning against germanium. Sequencing of phage DNA inserts corresponding to these peptides was conducted by Sharon E. Jones of AFRL. The amino acid residues histidine (H), arginine (R) lysine (K), serine (S), threonine (T), and tyrosine (Y) proposed to be associated with germania precipitation activity are indicated by color. pI = isoelectric point. H = number of histidine residues. K+R = combined number of lysine and arginine residues, respectively. D + E = combined number of aspartic and glutamic acid residues, respectively. Values for starting library taken from reference 24. *Asterisk designates those peptides selected for germania precipitation trials. **Isoelectric point of peptides calculated using MW, pI, titration curve program available at www.expasy.org.

Clone Name	Amino Acid Sequence	pI**	H	S+T+Y	K+R
Ge32	E P W L D S **R** Y S P L S	4.1	0.0	4.0	1.0
Ge7	G H G L L Q Y T D V M F	4.9	1.0	2.0	0.0
*Ge2	T S L Y T D **R** P S T P L	6.8	0.0	6.0	1.0
Ge36	L P I P S S L G G P F P	6.0	0.0	2.0	0.0
Ge4	S Y E M P F S T **R** P W F	7.0	0.0	4.0	1.0
Ge5	L P G W P L A E **R** V G Q	7.0	0.0	0.0	1.0
*Ge34	T G H Q S P G A Y A A H	8.0	2.0	3.0	0.0
Ge31	N F M E S L P **R** L G M H	7.8	1.0	1.0	1.0
Ge7	H S T W **K** L L **R** L D M E	7.8	1.0	2.0	2.0
Ge28	H A T G T H G L S L S H	8.1	3.0	4.0	0.0
Ge20	S F L Y S Y T G P **R** P L	9.7	0.0	5.0	1.0
Ge37	T M G F T A P **R** F P H Y	9.8	1.0	3.0	1.0
*Ge8	S L **K** M P H W P H L L P	10.1	2.0	1.0	1.0
Ge16	**K** A W I V Q P P F H Y S	9.8	1.0	2.0	1.0
Ge3	Q L P **K** H N Y W P G A F	9.8	1.0	1.0	1.0
Ge6	Y T T S N T L Q V I A **R**	9.8	0.0	5.0	1.0
Ge14	N T P G I **R** P Q A T Y S	9.8	0.0	4.0	1.0
Ge35	A L H P L T N **R** H Y A T	9.8	2.0	3.0	1.0
Ge15	S N T S I I **R** N A F P Q	11.0	0.0	3.0	1.0
Ge39	G V S Q N T N S L H L **R**	11.0	1.0	3.0	1.0
Ge11	G M V S T S **R** M H A G W	11.0	1.0	3.0	1.0
	average	8.5	0.8	2.9	0.9
	starting library	-	0.8	3.0	0.9

to yield any DNA from phage that remain attached to the germanium particles after elution with glycine-HCl pH 2.2[22]. This indicated that the glycine-HCl elution was effective in releasing all of the germanium surface-binding, peptide-displaying phages.

2.3.2 Germania Precipitation Assay

Insight into which residues are likely to be significant for the formation of germanium oxide was gained by purchasing several of these Ge surface-binding peptides and assessing their specific precipitation activity. Three peptides, Ge2, Ge8, and Ge34, which possess a range of pIs (6.8-10.1) and amino acid contents were selected for further evaluation (peptides marked with an asterisk in Table 2.1). In order to assess the ability of these germania-binding peptides to promote germania precipitation, the peptides were introduced (1 mg/ml) into a germanium alkoxide-bearing solution (135 mM tetramethoxygermanium dissolved in methanol) at room temperature. Precipitation occurred rapidly upon introduction of either the Ge8 or Ge34 peptide into the alkoxide solution. In contrast, germania precipitation induced by the Ge2 peptide was difficult to detect by visual observation. Control experiments conducted with non-germania-binding peptides Ag5 (SLATQPPRTVPP, pI=11.0) and Ag-p28 (SPLLYATTSNQS, pI=6.0), or in the absence of the germania-binding peptides (i.e., addition of an equal volume of water), failed to yield germania precipitates from the alkoxide solution[18,22]. The amount of germania formed (i.e., the germania precipitating activity) in the presence of the germanium surface-binding peptides was quantified by adapting the β-silicomolybdate colorimetric assay[16]. As shown in Figure 2.1, the Ge8 and Ge34 peptides exhibited relatively high germania- precipitating activities, whereas the Ge2 peptide exhibited much lower activity.

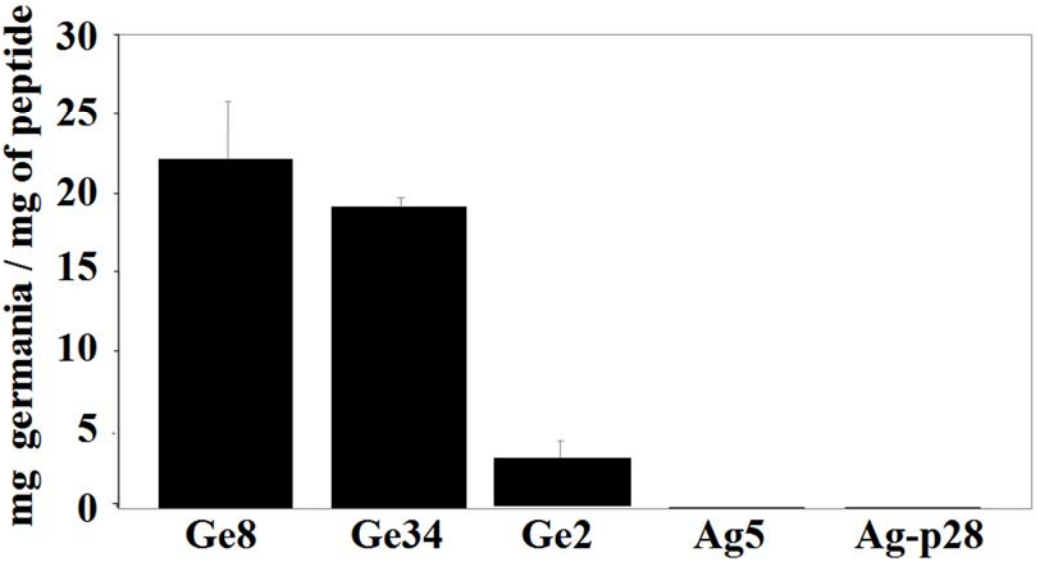

Figure 2.1: Germania precipitating activity of library-identified and control peptides.

The amino acids within peptides can provide molecular recognition motifs for strong binding to specific inorganic surfaces. The molecular characteristics that result in strong binding of a particular peptide to a specific inorganic surface may also enable that peptide to induce the precipitation of the inorganic solid from a solution[25]. In the present work, germania-binding peptides that were particularly effective in promoting germania precipitation from an alkoxide solution, Ge8 and Ge34, possessed hydroxyl- and imidazole-containing amino acid residues. The germania-binding peptide with the lowest germania precipitating activity, Ge2, lacked histidine residues and possessed a more acidic isoelectric point. The failure of the control peptides RN 28 and Ag5 to produce germania indicated that precipitation in the presence of the isolated germania clones was not due to non-specific peptide backbone interactions or a simple pH mediated hydrolysis. This indicates that germania precipitation activity was instead specific to

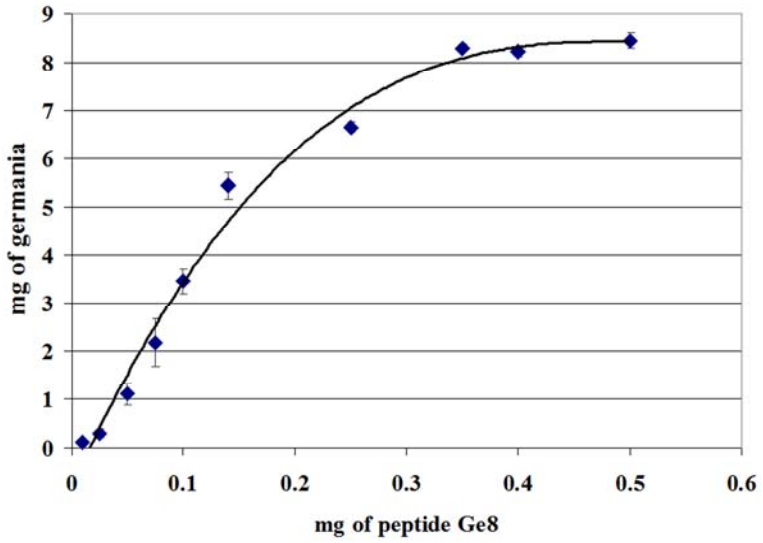

Figure 2.2: Milligrams of germania precipitated from solution as a function of the amount of peptide Ge8 introduced. The amount of germania precipitated increased roughly linearly with the amount of peptide added at low values and then reached a maximum value which corresponded to a 60% depletion of the initial concentration of available germanium in the solution. At this level of depletion, insufficient germanium may be left in solution to allow for further precipitation by additional Ge8.

those sequences isolated by the panning process. The observation that the amount of germania precipitated from solution directly correlated with peptide concentration, provided additional evidence that the identified peptides played a direct role in germania formation (Figure 2.2). It is interesting to note that similar molecular characteristics (hydroxyl- and imidazole-containing amino acid residues, basic isoelectric point) have been found in peptides that exhibited a high silica precipitating activity[20]. These silica-precipitating peptides were however, not among the 21 germania-binding peptides isolated in the present work.

In order to better assess the contributions of individual amino acid residues to the unique character of peptides isolated through the phage-displayed library screening

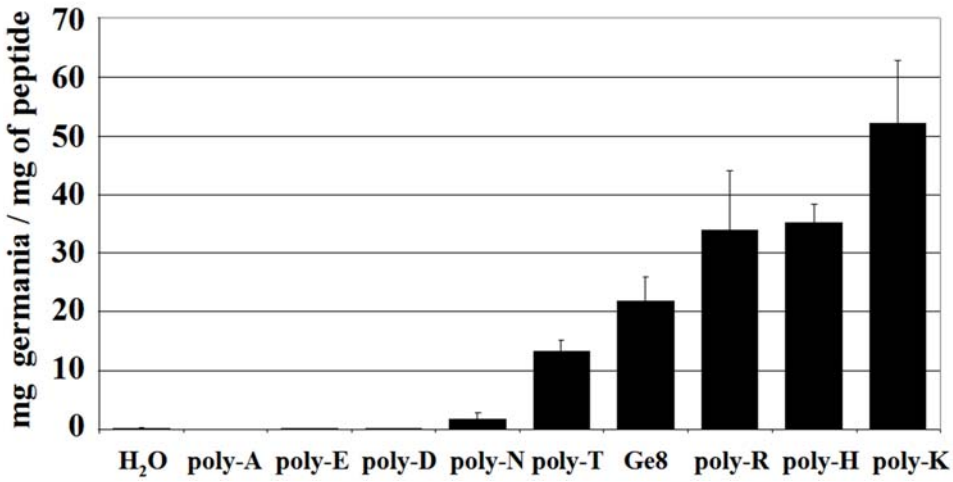

Figure 2.3: Germania precipitating activity of several homo poly-amino acids. Lysine = K, histidine = H, arginine = R, threonine = T, asparagine = N, aspartic acid = D, glutamic acid = E, alanine = A. H_2O= equal volume of water, with no peptide. Precipitation activity of Ge8 included for reference.

technique, the germanium oxide-forming nature of several commercially available homo poly-amino acids were investigated. The eight poly-amino acid peptides utilized in this study were selected on the basis of the side group character spectrum of the amino acids contained by the library-isolated peptides. Addition of the germanium oxide precursor solution to either of the anionic amino acid residues, poly-aspartic acid or glutamic acid, failed to produce any detectable precipitation product (Figure 2.3). The hydrophobic amino acid polymer, poly-alanine, also failed to produce germanium oxide from the precursor solution. Inspection of Figure 2.3 reveals that the poly-amino acids composed of residues capable of participating in hydrogen bonding interactions (i.e., threonine and asparagine) exhibited modest germania formation activity. Of poly-threonine and poly-asparagine, the hydroxyl-rich poly-threonine possessed greater precipitation activity. As expected from the relatively high precipitation yields of the histidine containing peptides Ge8 and Ge34, poly-histidine was observed to induce the formation of significant

amounts of germania. The cationic peptides poly-lysine and poly-arginine were also found to possess high germania precipitation activities. This correlated well with the results of a 2005 study by Patwardhan and Clarson in which the highly cationic molecule poly-allylamine was found to precipitate germania from alkoxide precursor solutions[26]. The results of the interaction of poly-alanine, asparagine, threonine, glutamate, aspartate, histidine, lysine, and arginine in the formation of germanium oxide correlated well with previously observed interactions, or lack of interaction, with chemically-similar silica precursors[27-29].

2.3.3 Characterization of Germania Precipitates

The germania precipitates generated in the presence of peptides Ge8, Ge34, poly-threonine, poly-histidine, poly-lysine, or poly-arginine were characterized by scanning electron microscopy (SEM) and transmission electron microscopy (TEM). Although the chemical character, polymer length, and the germanium oxide precipitation activities of the studied peptides differed substantially, the morphologies of their germania precipitates were remarkably similar. SEM micrographs (Figure 2.4) revealed that the precipitation products generated by all biomolecules tested consisted of porous, inter-connected networks of agglomerates of fine particles. Energy dispersive x-ray analyses revealed that the precipitates were enriched in germanium and oxygen (see Figure 2.4D; the minor Au and Pd peaks were a result of the coating applied to the particles to avoid surface charge buildup in the SEM, and the minor Si peak was generated by the silicon substrate on which the precipitates were placed). High-resolution TEM images, taken by Dr. Ye Cai (Georgia Institute of Technology), (Figure 2.5) confirmed the open network structures and revealed that the fundamental germania particles possessed diameters on

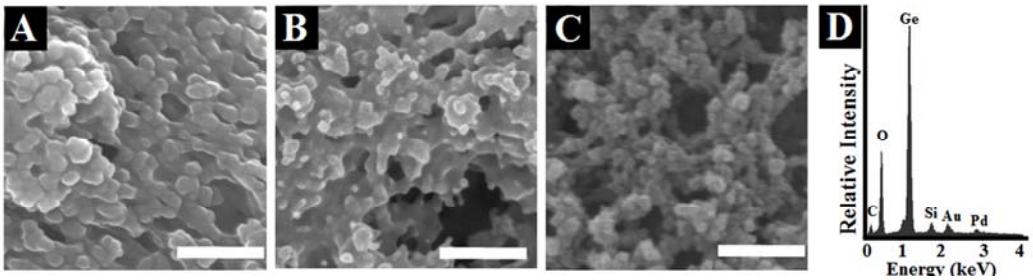

Figure 2.4: Morphologies of the germania nanoparticle networks induced to form at room temperature from an alkoxide precursor solution in the presence of peptides. Secondary electron images reveal typical germania precipitates generated in the presence of the: A) Ge8, B) Ge34, and C) homo poly-amino acids. D) Representative elemental analysis by EDS of the GeO_2 precipitate formed in the presence of all peptides tested. Scale bars correspond to 250 nm. Analyses shown in C) and D) were specifically generated by poly-histidine and Ge8, respectively.

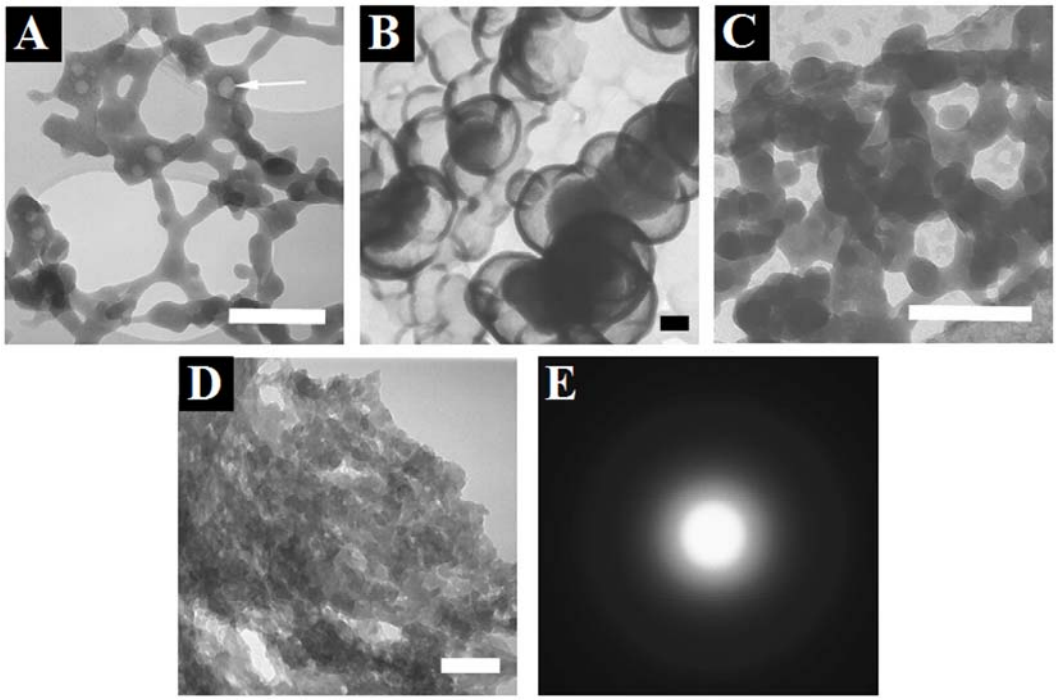

Figure 2.5: Bright field transmission electron images of the germania precipitates formed in the presence of the: A) and B) Ge-8, C) Ge-34, and D) poly-lysine peptides. The arrow in A designates a low density area found in Ge-8 induced precipitates. These low density areas were occasionally observed to be quite large, resulting in the hollow sphere or core-shell structures observed in B). Representative electron diffraction pattern from all peptide precipitated germania samples presented in E). The scale bars correspond to 200 nm. Images taken by Dr. Ye Cai (Georgia Institute of Technology).

the order of 50 nm. TEM analyses, conducted by Dr. Ye Cai also revealed that the particle agglomerates contained regions of low density (relatively bright regions in Figures 2.5A), which were consisted of either entrapped pores or residual organic material. Occasionally, these pores were observed to be quite large, conferring a hollow sphere or core/shell architecture onto the Ge8-induced germania (Figure 2.5B). Hollow sphere morphology was also recently noted for TiO_2 formed under the influence of a recombinant silaffin (rSilC)[30]. Electron diffraction (ED) analyses (conducted by Dr. Ye Cai) obtained at numerous locations within the peptide induced precipitation products indicated that the germania was amorphous (a representative ED pattern is shown in Figure 2.5E).

2.4 Summary and Outlook

A phage display peptide library was used to identify germania-binding peptides that promoted the rapid, room-temperature precipitation of amorphous germania nanoparticle networks from an alkoxide solution. The assessment of the precipitation activity of three of these library-identified peptides in conjunction with several homo poly-amino acids revealed that cationic (arginine and lysine), histidine, and hydroxyl-bearing (threonine, serine, and tyrosine) amino acid residues were effective at producing germania from a TMOG solution. It is likely that the chemistry, and resulting optical properties, of the germania-bearing precipitates can be adjusted by doping of the alkoxide precursor solution and/or by using combinations of peptides that promote the co-precipitation of germania with other oxides (e.g., germania-silica compositions for optical waveguides). The ability of such peptides to promote the rapid, room-temperature precipitation of tailored oxide compositions, coupled with the ability to pattern peptides

on various surfaces, enables exciting new opportunities for the integration of functional oxides with low-temperature or reactive materials (e.g., polymer-, bio-organic-, or silicon-based devices). Such germania-based composite materials may find use as technologically-important solids for electronic, optical, energy-generation and catalytic applications[7-10,31-33]. Indeed, following the publication of our initial study, the Ge34 peptide has found use in the preparation of porous germania nanospheres[33]. These GeO_2 nanospheres were utilized as a host matrix for the growth of catalytic Au-Pd (1:4) nanoparticles, capable of degrading p-nitroaniline[33].

2.5 References

1. Hildebrand, M.; Wetherbee, R. *Progress in Molecular and Subcellular Biology*, Springer-Verlag, **2003**, 11.
2. Crawford, S.; Higgins, M.; Mulvaney, P.; Wetherbee, R. *J. Phycol.*, **2001**, *37*, 543.
3. Mann, S. *Biomineralization: Principles and Concepts in Bioinorganic Materials Chemistry,* Oxford Univ. Press, **2001**.
4. Round, F.; Crawford, R.; Mann, D. *The Diatoms. Biology and Morphology of the Genera*, Cambridge Univ. Press, **1990**.
5. Sumper, M.; Brunner, E. *Adv. Func. Mater.*, **2006**, *16*, 17.
6. Lide, D. *CRC Handbook of chemistry and physics 77th Edition*, CRC press, **1996**, 4-130-4-136.
7. Kojima, K.; Tsuchiya, K.; Wada, N. *J. Sol-Gel Sci. Tech*., **2000**, *19*, 511.
8. Layne, C.; Lowdermilk, W.; Weber, M. *Phys. Rev.*, **1977**, *B16*, 10.
9. Honkanen, S.; Jiang, S. *Rare-Earth Doped Devices II*, International Society for Optical Engineering, Washington, DC, **1998**.
10. Brusatin, G.; Guglielmi, M.; Marucci, A. *J. Am. Ceram. Soc.*, **1997**, *80*, 3139.
11. Robinson, M.; Brown, L.; Hall, B. *J. Coat. Tech.,* **1986**, *58*, 57.
12. Simpson, T.; Garrone, R.; Mazzorana, M, *J. Ultrastruct. Res.,* **1983**, *85*, 159.

13. Shimizu, K.; Cha, J.; Stucky, G.; Morse, D. *Proc. Nat'l. Acad. Sci., USA* **1998**, *95*, 6234.

14. Cha, J.; Shimizu, K.; Zhou, Y.; Christiansen, S.; Chmelka, B.; Stucky, G.; Morse, D. *Proc. Nat'l. Acad. Sci., USA*, **1999**, *96*, 361.

15. Sumper, M.; Kröger, N. *J. Mater. Chem.*, **2004**, *14*, 2059.

16. Iler, R. *The Chemistry of Silica*, Wiley, New York, **1979**.

17. Whaley, S.; English, D.; Hu, E.; Barbara, P.; Belcher, A. *Nature*, 2000, *405*, 665.

18. Naik, R.; Stringer, S.; Agarwal, G.; Jones, S.; Stone, M. *Nat. Mater.*, 2002, *1*, 169.

19. Brown, S.; Sarikaya, M.; Johson, E. *J. Mol. Biol.,* 2000, *299*, 725.

20. Naik, R.; Brott, L.; Clarson, S.; Stone, M. *J. Nanosci. Nanotech.*, 2002, *2*, 95.

21. Ahmad, G.; Dickerson, M. B.; Church, B. C.; Cai, Y.; Jones, S. E.; Naik, R. R.; King, J. S.; Summers, C. J.; Kroger, N., Sandhage, K. H. *Adv. Mater.*, **2006**, *18*, 1759.

22. Naik, R.; Jones, S.; Murray, C.; McAuliffe, J.; Vaia, R.; Stone, M. *Adv. Func. Mater.* **2004**, *14*, 25.

23. Reiss, B.; Mao, C.; Solis, D.; Ryan, K.; Thomson, T.; Belcher, A. *Nanoletters,* **2004**, *4*,1127.

24. Instructional and informational materials version 2.7 accompanying *Ph.D. 12 Phage Display Peptide Library Kit*, New England BioLabs, Inc., Ipswich, MA, **2006**.

25. Bäuerlein, E., *Biomineralization: Progress in Biology, Molecular Biology, and Application;* Wiley-VCH, Weinheim, **2004**.

26. Patwardhan, S.; Clarson, S. *Polymer*, **2005**, *46*, 4474.

27. Belton, D.; Paine, G.; Patwordhan, S.; Perry, C. *J. Mater. Chem.*, **2004**, *14*, 2231.

28. Sudheendra, L.; Raju, A. *Mater. Res. Bull.*, **2002,** *37*, 151.

29. Coradin, T.; Durupthy, O.; Livage**,** J.; *Langnuir*, **2002**, *18*, 2331.

30. Kröger, N; Dickerson, M.; Ahmad, G.; Cai, Y.; Haluska, M.; Sandhage, K.; Poulsen, N.; Sheppard, V. *Angew. Chem. Int. Ed*. **2006**, *45*, 7239.

31. Kitiyanan, A; Kato, T; Suzuki, Y; Yoshikawa, S. *J. Photochem. Photobiol., A: Chem.,* **2006**, *179*, 130.

32. Bellman, R.; Bourdon, G.; Alibert, G.; Beguin, A.; Guiot, E.; Simpson, L.; Lehuede, P.; Guiziou, L.; LeGuen, E. *J. Electrochem. Soc.*, **2004**, *151*, G541.

33. Regan, M.; Banerjee, I. *Scripta Mater.*, **2006**, *54*, 909.

CHAPTER 3: THE IDENTIFICATION AND DESIGN OF PEPTIDES FOR THE SYNTHESIS OF NANOPARTICULATE TITANIA FROM AQUEOUS SOLUTIONS AT ROOM TEMPERATURE

The research in this chapter is distinct from, though represents a summary of the study presented for publication in:

Dickerson, M. B.; Jones, S. E.; Cai, Y.; Ahmad, G.; Naik, R. R.; Kröger, N.; Sandhage, K. H. *Chem. Mater.,* **2007,** (submitted).

3.1 Introduction

The biomimetic or biomolecule-enabled formation of inorganic materials is a field of growing prominence in materials science[1-6]. This work has been inspired by the ability of certain organisms to produce minerals under physiological conditions (biomineralization) through the use of specific biomolecules[1,2]. Examples of such biomolecules include proteins such as silicateins and silaffins, isolated from the SiO_2 (silica) structures generated by sponges and diatoms, respectively[7-14]. These proteins have also been utilized to induce the *in vitro* formation of silica, and of non-biological inorganic materials, from precursor solutions at room temperature[8,10-19]. Examples of the latter include the formation of TiO_2, Ga_2O_3, ZrO_2, and $BaTiOF_4$ with the aid of native and recombinant silicateins, and the formation of fully-crystallized rutile TiO_2 with the aid of a recombinant silaffin[15-19]. In several recent studies, the formation of titania from precursor solutions exposed to lysozyme (a bactericidal enzyme), peptide R5 (a synthetic analog of silaffin natSil1), poly-l-lysine (PLL), poly-allylamine (PAA), spermidine, and spermine has been reported[20-24]. Such room temperature biomolecule-enabled and biomimetic syntheses can be attractive alternatives to higher temperature processes for

forming titania for use in a variety of existing or emerging applications (e.g., for (photo)catalysis, chemical sensing, cosmetics, photovoltaics, energy storage and photonics)[25-31].

While these recent observations demonstrate that proteins and biomolecule analogs can be used to induce the formation of titania under mild conditions, the influence of protein primary structure on the titania morphology or yield at room temperature is not well understood. Through the selective binding of a phage-displayed 12-mer peptide library to TiO_2 crystals, we have identified 20 peptides with an affinity for titania. The titania precipitation activities of these peptides upon exposure to a water stable Ti(IV) complex have been quantified through the use of spectrophotometric analyses. Correlations obtained between the peptide primary structure and the titania precipitation activity have been used to design a peptide that exhibits an enhanced titania yield with a reduced pH dependence for such titania precipitation.

3.2 Experimental Procedure

3.2.1 Peptide Library Screening ("Biopanning")

TiO_2-binding peptides were identified using the Ph.D.-12™ phage display library (New England Biolabs; Beverly, MA) by MBD. The target binding, elution, and phage amplification steps were conducted according to the manufacturer's instructions[32]. Rutile TiO_2 single crystals of (100), (110), or (001) orientation (10 × 10 × 0.5 mm, double side polished, MTI Corporation, Richmond, CA) were used as targets. A given crystal was washed three times with a 150 mM NaCl solution containing 50 mM tris-(hydroxymethyl)-aminomethane buffer and 0.2% Tween-20 detergent (referred to herein as 0.2% TBST). The phage library was then incubated with the TiO_2 crystal for one hour

in a 0.2% TBST solution with rotation at 30 rpm. The TiO_2 substrate was then washed repeatedly with 0.2% TBST to remove any non-bound phage particles, after which the bound phages were eluted by incubation for 10 minutes with a solution containing 0.2 M glycine-HCl pH 2.2. The supernatant was removed from the TiO_2 target by centrifugation and then neutralized with 1M Tris-HCl pH 9.1. The eluted phages were amplified through infection of *Escherichia coli* strain ER2738 grown in Luria Broth (LB). The phage population was further enriched for titania binding clones by four subsequent attachment/elution ("biopanning") cycles utilizing 0.2% TBST. The fifth round of biopanning was conducted with 0.5% TBST. To select for high-affinity TiO_2 binding clones, additional biopanning rounds were conducted using more stringent washing conditions (i.e., with 0.5 or 0.8% TBST solutions). All other aspects of the biopanning procedure remained unchanged for these additional rounds. After the final biopanning round, *E. coli* ER2738 cells were infected with the eluted phages and plated on LB plates containing 5-bromo-4-chloro-3-indolyl-β-D-glactoside (X-gal, Invitrogen, Carlsbad, Ca) and isopropyl β-D-thioglactoside (IPTG, Invitrogen, Carlsbad, Ca). DNA was isolated from 225 independent blue plaques and sequenced using an 3100 Avant (Applied Biosystems, Ca) automated sequencer by Sharon E. Jones (Air Force Research Laboratory).

3.2.2 Titania Precipitation

The peptides used in this study were purchased from EZBiolab, Inc. (Westfield, IN), and received as desalted grade. All peptides contained the C-terminal tetrapeptide Gly-Gly-Gly-Trp in order to enable quantification by spectrophotometry at 280 nm. Peptide stock solutions were prepared with 0.2 μm filtered 18.2 MΩ H_2O (Nano-Pure

Diamond Ultrapure Water System, Barnstead International, Dubuque, IA). Select peptides possessing high titania precipitation activities were chemically synthesized and purified to >70% by EZBiolab, Inc. (Westfield, IN). These peptides were further purified by gel-filtration chromatography utilizing a Superdex Peptide 10/300 GL column (GE Healthcare, Piscataway, NJ) and a Dionex FPLC system (Sunnyvale, CA) with the assistance of Dr. Nicole Poulsen and Ms. Vonda C. Sheppard (Georgia Institute of Technology). In a typical precipitation experiment, 50-250 μl of 110 mM Titanium-bis-ammonium-lactato-dihydroxide (TiBALDH) (Alfa Aesar, Ward Hill, Ma) were added to an equal volume of a 200 mM phosphate-citrate buffer solution that contained the peptide at a concentration of 2 mg/ml. This solution was mixed by vortexing and incubated for 10 min. The precipitates were recovered by centrifugation at 13,200 rpm, washed five times with 1 ml H_2O, and once with 1 ml methanol (Fisher Scientific, Waltham, MA). The precipitates were then dried for 30 min in a vacuum centrifuge (Eppendorf North America, Inc., Westbury, NY) at 30°C. Where indicated, the phosphate-citrate buffer was replaced with an equal concentration of 4-morpholino-ethanesulfonic acid (MES), N-(2-Acetamido)iminodiacetic acid (ADA) or bis(2-hydroxyethyl)amino-tris(hydroxyl methyl)methane (Bis-Tris) obtained from Amresco, Inc. (Solon, OH), or with sodium citrate or sodium phosphate buffers (Sigma-Aldrich, St. Louis, MO).

3.2.3 Colorimetric Assay for Titanium Dioxide

Quantitative evaluation of the amount of titania precipitated by the peptides tested in this study was conducted with a colorimetric assay[33]. At least three precipitation reactions were conducted and measured for each data point, error bars represent one standard deviation. Briefly, the precipitates were dissolved in a solution of concentrated

sulfuric acid and ammonium sulfate at 90°C for 1 hour. A portion of the dissolved precipitate was combined with an ethanolic solution of $NaClO_4$ (Sigma, Milwaukee, WI) and 5-chlorosalicylic acid (Fluka, Seelze, Germany). Ammonium hydroxide was used to adjust the solution pH to 3, and the absorbance was measured at 355 nm utilizing a Thermo Scientific GENESYS UV/Vis spectrometer (Waltham, MA).

3.2.4 Materials Characterization

Scanning electron microscopy was conducted with a field emission gun microscope (Leo 1530 FEG SEM, Carl Zeiss SMT Ltd., Cambridge, UK) equipped with an energy dispersive x-ray spectrometer (INCA EDS, Oxford Instruments, Bucks, UK). Transmission electron microscopy was conducted by Dr. Ye Cai (Georgia Institute of Technology) with a JEOL 4000 EX instrument. X-ray diffraction analyses were conducted with Cu Kα radiation at a scan rate of 0.003°/min using a X-Pert ProAlpha 1 diffractometer equipped with an incident beam Johannsen monochromator, 1/28 divergence slits, 0.048 soller slits, and an Xcelerator linear detector (PANalytical, Almelo, The Netherlands). Quantitative evaluation of the amount of pyrolyzable material contained in the titania precipitates was obtained by thermogravimetric analysis (Netzsch 449C Simultaneous Thermal Analyzer, Selb, Germany) at a heating rate of 5°C/min to 600°C in air. Thermogravimetric analysis was conducted with the assistance of Dr. Yunshu Zhang (Georgia Institute of Technology).

3.3 Results and Discussion

3.3.1 Phage-Displayed Peptide Library Screening

To identify TiO_2-binding peptides, a commercially available combinatorial phage-displayed peptide library (M13 phage) was screened against rutile TiO_2 single crystal

substrates of (100), (110), and (001) orientation. The surface of each phage displayed five copies of the minor coat protein pIII fused to a 12-mer peptide characteristic for the clone. The library contained approximately 3×10^9 different phage clones representing the same number of different 12-mer peptides[32]. Four rounds of screening were conducted (i.e., with each round comprised of phage binding, removal of phages with low affinity by washing, and elution of bound phages via a brief decrease in pH) utilizing a 0.2% TBST wash solution for removal of non-specifically-bound phage, followed by a final round using a more stringent 0.5% TBST wash solution. DNA from 55 phage clones selected after the final round of biopanning against the three distinct TiO_2 substrates were isolated and sequenced by Sharon E. Jones (Air Force Research Laboratory), which led to the identification of 53 unique 12-mer peptide sequences (see Appendix I). A summary of the peptide characteristics identified from the (001)-oriented TiO_2 substrate is provided in Table 3.1. The peptides identified from the initial screening possessed calculated isoelectric points (pI) ranging from strongly acidic (3.1) to highly basic (12.0), with a modest average enrichment of lysine (K) and arginine (R) residues relative to the starting phage-displayed library. Additional rounds of biopanning were then conducted using washing conditions of higher stringency. In one set of experiments (modified biopanning method 1), three additional rounds of screening were conducted with a 0.5% TBST wash solution (for a total of 8 rounds of biopanning). In another set of experiments (modified biopanning method 2), two additional rounds (7 rounds total) were conducted using a 0.8% TBST wash solution. The results of such modified screening against the (001)-oriented TiO_2 crystal are summarized in Table 3.1, with sequence details provided in Tables 3.2 and 3.3. Through successive rounds of selection with the more stringent washes in modified biopanning method 1, the number of unique

peptides detected decreased from 19 down to 2, while the average isoelectric points increased significantly (from 8.3 to 11.3) due to the enrichment of the basic amino acid residues, K and/or R (Tables 3.1, 3.2). A distinct enrichment in the histidine (H) content was also noted. Similar trends were observed with modified biopanning method 2, which resulted in a final population of 3 unique sequences with an average pI of 10.0 (Table 1). The increase in K, R, and H residues in the peptides identified with the modified biopanning methods occurred largely at the expense of hydrophobic residues, which decreased from the population average of 50% after the initial (less stringent) five rounds

Table 3.1: Summary of the properties and amino acid residue compositions of the peptides identified through additional high stringency biopanning rounds (modified biopanning methods 1 and 2) using a Ph.D.-12 peptide library and a single crystal (001)-oriented rutile TiO_2 target. Starting library peptide sequence enrichment information is as reported by the manufacturer[33].

	No. of unique sequences identified	Average pI	Average number of H/peptide	Average number of (K+R)/peptide	Average number of (D+E)/peptide	Average number of (S+T+Y)/ peptide
Starting Library	-	-	0.8	0.9	0.7	3.0
Initial Screening	19	8.3	0.4	1.2	0.7	2.6
First additional 0.5% TBST round*	6	8.6	1.7	1.0	0.5	2.7
Second additional 0.5% TBST round*	5	9.6	1.8	1.6	0.6	3.4
Third additional 0.5% TBST round*	2	11.3	2.5	2.0	0.5	3.5
First additional 0.8% TBST round**	10	8.3	1.1	0.8	0.5	3.0
Second additional 0.8% TBST round**	3	10.0	2.3	1.7	0.3	3.7

*Modified biopanning method 1. **Modified biopanning method 2.

Table 3.2: Peptides identified through the additional rounds of modified biopanning method 1 (using a relatively stringent 0.5% Tween-20 wash solution).

Additional Round 1

Peptide Sequence	Frequency	pI	(D+E)	H	(K+R)	(S+T+Y)
T T A A V D M P R S T P	3/16	6.8	1	0	1	3
H E S F W Y L P H Q S Y	1/16	6.0	0	2	0	4
L L A D T T H H R P W T	8/16	8.0	1	2	1	3
Q S N Y P R A S Y V F Q	1/16	9.7	0	0	1	4
K S L S R H D H I H H H	2/16	10.1	1	5	2	2
M P W A H R A P Q G I A	1/16	11.0	0	1	1	0
Averages		8.6	0.5	1.7	1.0	2.7

Additional Round 2

Peptide Sequence	Frequency	pI	(D+E)	H	(K+R)	(S+T+Y)
L L A D T T H H R P W T	2/17	8.0	1	2	1	3
S H A F T A S P R Y L H	4/17	9.8	0	2	1	4
K S L S R H D H I H H H	6/17	10.1	1	5	2	2
Y A K S P P T P Y Y T P	4/17	9.6	0	0	1	6
L A P K P F E P R Y T R	1/17	10.3	1	0	3	2
Averages		9.6	0.6	1.8	1.6	3.4

Additional Round 3

Peptide Sequence	Frequency	pI	(D+E)	H	(K+R)	(S+T+Y)
K S L S R H D H I H H H	17/20	10.1	1	5	2	2
S R P S R Q P S A S P T	3/20	12.4	0	0	2	5
Averages		11.3	0.5	2.5	2.0	3.5

Table 3.3. Peptides identified through the additional rounds of modified biopanning method 2 (using a relatively stringent 0.8% Tween-20 wash solution).

Additional Round 1

Peptide Sequence	Frequency	pI	(D+E)	H	(K+R)	(S+T+Y)
D P I Y A L S W S G M A	1/19	3.1	1	0	0	3
T M A T Y V N Q S L T G	1/19	6.0	0	0	0	5
S V S L P Y A N L A T H	1/19	7.8	0	1	0	4
S L Y N T A A S H V P T	1/19	7.8	0	1	0	5
D L N T N R T G M V L H	2/19	7.8	1	1	1	2
N Y L H N H P Y G T V G	1/19	8.0	0	2	0	3
L T P T S R P T P Y P A	1/19	9.8	0	0	1	5
K S L S R H D H I H H H	9/19	10.1	1	5	2	2
N F R P V T A M P R L D	1/19	10.9	1	0	2	1
N I N A N A A Q I K R H	1/19	11.5	0	1	2	0
Averages		8.3	0.5	1.1	0.8	3.5

Additional Round 2

Peptide Sequence	Frequency	pI	(D+E)	H	(K+R)	(S+T+Y)
T Q H L S H P R Y A T K	9/22	10.3	0	2	2	3
Y A K S P P T P Y Y T P	8/22	9.6	0	0	1	6
K S L S R H D H I H H H	5/22	10.1	1	5	2	2
Averages		10.0	0.3	2.3	1.7	3.7

of biopanning to an average of 29.2% for the final pool of unique sequences isolated through the higher-stringency modified screening procedures. The enrichment of K, R, and H residues was also observed in peptides identified via the increased stringency biopanning methods conducted with the (110)- and (100)-oriented TiO_2 crystal substrates (see Table 3.4). These screening results are consistent with the recent report of Chen, et al., who identified two anatase TiO_2-binding heptapeptides enriched in basic amino acid residues via screening with a phage-displayed constrained-heptapeptide library[34].

Table 3.4: The characteristics and sequences of peptides identified during high stringency biopanning (methods 1 and 2) against rutile crystal substrates. The amino acid residues histidine (H), arginine (R) and lysine (K) proposed to be associated with TiO_2 binding and precipitation activities are indicated in bold. pI = isoelectric point. H = number of histidine residues. K+R = combined number of lysine and arginine residues, respectively. D + E = combined number of aspartic and glutamic acid residues, respectively. Plus and minus signs indicate that the peptide was or was not identified via biopanning against a particular rutile crystal substrate, respectively. Asterisk (*) values correspond to averages.

Peptide Name	(001) TiO_2 Target	(100) TiO_2 Target	(110) TiO_2 Target	Sequence	pI	H	K+R	D+E	S+T+Y
Ti-1	-	-	+	**R K K R** T **K** N P T **H K** L	12.4	1	6	0	2
Ti-2	+	+	+	T Q **H** L S **H** P **R** Y A T **K**	10.0	2	2	0	3
Ti-3	+	-	+	**K** S L S **R H** D **H** I **H H H**	10.1	5	2	1	2
Ti-4	-	+	-	M **R** M I **R R** F P S S L **K**	12.3	0	4	0	2
Ti-5	+	-	-	S **R** P S **R** Q P S A S P T	12.0	0	2	0	5
Ti-6	-	+	-	L **K** M N P S I S S S L **K**	10.5	0	2	0	4
Ti-7	-	+	-	F A V N P S **K** P A Y F **K**	10.1	0	2	0	2
Ti-8	-	-	+	A S I E E L **R** V P **R** Q A	7.1	0	2	2	1
Ti-9	-	-	+	N **H H H** Q P L A **R** N Q S	11.0	3	1	0	1
Ti-10	-	+	-	F T T S N **H** T S **R H** G S	11.0	2	1	0	6
Ti-11	+	-	-	L L A D T T **H H R** P W T	9.6	2	1	1	6
Ti-12	-	-	+	L L P Q N G S T P **R H** S	11.0	1	1	0	3
Ti-13	-	+	-	Y P M L P Q N **K H** A Q F	10.5	1	1	0	1
Ti-14	-	-	+	S F S A I T **K** N V **H** W M	10.1	1	1	0	4
Ti-15	-	+	-	Q N L I N W P P P **R** F S	11.0	0	1	0	1
Ti-16	-	-	+	T F S N P L Y M W P **R** P	9.8	0	1	0	3
Ti-17	-	+	-	N V T T M T N **H** L V Y S	7.8	1	0	0	5
Ti-18	-	-	+	S P G L S L V S **H** M Q T	7.8	1	0	0	4
Ti-19	-	-	+	S A **H** G T S T G V P W P	7.8	1	0	0	4
Ti-20	-	+	-	L A T P F T A T S A T G	6.0	0	0	0	5
					9.9*	1.1*	1.5*	0.2*	3.2*

Of the total of 20 unique 12-mer peptides (sequences provided in Table 3.4) identified through the higher stringency biopanning methods, one peptide sequence (Ti-4) was identified after screening against all three TiO_2 single crystal substrates (Figure 3.1). This peptide appears to have a high affinity for several inorganic and organic surfaces, as it has also been identified through the Ph.D.-12 library screening of FePt and GaN, as well as several acrylate-based polymers[35,36]. Peptide Ti-3 was also repeatedly identified during high stringency biopanning against both the (001)- and (110)-oriented TiO_2 crystal substrates. The remaining 18 peptides were identified via the higher stringency biopanning against one of the three different TiO_2 substrates (Figure 3.1).

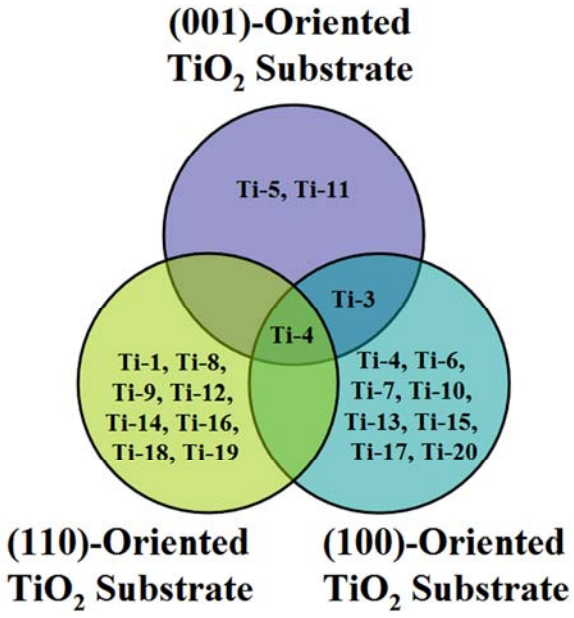

Figure 3.1: Venn diagram indicating the unique and common peptide sequences identified from the higher stringency (i.e., with 0.5% or 0.8% TBST wash solutions) panning experiment against three TiO_2 crystal substrates.

3.3.2 Peptide-induced Titania Formation

A select number of peptides (eleven) with a range of pI values was chosen to evaluate their capabilities of inducing the formation of TiO_2 from an aqueous solution of titanium(IV) bis-ammonium-lactato-dihydroxide (TiBALDH). The peptides were added to the TiBALDH solution buffered to pH 6.3 by a sodium phosphate/citrate buffer, and incubated for 10 min at room temperature. The precipitates were then collected by centrifugation and washed repeatedly with H_2O. The amount of titanium present in the precipitates was quantified by a colorimetric assay[33]. Four of the eleven assayed peptides, Ti-1, Ti-2, Ti-3, and Ti-4, displayed relatively high titania precipitation activities (0.36-1.66 mg TiO_2 per mg of peptide; see Table 3.5 and Figure 3.2). The titania precipitation activities of the peptides increased with the number of calculated

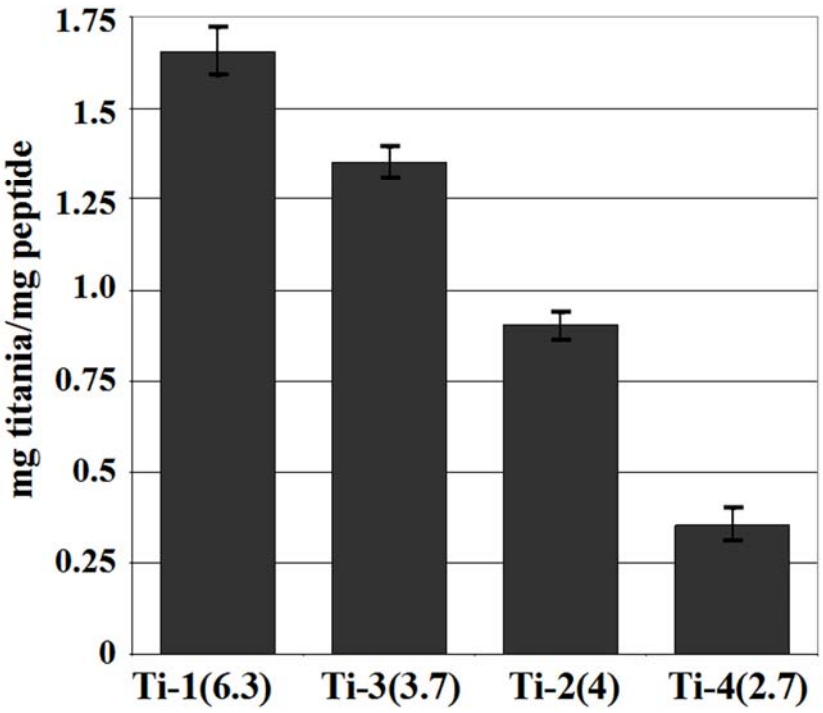

Figure 3.2: Quantification of the titania precipitation activities of several purified peptides identified via phage-display biopanning. The number of positive charges carried by the amino acid side groups are shown in brackets (values calculated at the pH 6.3 condition of the assay).

positive charges carried by the peptides at the assay pH of 6.3. The precipitation yield of peptide Ti-1 (with 6.3 side group positive charges) exceeded the yields of peptides Ti-2 and Ti-3 (with 4 and 3.7 side group positive charges, respectively) that, in turn, exceeded the yield of peptide Ti-4 (with 2.7 side group positive charges). Thus, it appears that both the binding of peptides to TiO_2 surfaces, and the induction of TiO_2 formation from aqueous TiBALDH solutions, were promoted by the presence of multiple positive charges within the peptide. These results are in accordance with previous observations that strongly polycationic molecules (natural and synthetic polyamines, highly basic recombinant silaffins rSilC and rSil1L) are capable of precipitating titania from aqueous Ti(IV)-complexes under near neutral conditions[17,19-24].

Table 3.5: Titania precipitation activities of peptides identified via biopanning and of designed peptides. The number of positive charges carried by residue side groups was calculated at pH 6.3 (the standard precipitation condition). Chromatographically-purified and as-desalted grade peptides were utilized to generate the activities reported in this table (differences in titania precipitation activity of the same peptide reflect this purity difference). pI = isoelectric point. H = number of histidine residues. K+R = combined number of lysine and arginine residues.

Peptide (purified)	Sequence	pI	H	K+R	#of Positive Charges	mg titania/ mg peptide
dTi-1(RKK)	**R K K R K K R K K R K K G** G G W	12.8	0	12	12	1.84 ± 0.08
Ti-1	**R K K R** T **K** N P T **H K** L G G G W	12.4	1	6	6.3	1.66 ± 0.07
dTi-1(H/R)	**R K K R** T **K** N P T **R K** L G G G W	12.6	0	7	7	1.48 ± 0.03
Ti-3	**K** S L S **R H** D **H** I **H H H** G G G W	10.1	5	2	3.7	1.35 ± 0.05
Ti-2	M **R** M I **R R** F P S S L **K** G G G W	12.3	0	4	4	0.90 ± 0.04
Ti-4	T Q **H** L S **H** P **R** Y A T **K** G G G W	10.0	2	2	2.7	0.36 ± 0.05
Peptide (as desalted)	Sequence	pI	H	K+R	# of Positive Charges	mg titania/ mg peptide
Ti-1	**R K K R** T **K** N P T **H K** L G G G W	12.4	1	6	6.3	1.80 ± 0.12
Ti-3	**K** S L S **R H** D **H** I **H H H** G G G W	10.1	5	2	3.7	1.04 ± 0.04
Ti-2	M **R** M I **R R** F P S S L **K** G G G W	12.3	0	4	4	0.85 ± 0.09
Ti-4	T Q **H** L S **H** P **R** Y A T **K** G G G W	10.0	2	2	2.7	0.26 ± 0.01
Ti-9	N **H H H** Q P L A **R** N Q S G G G W	11.0	3	1	2	0.11 ± 0.01
Ti-8	A S I E E L **R** V P **R** Q A G G G W	7.1	0	2	2	0.03 ± 0.00
Ti-6	L **K** M N P S I S S S L **K** G G G W	10.5	0	2	2	0.02 ± 0.00
Ti-20	L A T P F T A T S A T G G G G W	6.0	0	0	0	0.02 ± 0.00
Ti-5	S **R** P S **R** Q P S A S P T G G G W	12.0	0	2	2	0.01 ± 0.00
Ti-11	L L A D T T **H H R** P W T G G G W	9.6	2	1	1.7	0.00 ± 0.00
Ti-18	S P G L S L V S **H** M Q T G G G W	7.8	1	0	0.3	0.00 ± 0.00

The peptide-titania precipitation analyses were then used to design peptides with enhanced titania precipitation activity. Based on the sequence of the peptide with the highest titania precipitation activity, Ti-1, two modified peptides were designed: dTi-1(H/R) and dTi-1(RKK) (see Table 3.5). For the designed peptide dTi-1(H/R), the single histidine residue of peptide Ti-1 was replaced by an arginine residue. This modification was expected to decrease the pH dependence of the titania precipitation activity in the range $4 < pH \leq 8$, since the arginine side chain should remain positively charged over this range, whereas the positive charge of the histidine side chain should become more and more reduced with increasing pH values (i.e., above the histidine side group pKa = 6).

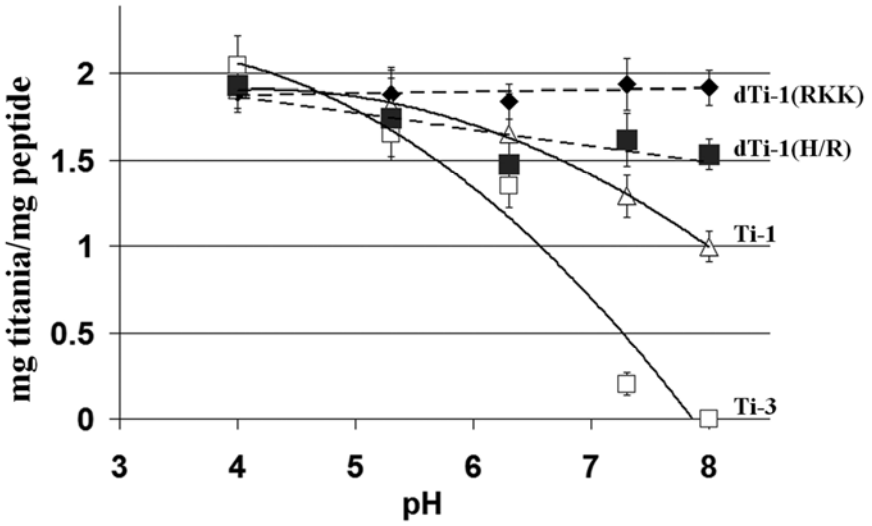

Figure 3.3: Precipitation activities of peptides with varying pH. The titania precipitation activities of peptides possessing histidine residues (solid lines) are more affected (reduced) by increasing pH than those lacking such residues (dashed lines). The precipitation activities of peptides Ti-1 and Ti-3 are marked with open triangles and squares, respectively, and are indicated with solid lines. The precipitation activities of peptides dTi-1(H/R), and dTi-1(RKK) are marked with filled squares and diamonds, respectively, and are indicated with dashed lines.

Indeed, as shown in Figure 3.3, the titania formation activity of Ti-1 was substantially lower at pH 8 than at pH 4. Figure 3.3 also reveals that, by replacing the histidine with arginine in the dTi-1(H/R) peptide, the pH dependence of the precipitation activity was reduced in the pH range 7–8 (Figure 3.3). The influence of histidine residues on the pH dependence of titania precipitation activity was further confirmed by the observation that the histidine-rich peptide Ti-3, which generated the highest titania yield at pH 4, failed to induce the formation of any titania at pH 8 (Figure 3.3). The second designed peptide, dTi-1(RKK), contained a tetrameric repeat of the first three amino acid residues (RKK) of peptide Ti-1 (Table 3.5). As a result, dTi-1(RKK) possessed the highest number of positive charges of all peptides tested in this study. Consistent with the observed correlation between titania yield and positive peptide charges, the dTi-1(RKK) peptide

generated the highest (biomolecule induced) titania yield observed to date at neutral pH (1.84 mg TiO_2/mg peptide, Table 3.5). Furthermore, because the number of positive charges carried by this designed peptide remained unchanged from pH 4-8, the titania formation activity was virtually pH independent over this range (Figure 3.3).

3.3.3 Characterization of the Peptide-Induced Titania

The structures of the precipitates generated by the peptides Ti-1, Ti-2, Ti-3, Ti-4, dTi-1(H/R), and dTi-1(RKK) were evaluated by scanning electron microscopy (Figure 3.4). Secondary electron micrographs revealed that the precipitation products generated by peptides Ti-1, Ti-2, Ti-3, and dTi-1(RKK) consisted of particles approximately 50-100 nm in diameter that were necked together to form a nanoparticulate network (such as shown in Figure 3.4A). The Ti-4 and dTi-1(H/R) also induced the formation of nanoparticulate networks, but the apparent particles possessed larger diameters (Figure 3.4B, C). Energy dispersive x-ray spectroscopy (EDXS) indicated that the peptide-induced precipitates contained titanium, oxygen, and phosphorous (see Figure 3.4D, E). The presence of phosphorous indicated the incorporation of phosphate ions from the buffer solution in the precipitate. The presence of sulfur in the Ti-2 induced precipitate was due to incorporation of the peptide, which contained two residues of the sulfur-bearing amino acid, methionine. This was consistent with TGA analysis, which detected the presence of 48.1% pyrolyzable material in the Ti-2-induced titania. Similar amounts of pyrolyzable material (45.8$\pm$2.5%) were present in the precipitates formed in the presence of the Ti-1, Ti-3, and Ti-4 peptides.

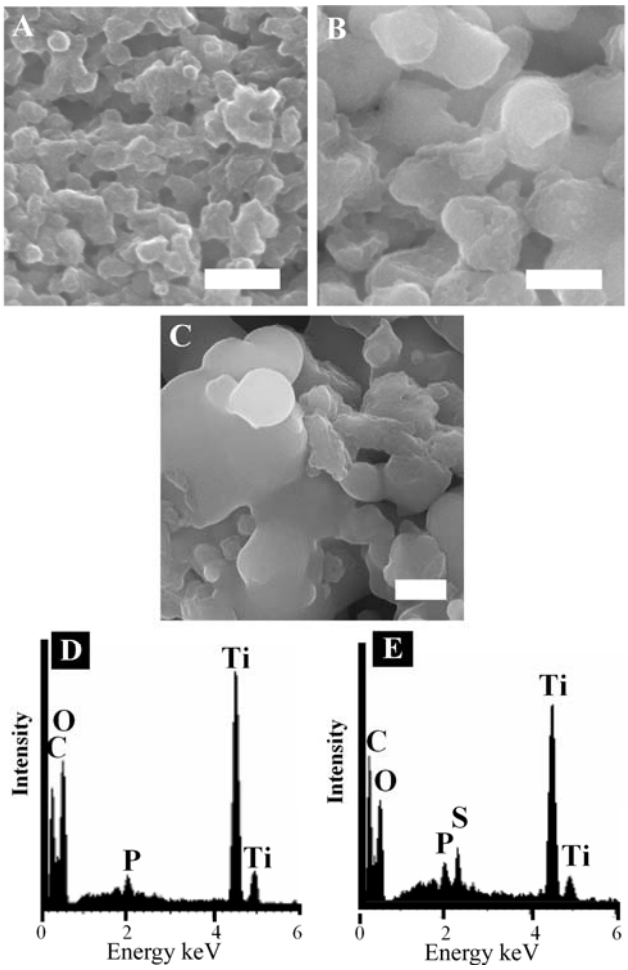

Figure 3.4: Morphologies of the nanoparticulate titania induced by peptides at room temperature from an aqueous TiBALDH solution at pH 6.3. Secondary electron images of the TiO_2 precipitate generated in the presence of: A) Ti-1 peptide (similar to Ti-2, Ti-3, dTi-1(RKK) precipitates), B) Ti-4 peptide, and C) dTi-1(H/R) peptide. Elemental analysis by EDXS of the TiO_2 precipitate formed in the presence of the: D) Ti-1 peptide and E) Ti-2 peptide. Scale bars: A), B) 200 nm; C) 400 nm.

High-resolution transmission electron microscope (TEM) analyses revealed that the peptide-induced titania precipitates consisted of a mixture of fine nanocrystals along with an amorphous phase (Figure 3.5). A mixture of anatase and amorphous oxide was also reported by Sumerel, et al., in their investigation of TiO_2 formed under the influence of silicateins[17]. In that work, the anatase crystals formed at interfaces between

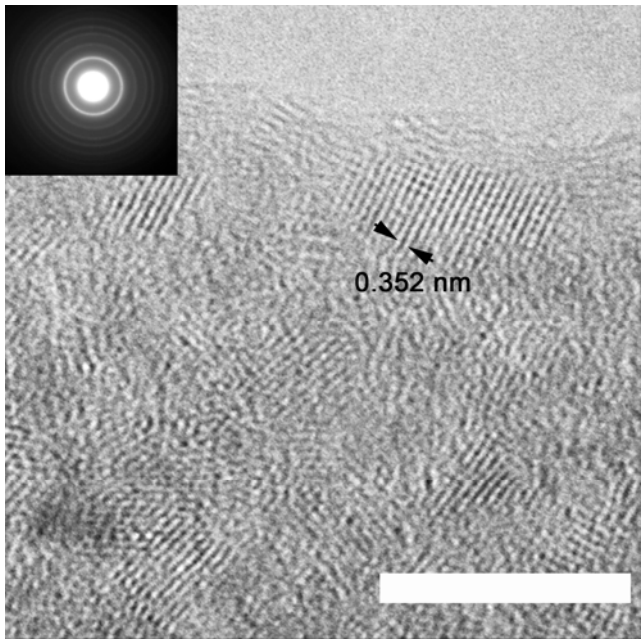

Figure 3.5: High resolution transmission electron image and electron diffraction pattern (as an inset) of the titania precipitate induced to form from the TiBALDH precursor solution at pH 6.3 in the presence of the dTi-1(H/R) peptide. The lattice fringe spacing indicated by arrows was consistent with the (101) plane spacing of anatase and the (110) plane spacing of monoclinic β-TiO_2. Similar results were obtained with the titania induced by the other peptides. The scale bar corresponds to 10 nm. HRTEM image taken by Ye Cai (Georgia Institute of Technology).

amorphous titania and protein filaments[17]. High resolution TEM images, such as Figure 3.5, indicated that the crystalline and amorphous phases formed in the present work were distributed throughout the titania nanoparticles.

The crystallinity of the peptide-induced precipitates was also evaluated by x-ray and electron diffraction analyses, which indicated that the room-temperature synthesized titania contained both anatase and monoclinic β-TiO_2 crystals. Indexing of several electron diffraction patterns yielded d spacings of 3.5, 2.1, 1.73 and 1.22 Å, which were consistent with the d spacings associated with the (101) plane of anatase and the (110) plane of β-TiO_2, the ($\bar{6}$01) plane of β-TiO_2, the (105) plane of anatase, and the (910)

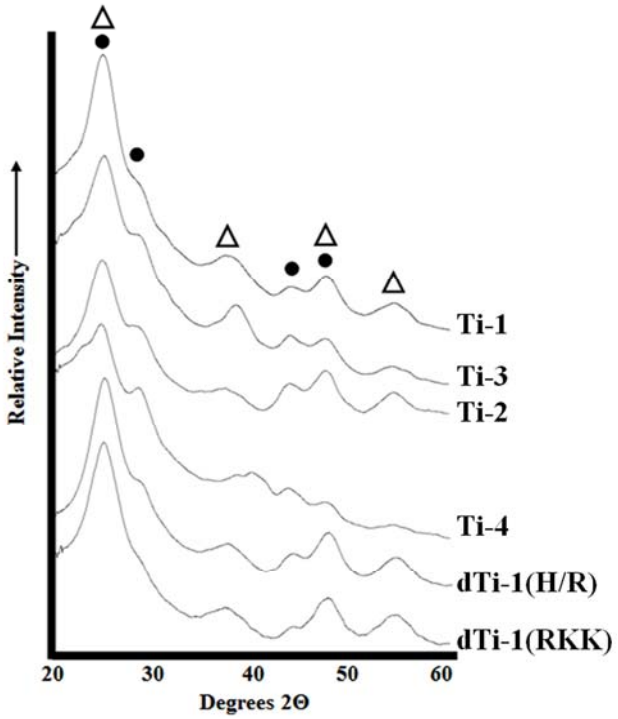

Figure 3.6: X-ray diffraction analyses of the TiO_2 precipitates generated under the influence of the Ti-1, Ti-3, Ti-2, Ti-4, dTi-1(H/R), and dTi-1(RKK) peptides. Filled circles and open triangles represent diffraction peaks attributable to the monoclinic (β-TiO_2) and anatase polymorphs of TiO_2, respectively.

plane β-TiO_2, respectively. The x-ray diffraction peaks (Figure 3.6) and electron diffraction rings (Figure 3.5 inset) were quite broad, which indicated that the titania crystallites were very small. Indeed, Scheerer analysis of the x-ray diffraction patterns yielded an average (global) anatase crystallite size on the order of 2 nm, which was consistent with the crystallites observed via (localized) high magnification TEM (Figure 3.5). The collected x-ray diffraction patterns also exhibited relatively high background intensities at low 2θ values, which was consistent with the presence of an amorphous phase within the precipitates.

The titania-forming peptides identified through extensive biopanning against three different rutile TiO_2 single crystals yielded precipitates containing nanocrystals of

only the anatase and monoclinic (β) polymorphs of titania. While nanocrystalline mixtures of anatase and monoclinic titania can exhibit attractive photocatalytic properties[41,42], the inability of any of the titania-forming peptides to induce rutile titania formation was striking. Recent work has shown that a recombinant silaffin possessing a highly repetitive arrangement of arginine and lysine residues can induce the formation of rutile TiO_2 from an aqueous TiBALDH solution under ambient conditions and neutral pH[20]. Those results coupled with the present work suggest that 12-mer titania-forming peptides may lack the molecular complexity (e.g., three-dimensional structure) required for rutile TiO_2 formation under ambient conditions.

3.3.4 Influence of Reaction Conditions

In several recent studies, solution conditions (i.e., pH, buffer chemistry, buffer and salt concentrations) have been found to influence both the ability of biomolecules to induce precipitation and the morphology of the resulting precipitates[10, 11, 21, 24, 37-39]. In order to assess the possible influence of these factors on the peptide-mediated formation of titania, precipitation trials were conducted utilizing pH 3-8 phosphate-citrate buffers (i.e., constant chemistry, variable pH) and several pH 6 buffers (i.e., variable chemistry, constant pH). The peptide Ti-1 was qualitatively observed to generate similar amounts of white precipitate upon introduction into each of the solutions under the various buffer chemistries examined. SEM analyses indicated that the TiO_2 nanoparticulate networks formed in the presence of the Ti-1-peptide possessed similar morphologies under all of the conditions tested (see Figures 3.7 and 3.8). Similar x-ray diffraction patterns were also obtained for the precipitates formed in the presence of the Ti-1 peptide under varying conditions of buffer chemistry or pH (see Figures 3.9 and 3.10).

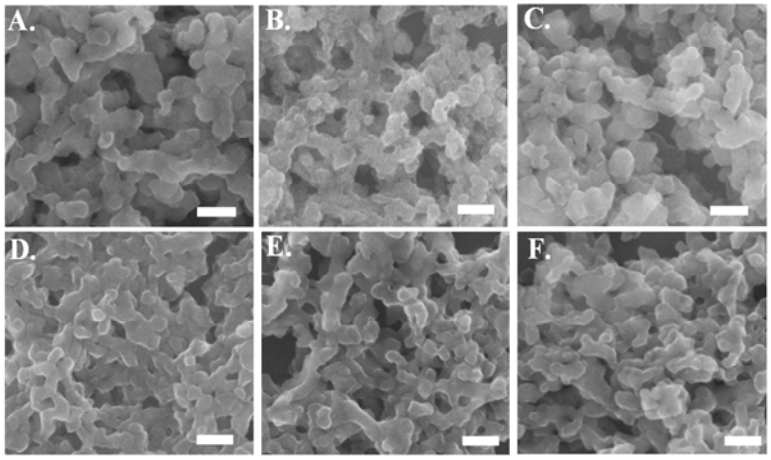

Figure 3.7: Secondary electron images of the TiO_2 precipitates formed under the influence of the peptide Ti-1 from an aqueous TiBALDH solution buffered with pH 6: A) phosphate-citrate, B) phosphate, C) sodium citrate, D) Bis-Tris, E) ADA, and F) MES buffer solutions. The scale bars correspond to 200 nm.

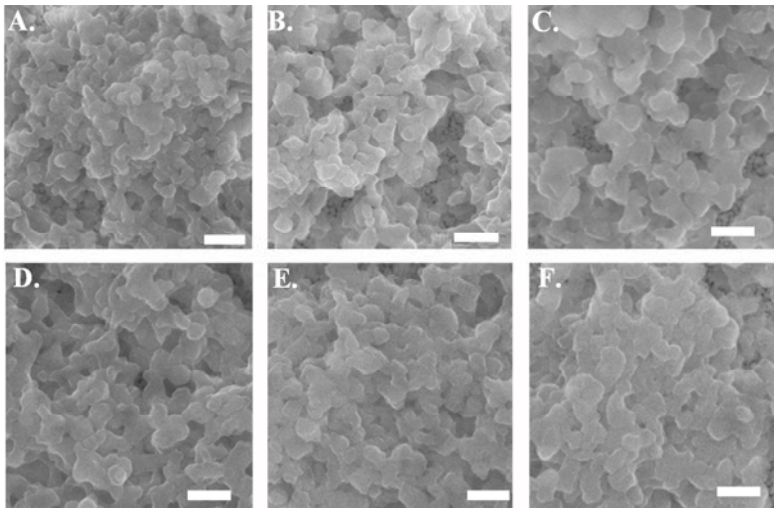

Figure 3.8: Secondary electron images of the TiO_2 precipitates formed under the influence of the peptide Ti-1 from an aqueous TiBALDH solution buffered with: A) pH 3, B) pH 4, C) pH 5, D) pH 6, E) pH 7, and F) pH 8 phosphate-citrate buffers. The scale bars correspond to 200 nm.

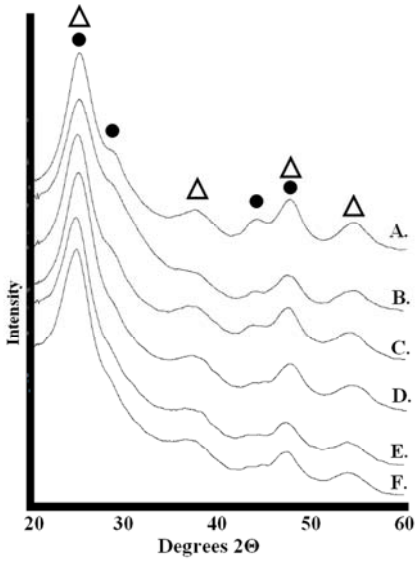

Figure 3.9: X-ray diffraction analyses of the TiO_2 precipitates generated under the influence of peptide Ti-1 from aqueous TiBALDH solutions buffered with pH 6: A) phosphate-citrate, B) phosphate, C) sodium citrate, D) Bis-Tris, E) ADA, and F) MES buffer solutions. Filled circles and open triangles represent diffraction peaks attributable to the monoclinic (β-TiO_2) and anatase phases of TiO_2, respectively.

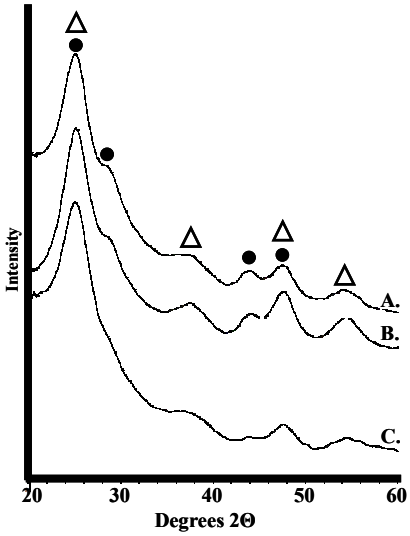

Figure 3.10: X-ray diffraction analyses of the TiO_2 precipitates generated under the influence of peptide Ti-1 from aqueous TiBALDH solutions buffered with: A) pH 8 B) pH 6, C) pH 3 phosphate-citrate buffers. Filled circles and open triangles represent diffraction peaks attributable to the monoclinic (β-TiO_2) and anatase phases of TiO_2, respectively.

3.4 Summary

Phage-displayed, 12-mer peptides, that were identified on the basis of their binding affinity to titania single crystals, were found to exhibit a strong enrichment in arginine, lysine, and histidine residues. Incubation of these titania-binding peptides in an otherwise stable aqueous TiBALDH-bearing solution at pH 6.3 yielded nanoparticulate titania within 10 min at room temperature. The amount of titania formed by a given peptide was found to increase with the number of positive charges carried by the peptide. X-ray diffraction analyses, electron diffraction analyses, and high resolution transmission electron microscopy revealed that the peptide-induced TiO_2 contained fine ($\leq$10 nm) anatase and monoclinic β-TiO_2 nanocrystals. These observations were used to design a peptide that generated the highest biomolecule-induced titania yield reported to date (1.84 mg TiO_2/mg peptide) from a water-stable precursor solution over a relatively wide pH range of 4-8.

3.5 References

1. Mann, S. *Biomineralization: Principles and Concepts in Bioinorganic Materials Chemistry*; Oxford University Press: Oxford, NY, 2001.
2. Bäuerlein, E., Biomineralization: Progress in Biology, Molecular Biology, and Application; Wiley-VCH, Weinheim, 2004.
3. Flynn, C. E.; Lee, S; Peelle, B. R.; Belcher, A. M. *Acta. Mater.* **2003**, *51*, 5867.
4. Sarikaya, M., Tamerler, C.; Jen, A. K.; Schulten, K.; Baneyx, F. *Nat. Mater.* **2003**, *2*, 577.
5. Xu, A.; Ma, Y; Helmut, D. *J. Mater. Chem.* **2007**, *17*, 415.
6. Naik, R. R.; Stone, M. O.; *Mater. Today* **2005**, 8, 18.
7. Shimizu, K.; Cha, J.; Stucky, G. D.; Morse, D. E. *Proc. Natl. Acad. Sci. U.S.A.* **1998**, *95*, 6234.

8. Cha, J. N.; Shimizu, K.; Zhou, Y.; Christiansen, S. C.; Chmelka, B. F.; Stucky, G. D.; Morse, D. E. *Proc. Natl. Acad. Sci. U.S.A.* **1999**, *96*, 361.

9. Schröder, H. C; Boreiko, A.; Korzhev, M.; Tahir, M. N.; Tremel, W.; Eckert, C.; Ushijima, H.; Müller, I. M.; Müller, W. E. G.; *J. Biol. Chem.* **2006**, *281*, 12001-9.

10. Kröger, N.; Deutzmann, R.; Sumper, M. *Science* **1999**, *286*, 1129.

11. Kröger, N.; Lorenz, S.; Brunner, E.; Sumper, M. *Science* **2002**, *298*, 584.

12. Poulsen, N.; Sumper M.; Kröger N. *Proc. Natl. Acad. Sci. U.S.A.* **2003**, *100*, 12075.

13. Poulsen, N.; Kröger, N. *J. Biol. Chem.* **2004**, *279*, 42993.

14. Wenzl, S.; Deutzmann, R.; Hett, R.; Hochmuth, E.; Sumper, M; *Angew. Chem. Int. Ed.* **2004**, *43*, 5933.

15. Brutchey, R. L.; Yoo, E. S; Morse, D. E. *J. Am. Chem. Soc.* **2006**, *128*, 10288.

16. Tahir, M. N.; Théato, P.; Müller, W. E. G.; Schröder, H. C.; Borejko, A.; Faiß, S.; Janshoff, A.; Huth, J.; Tremel, W. *Chem. Commun*. **2005**, *44*, 5533.

17. Sumerel, J. L.; Yang, W.; Kisailus, D.; Weaver, J. C.; Choi J. H.; Morse D. E.; *Chem. Mater*. **2003**, *15*, 4804.

18. Kisailus, D.; Najarian, M.; Weaver, J. C.; Morse, D. E. *Adv. Mater*. **2005**, *17*, 1234.

19. Kröger, N; Dickerson, M. B.; Ahmad, G.; Cai, Y.; Haluska, M. S.; Sandhage, K. H.; Poulsen, N.; Sheppard, V. C. *Angew. Chem. Int. Ed*. **2006**, *45*, 7239.

20. Luckarift, H. R.; Dickerson, M. B.; Sandhage, K. H.; Spain, J. *Small* **2006**, *2*, 640.

21. Cole, K. E.; Ortiz, A. N.; Schoonen, M. A.; Valentine, A. M. *Chem. Mater.* **2006**, *18,* 4592.

22. Pender, M. J.; Sowards, L. A.; Hartgerink, J. D.; Stone, M. O.; Naik, R. R.; *Nano Lett.* **2006**, *6*, 40.

23. Sewell, S. L.; Wright, D. W. *Chem. Mater.* **2006**, *18*, 3108.

24. Cole, K. E.; Valentine, A. M.; *Biomacromol*. **2007**, *8*, 1641.

25. Zhu, J.; Zhang, J.; Cehn, F.; Anpo, M. *Mater. Lett.* **2005**, *59*, 3378.

26. Wang, G.; Wang, Q.; Lu, W.; Li, J. *J. Phys. Chem. B* **2006**, *110*, 22029.

27. Nohynek, G. J.; Lademann, J.; Ribaud, C.; Roberts, M. S. *Crit. Rev. Toxicology* **2007**, *37*, 251.

28. Robel, I.; Subramanian, V.; Kuno, M.; Kamat, P. V. *J. Am. Chem. Soc.*. **2006**, *128*, 2385.

29. Armstrong, A. R.; Armstrong, G.; Canales, J.; Bruce, P. G. *Angew. Chem., Int. Ed.* **2004**, *43*, 2286.

30. Bavykin, D. V.; Friedrich, J. M.; Walsh, F. C. *Adv. Mater.* **2006**, *18*, 2807.

31. King, J. S.; Grangnard, E.; Roche, O. M.; Sharp, D. N.; Scrimgeour, J.; Denning, R. G.; Turberfield, A. J.; Summers, C. J.

32. Instructional and informational materials version 2.7 accompanying *Ph.D. 12 Phage Display Peptide Library Kit*, New England BioLabs, Inc., Ipswich, MA, 2006.

33. Sedaira, H.; Idriss, K. A.; Abdel-Aziz, M. S. *Analyst* **1996**, *8*, 1079.

34. Chen, H.; Xiaodi, S.; Neoh, K.; Choe, W. *Anal. Chem.*, **2006**, *78*, 4872.

35. Reiss, B. D.; Mao, C.; Solis, D.J.; Ryan, K. S.; Thomson, T.; Belcher, A. M. *Nanoletters,* **2004**, *4*,1127.

36. Ahmad, G.; Tomczak, M. M.; Dickerson, M. B.; Jones, S. E.; Naik, R. R.; Kröger, N.; Sandhage, K. H., Unpublished results.

37. Knecht, M. R.; Sewell, S. L.; Wright, D. W. *Langmuir* **2005**, *21*, 2058.

38. Brunner, E.; Lutz, K.; Sumper, M. *Phys. Chem. Chem. Phys.* **2004**, *6*, 854.

39. Sumper, M.; Lorenz, S.; Brunner, E. *Angew. Chem., Int. Ed.* **2003**, *42*, 5192.

40. Yin, S.; Wu, J.; Aki, M.; Sato, T. *Int. J. Inorg. Mater.* **2000**, *2*, 325.

41. Yin, S.; Sato, T. *Ind. Eng. Chem. Res.* **2000**, *39*, 4526.

CHAPTER 4: RAPID, ROOM-TEMPERATURE SYNTHESIS OF ANTI-BACTERIAL BIO-NANO-COMPOSITES OF HEN EGG WHITE LYSOZYME WITH AMORPHOUS TITANIA OR ZIRCONIA

The following chapter is distinct from, though presents the results of a collaborative project initiated by Dr. Heather R. Luckarift and Prof. Jim C. Spain.

Luckarift, H. R.; Dickerson, M. B.; Sandhage, K. H.; Spain, J. C. *Small*, **2006**, *2*, 640.

4.1 Introduction

The gentle reaction conditions offered by the biomolecule-initiated synthesis of silica have recently enabled the *in situ* formation of enzymatically-active bioinorganic composite materials[1,2]. The synthesis of these materials was accomplished by first mixing the enzyme to be entrapped with the silica-condensing R5 peptide[1,2]. Upon addition of silicic acid (the silica precursor), the enzymes were incorporated into the growing R5-initiated silica precipitates[1,2]. This one-pot synthesis technique has proven successful for the high efficiency encapsulation and stabilization of the enzymes horseradish peroxidise, catalase, and butyrylcholinesterase[1,2].

Building on the recent demonstrations that the cationic R5 peptide can be used to induce the formation of silica/enzyme nanocomposites, the rapid, economical, room temperature synthesis of anti-bacterial lysozyme/inorganic hybrid materials has been explored, in collaboration with Dr. Heather R. Luckarift (Air Force Research Laboratory). While a 2006 publication (see above) covered the production of enzymatically-active silica and titania composites, only those materials produced by Dr. Luckarift from the TiBALDH precursor are presented here as a comparison with the

peptide- and recombinant silaffin produced titania presented in this dissertation. The synthesis of enzymatically-active zirconia materials, described herein, is a divergence from the silica and titania/lysozyme composite work initiated by Luckarift and Spain. The role of lysozyme in the present study is two-fold; lysozyme is an ubiquitous antibacterial enzyme capable of lysing gram-positive bacterial cells by hydrolyzing specific peptidoglycan linkages in the cell wall and, secondly, lysozyme has previously been observed to initiate silica condensation[3,4]. The development of a simple, low-cost processing route to lysozyme/inorganic nanocomposites, and evaluation of their antimicrobial activity, provides an opportunity to create robust bionanocomposite materials that inhibit bacterial activity for use as broad-spectrum antifouling materials. Lysozyme/inorganic nanocomposites, could be attractive multifunctional materials for a variety of applications in cosmetics (i.e., antimicrobial and sunscreen properties) or food preparation (i.e., hard antimicrobial particles for cutting surfaces)[5,6].

4.2 Experimental Section

4.2.1 Materials

The zirconia precursor, Tyzor-217®, (sodium zirconium lactate) was provided free of charge by the DuPont Chemical Company. Titanium-bis-ammonium-lactato-dihydroxide (TiBALDH) was purchased from Alfa Aesar (Ward Hill, Ma). Hen egg white lysozyme (HEWL) (95%, 50,000 units/mg) and potassium phosphate (>99%) was obtained from Sigma-Aldrich. Tris-(hydroxymethyl)-aminomethane (Tris) (>99.8%) buffer was purchased from Amresco Inc. (Solon, Ohio).

4.2.2 Precipitation Trials

For precipitation of inorganics, a stock solution of lysozyme (100 mg ml^{-1}) was prepared in 0.2 μm-filtered 18.2 MΩ·cm water and dialyzed (against the same water) prior to use (Slide-A-Lyzer, Pierce Biotechnology). The precipitation mixture consisted of 800 μl of buffer (0.1 N NaOH, 0.1 M KH_2PO_4, pH 8), 100 μl of 1M titanium (IV) *bis* (ammonium lactato) dihydroxide (Ti-BALDH) (final concentration of 100 mM) or 200 mM Tyzor-217® (final concentration 20 mM) and 100 μl of lysozyme (10 mg/ml final concentration). The mixture was agitated for 5 minutes at room temperature. The resultant particles were removed by centrifugation (14k rpm) for 2 minutes and then washed twice with deionized water. The zirconia precipitation conditions were alternately prepared as described above, but with 50 mM, pH 8 Tris-HCl buffer replacing the phosphate buffer. Titania and zirconia precipitation reactions were conducted by Dr. H. R. Luckarift and MBD, respectively.

4.2.3 Entrapped Enzyme Analysis

Entrapped lysozyme was released from zirconia and titania particles by incubation of the nanocomposites materials in 1 M sodium hydroxide for 10 min at 37 ^{o}C. The resulting solutions were analyzed for the presence of HEWL by denaturing polyacrylamide gel (15%) electrophoresis (SDS-PAGE) and spectrophotometrically at 280 nm. Lysozyme activity assays were performed with *Micrococcus lysodeikticus* cells according to the supplier's (Sigma Aldrich) instructions. Activity measurements were conducted on at least three independent samples with error bars representing one standard deviation.

4.2.4 Precipitate Characterization

The morphology of the lysozyme/inorganic composite materials was characterized by scanning electron microscopy utilizing a Leo 1530 FEG SEM, (Carl Zeiss SMT AG). Transmission electron microscopy was conducted by MBD with a JEOL 100CX II or Dr. Ye Cai (Georgia Institute of Technology) with a JEOL 4000 EX. Microchemical analyses were conducted utilizing an Oxford Inca EDS detector attached to the scanning electron microscope, using at least 3 measurements for each sample. The crystalline phases of the resulting composite materials were evaluated by x-ray diffraction (Philips PW1800, PANalytical) utilizing Cu Kα radiation at a scan rate of 0.6° minute^{-1}. Thermogravimetric analyses (TGA) were preformed with a Netzsch STA 449 C instrument at a heating rate of 10°C minute^{-1} to 900°C in a synthetic air gas stream with the assistance of Dr. Benjamin C. Church (Georgia Institute of Technology).

4.3 Results and Discussion

In the present work, hen egg white lysozyme (HEWL) catalyzed the precipitation of titania or zirconia within seconds when added to a solution of titanium (IV)-bis-(ammonium-lactato) di-hydroxide (Ti-BALDH) or Tyzor-217®. Scanning electron microscopy (SEM) and transmission electron microscopy (TEM) revealed that the precipitated titania and zirconia consisted of highly-interconnected networks of very fine particles (Figures 4.1 and 4.2). The fundamental particles entrapped within the titania networks possessed diameters of only 10-50 nm, while the zirconia particles were determined to be slightly larger (i.e., possessing diameters of 25-150 nm).

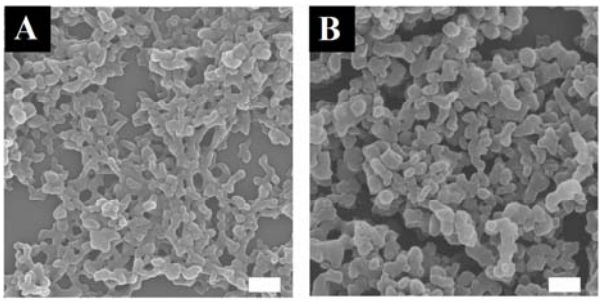

Figure 4.1: SEM micrographs of the titania and zirconia nanoparticles formed by precipitation with HEWL. A) precipitated from an aqueous Ti-BALDH solution in the presence of HEWL prepared by Dr. H. R. Luckarift. B) zirconia precipitated from sodium zirconium lactate by lysozyme. Scale bars represent 400 nm in each image.

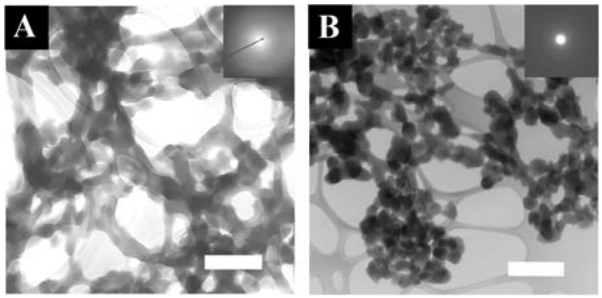

Figure 4.2: Bright field TEM micrographs of the nanoparticles formed by the interaction of HEWL with A) TiBALDH and B) Tyzor 217. Insets; SAED patterns of precipitates of the titania and zirconia precipitates. Scale bars represent 500 nm in A) and 150 nm in B. Image in B) was taken by Dr. Ye Cai (Georgia Institute of Technology). Material depicted in A) was precipitated by Dr. H. R. Luckarift (AFRL).

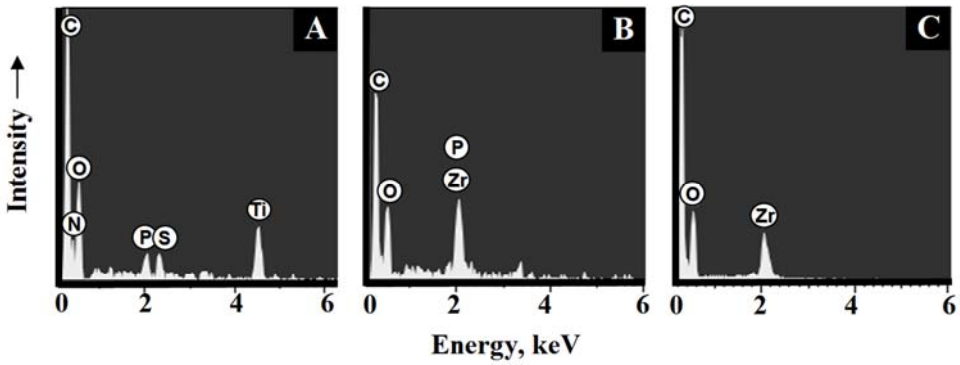

Figure 4.3: Energy dispersive spectroscopy (i.e., elemental analysis) of lysozyme-mediated titania and zirconia precipitates. Materials generated by the reaction of lysozyme with A) Ti-BALDH, B) sodium zirconium lactate, and C) sodium zirconium lactate in Tris-HCl buffer. HEWL/titania precipitates generated by Dr. H. R. Luckarift (AFRL).

EDS analysis indicated that the lysozyme/TiBALDH material was primarily composed of carbon, oxygen, titanium, phosphorus and sulfur (Figure 4.3A). Lysozyme is the likely origin of the carbon and sulfur signal as noted above, whereas the titanium and oxygen peaks present in this spectrum are associated with the newly formed inorganic phase. The phosphorous observed in this analysis can be traced to the incorporation of phosphate ions from the buffer solution during precipitation. Elemental analysis of the lysozyme/Tyzor-217® precipitate indicated the presence of zirconium, carbon and oxygen (Figure 4.3B). Unfortunately, the EDS peaks for zirconium and phosphorous coincide, making the unambiguous analyses of this material's exact composition difficult. Repetition of this HEWL/Tyzor-217® precipitation reaction in a phosphate-free solution (i.e., Tris-HCl buffer in place of potassium phosphate buffer) yielded an EDS pattern with peaks consistent with zirconium, oxygen, and carbon. SDS-PAGE and spectrophotometric (i.e., at 280 nm) analysis of the supernatant, recovered after the sodium hydroxide treatment of the titania and zirconia precipitates, indicated the presence of lysozyme within the composite material. The proportion of combustible components of these lactate precursor derived materials was found to be 70.3 and 73.6 wt%, for lysozyme-zirconia and lysozyme-titania, respectively (TG analysis conducted with the assistance of Dr. B. Church). SAED analyses (insets in Figure 4.2) and XRD analyses (not shown) indicated that the lysozyme-catalyzed titania and zirconia materials were amorphous.

The activity of the encapsulated lysozyme was compared with that of the free enzyme to determine the effect of immobilization. The physical entrapment of lysozyme within an inorganic matrix could, in principle, inhibit the ability of lysozyme to attach to

a bacterial cell wall and catalyze lysis. Bacteriolytic activity of the encapsulated lysozyme was investigated with *Micrococcus lysodeikticus* cells. Following the self-immobilization of lysozyme in titania, 69±7.8% of the free enzyme activity was retained in the lysozyme-inorganic nanocomposites (Figure 4.4). The HEWL precipitated zirconia materials were noted to have less preserved bactericidal activity (39±3.1%). The thermostability of the free and immobilized lysozyme was investigated to determine whether the inorganic matrices provided an environment that protected the immobilized lysozyme from denaturation (Figure 4.5). Free lysozyme in solution was denatured by incubation at 75 ^{o}C for 1 hour (90% decrease in activity). In comparison, the titania encapsulated lysozyme retained 45% of the native activity when incubated under the same conditions (Figure 4.5). Unfortunately, the zirconia encapsulated lysozyme was observed to completely lose its ability to hydrolyze *M. lysodeikticus* cell walls following

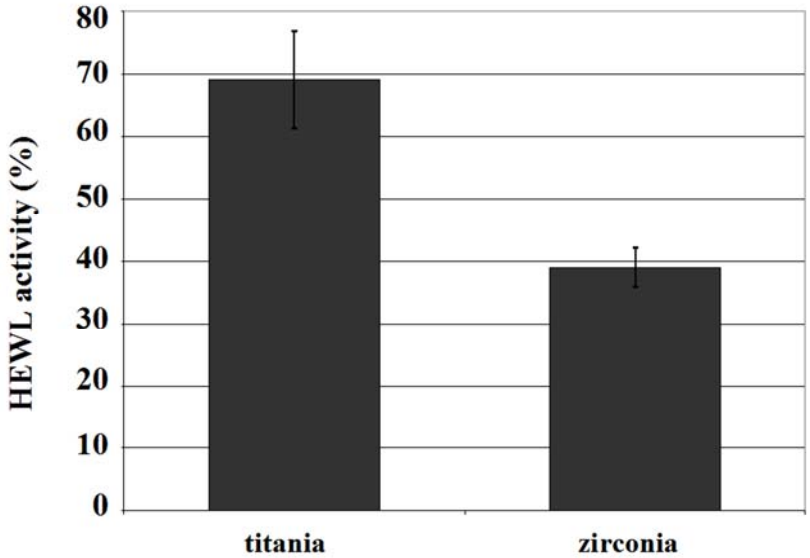

Figure 4.4: Activity of immobilized lysozyme as determined by lytic assay with *Micrococcus lysodeikticus* cells. Entrapping material precipitated by HEWL is noted in the x ordinate of the figure. Values reported are relative to the activity of native lysozyme in solution, taken as 100%. Data for titania collected by Dr. H. R. Luckarift (AFRL).

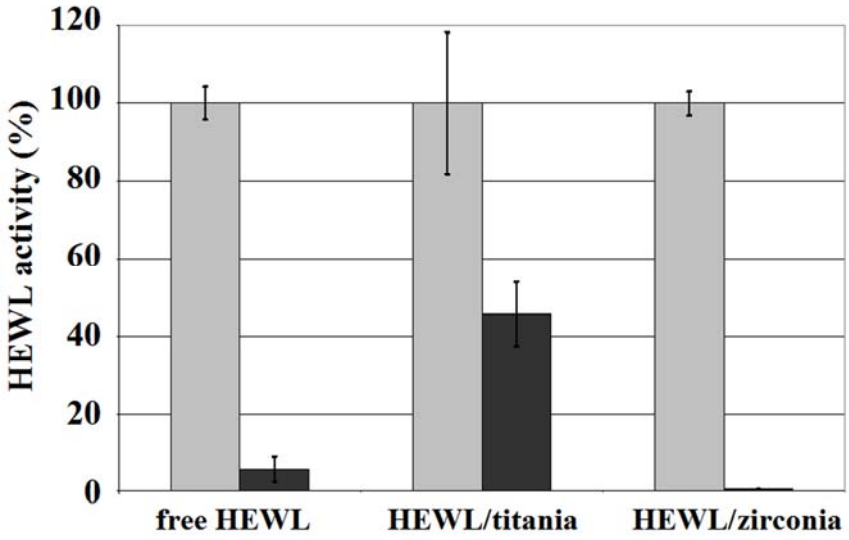

Figure 4.5: Thermostability of free and immobilized lysozyme in titania or zirconia nanoparticles. Activity of immobilized lysozyme as determined by lytic assay with *Micrococcus lysodeikticus* cells before (light gray bars) and following heat treatment at 75 ^{o}C for 1 hour (dark gray bars). Entrapping material precipitated by HEWL is noted in the x ordinate of the figure. Free lysozyme indicates HEWL in solution (i.e., no immobilizing matrix). Values reported are relative to the activity of the native lysozyme in solution (prior to heat treatment), taken as 100%. Free and titania entrapped data gathered by Dr. H. R. Luckarift (AFRL).

75 ^{o}C heat treatment.The reason for this differential loss of activity is currently unknown. The most direct answer for the poor degree of protection offered by zirconia may lie in the physical structure of this precipitated material. The zirconia matrix may possess a greater porosity or larger pore size than the HEWL precipitated titania, allowing the HEWL to escape the composite during the heat treatment procedure. Another possibility for the inferior performance of zirconia may partially lie in the isoelectric point (IEP) of the material; titania and zirconia possess IEPs of 5 and 6, respectively[8]. It is conceivable that, although lysozyme may initiate the formation of zirconia, the protein may not interact (i.e., through electrostatic interaction) as strongly with this particular ceramic, leading to poorer stabilization as compared to the more acidic ceramic matrices. The

more hydrophobic nature of zirconia (i.e., as compared to titania) may also contribute to the decreased stability of lysozyme by favoring the formation of amino acid residue-zirconia hydrophobic interactions (i.e., favoring the unfolding of lysozyme)[8].

The ability of lysozyme to induce the precipitation of titania and zirconia likely lies in the many characteristics that the protein shares with biomacromolecules involved in biosilicification; most importantly, HEWL is a highly basic protein, which possesses a pI of 11.1 and carries an excess of positive charges (+9) (Figure 4.6)[9,10]. Proteins believed to be associated with silica biogenesis, such as silicateins and silaffins, have been recently reported to initiate the formation of titania and/or zirconia from precursor solutions similar to those used in this study[11-13]. The ability of lysozyme to initiate materials synthesis has been exploited in this study to create enzymatically-active composites through the self-encapsulation of HEWL in its active form. The observation that lysozyme retains significant bactericidal activity when encapsulated in titania or zirconia suggests that the protein active site is not blocked or consumed in the precipitation of inorganic oxides.

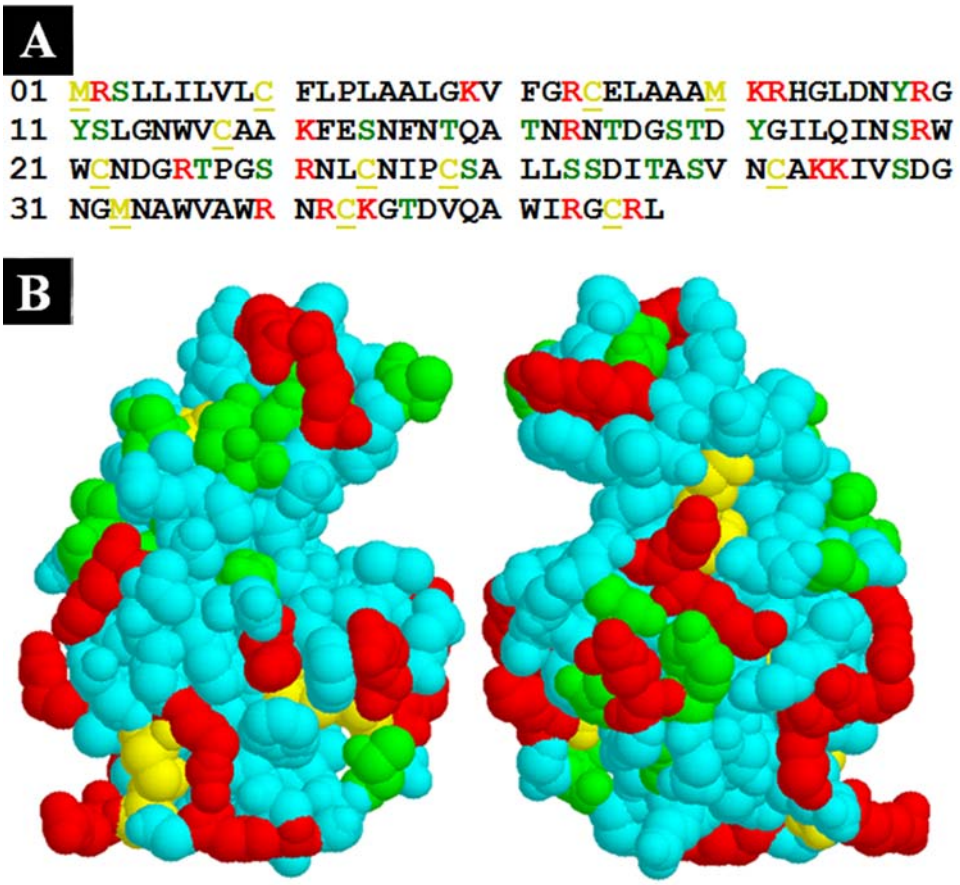

Figure 4.6: The structure of HEWL. A) The amino acid sequence of HEWL with the sulfur containing residues, Cys and Met, colored yellow and underlined, positively charge residues, Lys and Arg, coded red, and hydroxyl bearing residues, Tyr, Ser, and Thr, coded green. Amino acid numbering noted at right of sequence. B) Space filling model of lysozyme based on the x-ray crystal structure of the enzyme (opposing views). Color coding from A carried to B, non-specified residues colored light blue. Image in B) generated from protein data bank entered crystal structure of HEWL in protein explorer visualization software[9,14].

4.4 Summary

In summary, lysozyme induced the rapid, room-temperature precipitation of amorphous titania and zirconia. Lysozyme-mediated precipitation is a one-pot procedure that simultaneously results in lysozyme encapsulation within titania or zirconia, with moderate retention of anti-microbial activity. Titania was found to be an attractive

support matrix for this enzyme, as titania-encapsulated lysozyme retained significant hydrolytic activity even after exposure to denaturing conditions. This attractive bio-inspired mineralization/bioencapsulation strategy provides an economical and facile route for synthesizing a wide range of functional bionanocomposites containing functional biomacromolecules entrained within titania or zirconia nanostructures.

4.5 References

1. Luckarift, H. R.; Spain, J. C.; Naik, R. R.; Stone, M. O. *Nat. Biotech*., **2004**, *22*, 211.
2. Naik, R. R.; Tomczak, M. M.; Luckarift, H. R.; Spain, J. C.; Stone, M. O. *Chem. Commun.*, **2004**, 1684.
3. Pellegrini, A.; Thomas, U.; von Fellenberg, R.; Wild, P. *J. Appl. Bacteriol*., **1992**, *72*, 180.
4. Coradin, T.; Coupe, A.; Livage, J. *Colloid. Surf.,* **2003**, *29*, 189.
5. Ciccognani, D. T. *Cosm. Sci. Techn. Series*, **2006**, *31*, 185.
6. Conte, A.; Buonocore, G. G.; Sinigaglia, M.; Del Nobile, M. A. *J. Food Eng.*, **2006**, 78, 741.
7. Satyanarayan, M.; Deepthy, A.; Bhat, H. *Crit. Rev. Solid State Mater. Sci.,* **1999,** *24,*103.
8. Rezwan, K.; Studar, A. R.; Vörös, Gauckler, L. J. *J. Phys. Chem. B.*, **2005**, *109*, 14469.
9. Diamond, R. *J. Mol. Biol.*, **1974**, *82,* 371.
10. Sumper, M.; Kröger, N. *J. Mater. Chem*, **2004**, *14*, 2059.
11. Sumerel, J. L.; Yang, W.; Kisailus, D.; Weaver, J. C.; Choi J. H.; Morse D. E.; *Chem. Mater*. **2003**, *15*, 4804.
12. Tahir, M. N.; Théato, P.; Müller, W. E. G.; Schröder, H. C.; Borejko, A.; Faiß, S.; Janshoff, A.; Huth, J.; Tremel, W. *Chem. Commun*. **2005**, *44*, 5533.
13. Kröger, N; Dickerson, M. B.; Ahmad, G.; Cai, Y.; Haluska, M. S.; Sandhage, K. H.; Poulsen, N.; Sheppard, V. C. *Angew. Chem. Int. Ed*. **2006**, *45*, 7239.
14. Martz, E. *Trends Biochem. Sci.*, **2002**, *27*, 107.

CHAPTER 5: THE RECOMBINANT SILAFFIN MEDIATED *IN VITRO* SYNTHESIS OF TITANIA AT AMBIENT TEMPERATURE AND NEUTRAL pH

The following chapter presents the results of a collaborative project that resulted in the following publication:

Kröger, N; Dickerson, M. B.; Ahmad, G.; Cai, Y.; Haluska, M. S.; Sandhage, K. H.; Poulsen, N.; Sheppard, V. C. *Angew. Chem. Int. Ed*., **2006**, *45*, 7239.

5.1 Introduction

Many of the first materials utilized by our species were drawn from biology. Examples of such materials include animal bone (e.g., for cutting tools), wood (e.g., for shelter construction), and plant fibers (e.g., for clothing). Although the developments of metallurgy and chemistry have displaced many of these natural materials, recent advances in molecular biology have sparked a renewed interest in biologically-derived materials[1-5].

The ability to purify biomolecules in high yields from genetically manipulated expression hosts (e.g., *Escherichia coli* or *Pichia pastoris*) in particular, has enabled the study of proteins that mediate the formation of, or may be used directly as, functional materials[6-13]. Examples of the latter include proteins derived from spider drag line silks, which hold promise as high strength fibers as well as scaffolds for cell or tissue growth[6-8]. The second group of proteins, those that initiate or control the formation of minerals, include engineered viral capsids and proteins originally isolated from sponge silica (termed silicateins)[9-13].

Recently, Kaplan and colleagues have reported the generation of a recombinant protein (termed 15mer+R5) with a primary structure derived from both silk and silica

precipitating proteins[14]. The major domain of the chimeric 15mer+R5 protein was based on the consensus repeat sequence of the *Nephila clavipes* major ampullate spidroin protein 1 (MaSp1) [14]. Silica precipitation activity was introduced to this protein through the fusion of the R5 peptide to the c-terminus of the MaSp1-like domain[14]. The R5 peptide incorporated into Kaplan's chimeric protein is a synthetic analog to the silaffin, natSil-1a, first described by Kröger and colleagues[15]. Although the R5 peptide lacks the extensive post-translational modifications (i.e., phosphorylation, poly-amine addition, and lysine methylation) that are unique to natSil-1a, this 19 amino acid residue peptide is able to initiate the *in vitr*o precipitation of silica under very mild solution conditions (i.e., neutral pH, room temperature, containing multiply charged anions)[15].

While natSil-1a is believed to be associated with the flocculation of silica in diatom cell wall formation, the R5 peptide has recently been utilized to initiate the precipitation of titania, a material not currently known to be specifically mineralized in biology[15-19]. Expanding upon these prior studies of the R5 peptide-enabled formation of titania, Kröger, Dickerson, et al. have explored the construction, expression, purification, and TiO_2 precipitation activities of several recombinant silaffins derived from the diatoms *Cylindrotheca fusiformis* and *Thalassiosir pseudonana*[15,20].

5.2 Experimental Section

5.2.1 Recombinant silaffin production

Prof. Nils Kröger and Dr. Nicole Poulsen (Georgia Institute of Technology) amplified selected regions of silaffin genes by PCR, cloned them into pET16 plasmids, and introduced the plasmids into *E. coli* by transformation. The large scale expression and purification of the recombinant silaffins were conducted by Dr. Gul Ahmad and

Vonda C. Sheppard (Georgia Institute of Technology). The work undertaken by Ahmad and Sheppard was as follows: After induction of protein expression (1 mM isopropyl-β-thiogalactoside, 3 hours, 37^{o}C), cells were washed (150 mM NaCl) and lysed by sonication in HTPG buffer (1 M NaCl, 50 mM Tris-HCl pH 8.0, 6 M guanidine-HCl). Recombinant silaffins were isolated from the centrifuged supernatant (4^{o}C, 30 min, 10,000 g) by Ni-NTA chromatography. Recombinant silaffin rSilC was subjected to an additional purification step using cation exchange chromatography. Column eluants containing recombinant silaffins were dialyzed against 50 mM ammonium acetate, lyophyllized, and the residues dissolved in H_2O. The yield was ~5 mg recombinant silaffin per 1 liter of *E. coli* culture.

5.2.2 Titania precipitation

Titania precipitation reactions were conducted by Dr. Gul Ahmad (Georgia Institute of Technology). The work undertaken by Dr. Ahmad is as follows: Titania precipitation reactions were carried out in 200 µl volumes. For a given reaction, 20 µl of 500 mM sodium phosphate/citrate buffer of the desired pH (typically pH 7), 20 µl of 2 M TiBALDH (aq), and 140 µl of 0.2 µm-filtered 18.2 MΩ water were mixed and incubated for 20 minutes at room temperature. Titania precipitation was initiated by the addition of a 20 µl volume of recombinant silaffin (20 mg/ml) to the buffered TiBALDH solution. The reaction solution was mixed and incubated for 10 min at room temperature. The resulting precipitate was collected by centrifugation, and washed 3 times with 1 ml H_2O. The TiBALDH-based precursor solutions utilized in this work were observed by Dr. Ahmad to be stable for at least 24 hours in the absence of recombinant silaffins.

5.2.3 Materials Characterization

Scanning electron microscope (SEM) characterization of the titania precipitates was conducted with a field emission gun microscope (Leo 1530 FEG SEM, Carl Zeiss SMT Ltd., Cambridge, UK) equipped with an energy dispersive X-ray spectrometer (INCA EDS, Oxford Instruments, Bucks, UK). Precipitates were dried on a gold-coated aluminum SEM stub or silicon wafer at 37.5°C for 16 hours. FIB-SEM was performed with a Nova 200 DBFIB FE-SEM equipped with a gallium ion FIB (FEI Company, Hillsboro, USA). Transmission electron microscopy was conducted with a JEOL 4000 EX instrument by Dr. Ye Cai (Georgia Institute of Technology). HR-TEM analysis was conducted by Dr. Cai at an operating voltage of 400 kV. Typically, a drop of ethanol suspended titania precipitate was dried on a carbon-film-coated copper grid. rSilC-rutile titania precipitates were ground with a mortar and pestle prior to being deposited on a TEM grid. Thermogravimetric analyses were conducted by Dr. Benjamin C. Church (Georgia Institute of Technology) with a Netzsch 449C Simultaneous Thermal Analyzer (Selb, Germany). Prior to analysis, samples were dried for 16 hours at 65^{o}C. Powder X-ray diffraction was performed by Dr. Micheal S. Haluska (Georgia Institute of Technology) using a PANalytical X-Pert Pro Alpha 1 diffractometer with incident beam Johannsen monochromator, with 1/2^{o} divergence slits, 0.04^{o} soller slits and an Xcelerator linear detector. The powder sample was loaded on a zero background sample holder and the measurement performed over a 20-60^{o} 2θ range using a continuous scan with a 0.167° 2θ step size. For polarized light microscopy a Leica RDX microscope was used with 90° settings of polarizer and analyzer. Polarized light microscopy was conducted in

conjunction with Dr. Nicole Poulsen with the assistance of Matije Crne and Mohan Srinivasarao (Georgia Institute of Technology).

5.3 Results and discussion

5.3.1 Recombinant silaffin production

Four *E. coli* expression plasmids were constructed by Prof. Nils Kröger and Dr. Nicole Poulsen (Georgia Institute of Technology) that encoded selected regions from the silaffin genes *si1l*, *tpSil1,* and *tpSil3*[15,20]. Upon induction, these transformed *E. coli* cells produced 4 recombinant silaffins in respectable yields (i.e., ~5 mg purified protein/L of *E. coli*). Two of these engineered proteins, rSilN and rSilC, were based upon the 5' and 3' halves of *sil1* (i.e., the same gene that encodes the natSil-1a silaffin)[15]. The remaining two silaffins, rSil3 and rSil1L, were encoded by the *tpSil3* gene and 3'-half of the *tpSil1* gene, respectively[20]. A run of six histidine residues (His_6) engineered into the C-terminus of the recombinant silaffins was utilized to purify the proteins (i.e., by Ni^{2+} affinity chromatography) from the total *E. coli* lysate. The recombinant silaffin rSilC was subjected to an additional ion-exchange based chromatographic step in order to separate it from several extraneous proteins present in the initial purification procedure. All protein expression and purification work during the course of this investigation was conducted by Dr. Gul Ahmad (Georgia Institute of Technology). The primary sequences of rSilN, rSilC, rSil1L, and rSil3 are provided in Table 5.1, while a summary of the protein characteristics are provided in Table 5.2.

Table 5.1: Amino acid sequences of recombinant silaffins. To highlight the repetitive polypeptide structure of rSilC, the amino acid sequences of the repeated units have been aligned. The short repeat segment of rSil1L is designated by underlining. The charge distribution within recombinant silaffins is highlighted by depicting lysine (K) and arginine (R) residues in red, and aspartate (D) and glutamate (E) residues in green. Recombinant silaffin expression plasmids were designed and constructed by Prof. Nils Kröger and Dr. Nicole Poulsen (Georgia Institute of Technology).

rSil1L

```
  1 M V P G L T E M P T I S P T E D H Y F F G K S H K S H K S H K S K A
 35 T K T L K V S K S G K S A K S S K S S G R R P L F G V S Q L S E G I
 69 A V G Y A K S S G R S S Q Q A V G S W M P V A A A C I L G A L S F F
103 L N H H H H H H
```

rSilC

```
  1 M S S K K S G S Y Y S Y G T K K S G S Y S G Y S T K K S A S R R I L
 35   S S K K S G S Y S G Y S T K K S G S R R I L
 57   S S K K S G S Y S G S K G S K R R I L
 76   S S K K S G S Y S G S K G S K R R N L
 95   S S K K S G S Y S G S K G S K R R I L
114   S S K K S G S Y S G S K G S K R R N L
133   S S K K S G S Y S G S K G S K R R I L
152   S G G L R G S M H H H H H H
```

rSil3

```
  1 M E G H G G D G S I S M S M H S S K A E K Q A I E A A V E E D V A G
 35 P A K A A K L F K P K A S K A G S M P D E A G A K S A K M S M D T K
 69 S G K S E D A A A V D A K A S K E S H M S I S G D M S M A K S H K A
103 E A E D V T E M S T A K A G K D E A S T E D M C M P F A K S D K E M
137 S V K S K Q G K T E M S V A D A K A S K E S S M P S S K A A K I F K
171 G K S G K S G S L S M L K S E K A S S A H S L S M P K A E K V H S M
205 S A H H H H H H H H
```

rSilN

```
  1 M A A Q S I A D L A A A N L S T E D S K S A Q L I S A D S S D D A S
 35 D S S V E S V D A A S S D V S G S S V E S V D V S G S S L E S V D V
 69 S G S S L E S V D D S S E D S E E E E L R I L H H H H H H
```

Table 5.2. Properties of recombinant silaffins. K+R = number of lysine and arginine residues, D+E = number of aspartate and glutamate residues. The theoretical molecular masses of the unmodified polypeptides are listed.

	rSilC	**rSil1L**	**rSil3**	**rSilN**
pI	11.8	10.6	9.4	3.8
K+R	45 (27 %)	15 (14 %)	33 (16 %)	2 (2 %)
D+E	0	4 (4 %)	30 (14 %)	23 (27%)
kDa	17.6	11.8	22.1	9.9

Perhaps the most striking of the recombinant silaffins listed in Table 5.1 is rSilC, which possessed a highly-repetitive primary structure composed of seven nearly-identical segments. rSilC was also the most basic of the expressed silaffins, with an isoelectric point (pI) of 11.8, due to its high lysine and arginine content and lack of any acidic residues. The second most basic recombinant protein constructed for this study was rSil1L (i.e., pI=10.6). This silaffin possessed a short repetitive domain (amino acids 22-53) consisting of Lys-X-Z type sequences, where X was typically Ser and Z was often His. Unique to the recombinant silaffins explored in this study, rSil1L also contained a hydrophobic stretch of seventeen residues in its C-terminal domain. Silaffin rSilN, which corresponded to a gene product whose "fate" in the diatom is currently unknown, is strongly acidic (pI = 3.8) and lacked any notable sequence repetitions[15]. The final silaffin explored here, rSil3, contained almost equal numbers of basic and acidic residues, which is reflected in its pI of 9.4. Unlike rSilC or rSil1L, rSil3 did not possess any discernable repetitive sequence motifs.

5.3.2 Titania precipitation trials

Pushing beyond the natural chemistry of diatom biomineralization (i.e., silica), recombinant silaffins were investigated for their ability to control the formation of TiO_2 (titania). Titania-based materials are particularly interesting due to their wide variety of applications in photocatalysis, optoelectronics and photonics[21]. Titania precipitation experiments were conducted by Dr. Gul Ahmad (Georgia Institute of Technology) by introducing a given recombinant silaffin into a pH buffered solution containing the titania precursor titanium(IV) bis-(ammonium lactato)-dihydroxide (TiBALDH). The addition of either rSilC or rSil1L to TiBALDH precursor solutions resulted in the formation of a white material that precipitated from solution within a few minutes. The introduction of silaffins rSil3 and rSilN into TiBALDH solutions failed to produce such a reaction, even after incubation for several hours.

The findings of a growing number of studies suggest that a high positive charge density is critical for the precipitation of titania from TiBALDH solutions[16-19,22,23]. Considering these results, it was not surprising that only the most basic recombinant silaffins, rSilC and rSil1L, were able to induce titania formation. Although rSil3 contained a greater number of lysine and arginine residues than did the titania-precipitating protein rSilL, rSil3's enrichment in acidic amino acids evidently counteracted the contribution of these basic residues.

The mechanism by which polycationic proteins, peptides, or molecules inititate titania precipitation from TiBALDH is currently unknown. Presumably, the first step of the titania precipitation reactions in this study involved binding of the negatively charged Ti(IV)-lactato dihydroxy complex to either rSilC or rSilL. This may weaken the Ti-

lactato bonds due to Coulomb repulsion between the strongly polycationic protein environment and the positively polarized Ti(IV) center, thus inducing hydrolysis of the TiBALDH complex. The resulting hydrated titanium hydroxide is supersaturated with respect to titania formation (solubility: 1–10 μM at pH 3–10)[24]. In a manner analogous to their effect in the silicic acid/silica system, recombinant silaffins may promote the deposition of hydrated TiO_2 by aggregating the polytitanate molecules that develop spontaneously by autopolycondensation[25].

5.3.3 Characterization of rSilC and rSil1L-titania

The white precipitates generated by rSilC and rSil1L from a pH 7 phosphate-citrate buffered TiBALDH solution were collected by centrifugation, rinsed with water, and characterized by energy dispersive x-ray analysis (EDS), scanning electron microscopy (SEM), and transmission electron microscopy (TEM). Elemental analysis (i.e., by EDS) indicated that both the rSilC- and rSil1L-induced materials contained titanium, oxygen, carbon, nitrogen, and small amounts of phosphorous (Figure 5.1). The presence of organic material within these precipitates was confirmed by thermogravimetric analyses, conducted by Dr. Benjamin C. Church (Georgia Institute of Technology), which indicated an organic content of 56 % for rSilC-titania and 50 % for rSil1L-titania.

Although nominally composed of the same elemental constituents, analysis by SEM revealed marked differences in the titania structures produced by rSilC and rSil1L. The rSil1L-titania was composed of aggregates of nanospherical particles (diameters 100-300 nm) that were interconnected (Figure 5.1C). The precipitates generated by rSilC were observed to have larger particle sizes than those produced by rSil1L, with diameters

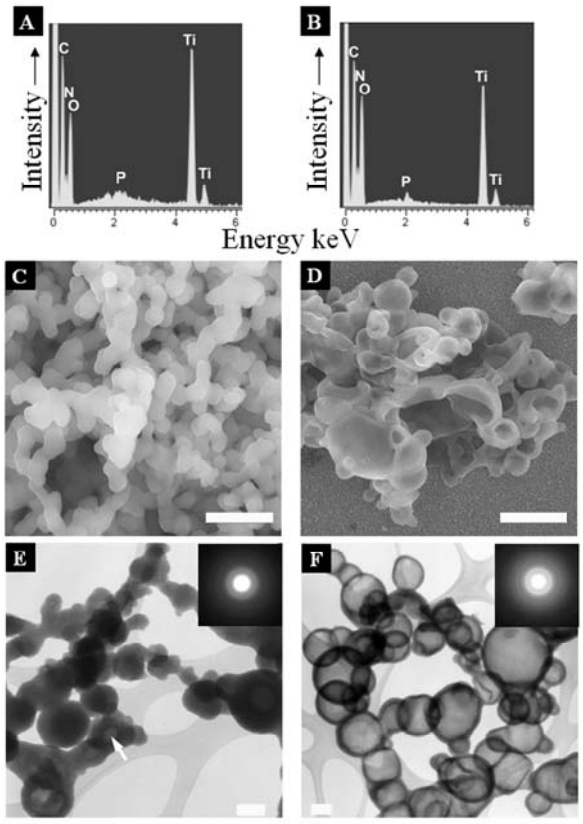

Figure 5.1: Characterization of the titania precipitates generated by rSilC and rSil1L. Energy dispersive x-ray spectroscopy analysis of: A) rSil1L-titania and B) rSilC-titania. SEM micrographs of: C) rSil1L-titania and D) rSilC-titania. Bright field TEM images of: E) rSil1L-titania and F) rSilC-titania, with electron diffraction patterns as insets. The arrow in E) designates a small void in the precipitate. Scale bars represent: 1 μm in C) and D), 100 nm in E) and F). Images E) and F) were taken by Dr. Ye Cai (Georgia Institute of Technology).

that ranged between 100 nm – 1 μm (Figure 5.1D). In many cases these rSilC-titania particles appeared to be partially collapsed, suggesting that they might be hollow. While small voids were occasionally observed in rSil1L-precipitated titania (Figure 5.1E), the rSilC particles proved to be almost completely hollow (Figure 5.1F). The hollow nature of these particles was also confirmed after the precipitates were examined by SEM before and after sectioning with a focused ion beam (Figure 5.2). The crystallinity of the recombinant silaffin-induced precipitates was evaluated by x-ray (Dr. M. Haluska) and

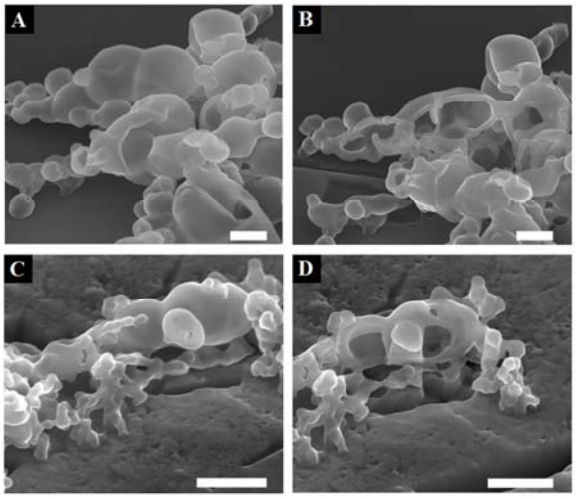

Figure 5.2: Scanning electron images of rSilC precipitates before A) and C) and following milling with a focused ion beam, B) and D). Matched images are A) and B) and (C and D). Scale bars represent 500 nm.

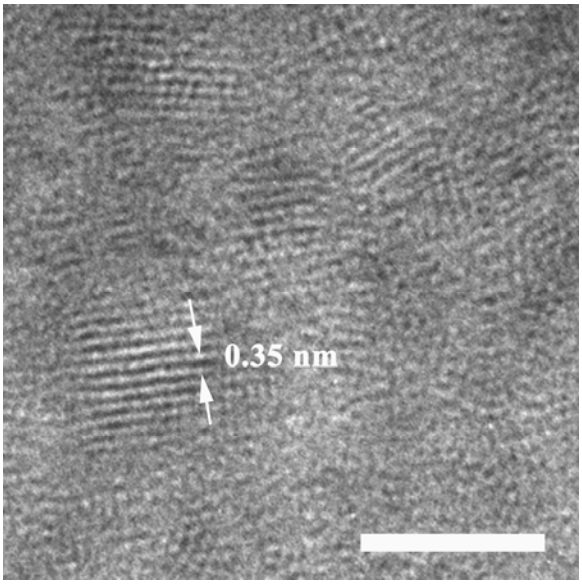

Figure 5.3: High-resolution transmission electron image of a cross-section of a rSilC-titania hollow spherical precipitate. The lattice fringe spacing indicated by arrows is consistent with the (101) plane spacing of anatase and/or the (110) plane spacing of monoclinic β-TiO_2. The scale bar corresponds to 5 nm. Image taken by Dr. Ye Cai (Georgia Institute of Technology).

electron (Dr. Y. Cai) diffraction analyses. Indexing of several selected area electron diffraction patterns from the rSil1L and rSilC produced titania, yielded d spacings of 3.5, 2.1, 1.73 and 1.22 Å. These values were found to be consistent with the d spacings associated with several planes of anatase and a metastable monoclinic phase of titania, β-TiO_2. Very small (2-5 nm) crystallites possessing lattice spacings corresponding to anatase or β-titania were observed (i.e., by high resolution TEM) to be embedded within the solid walls of the rSilC induced hollow spheres (Figure 5.3).

The XRD characterization of rSil1L-titania (i.e., not rSilC-titania, see below), conducted by Dr. Michael S. Haluska (Georgia Institute of Technology), yielded a diffraction pattern with broad peaks which were indexable to either β-TiO_2 or a mixture of β-TiO_2 and anatase titania. The large widths of these XRD peaks were associated with the presence of very small titania crystallites in the rSil1L induced titania. Inspection of Figure 5.4 also reveals that the XRD pattern of the rSil1L-titania precipitate exhibited relatively high background intensities at low 2θ values, which is a result indicative of the presence of an amorphous phase within the precipitates (Figure 5.4).

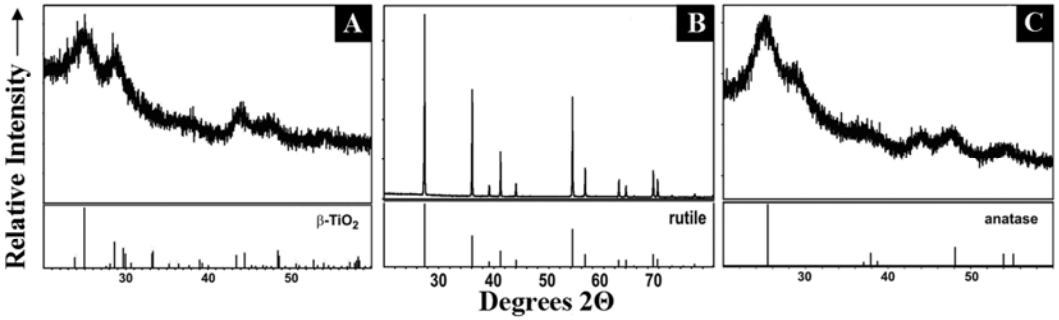

Figure 5.4: X-ray diffraction patterns of A) rSil1L-titania, B) rSilC-titania, and C) poly-l-lysine-titania precipitates. XRD patterns A) and B) collected by Dr. Micheal S. Haluska (Georgia Institute of Technology).

5.3.4 Phase transformation in rSilC-titania

The XRD characterization (Conducted by Dr. M. Haluska) of rSilC-titania yielded results which were inconsistent with the TEM and SAED characterization of this same material. As can be clearly seen in Figure 5.4, the x-ray diffraction pattern of rSilC-titania contained sharp peaks consistent with coarse crystals of rutile TiO_2. This was markedly different from the diffraction pattern seen for rSil1L-titania (Figure 5.4A). Repetition of the precipitation (by Dr. G. Ahmad) and characterization (by Dr. M. Haluska) of rSilC-titania consistently produced diffraction patterns possessing only sharp peaks for rutile. These conflicting accounts of the crystalline identity of rSilC-titania from SAED and XRD analyses were found to be linked to the different methods of sample preparation used for both types of analyses.

Specimens of hollow shell rSilC-titania materials characterized by electron microscopy were prepared from a final aqueous rinse solution by being placed onto a stub or grid and air dried at 37.5°C. Due to the larger size of the samples required for XRD analysis, these rSilC-titania materials were rinsed two additional times in anhydrous methanol (i.e., to facilitate drying) and dried at 30°C in a vacuum centrifuge.

SEM characterization of these methanol and vacuum-dried rSilC-titania precipitates revealed particles of a morphology not previously observed in the water rinsed and air dried samples. The methanol rinsed and vaccum dried rSilC-titania precipitates were found to have transformed into large microspheres (20-50 μm in diameter) that were frequently cracked and/or fragmented (Figures 5.5A and B). While the structure of these microspheres is unremarkable when viewed at low magnifications, higher magnification SEM characterization revealed that these spheres possessed a

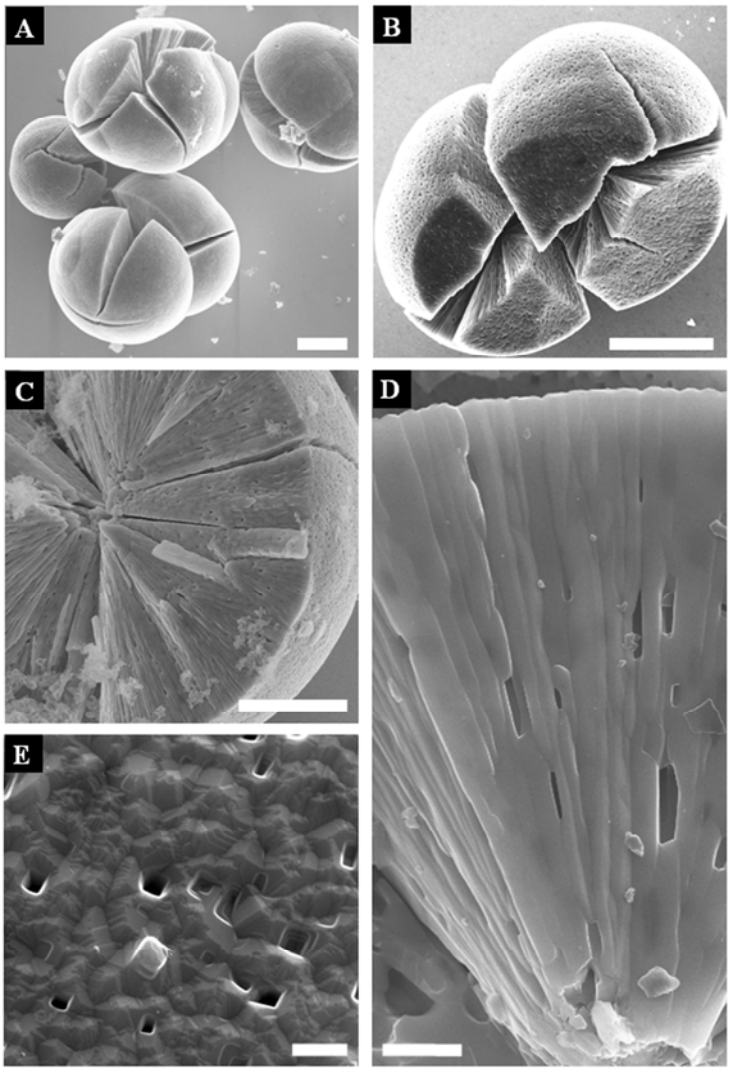

Figure 5.5: SEM characterization of rutile microspheres formed after the methanol treatment and vacuum drying of rSilC-titania. (Panels described in text).

remarkable hierarchical architecture (Figures 5.5C and D). The bulk of the microspheres were observed to be composed of radially-arranged, densely packed, conically-shaped columns exhibiting diameters of 400–800 nm and 100–200 nm on the surface and at the center of the microspheres, respectively (Figures 5C and D). Numerous rectangular pores were also noted to decorate the surface and the cross-sections of the microspheres (Figure 5.5 D and E). The faceted structure of the microspheres' columnar subunits and surface,

as well as the appearance of rectangular pores, strongly suggested that these structures may be composed of crystalline titania. Indeed, selected area electron diffraction (SAED) analysis (conducted by Dr. Y. Cai), of the columnar subunits yielded well-defined diffraction spots that could all be assigned to lattice planes of the titania polymorph rutile (Figure 5.6). The crystalline nature of the columns was further confirmed by high resolution transmission electron microscopy (HR-TEM), which revealed exclusively crystalline regions with lattice constants again characteristic for rutile (Figure 5.6).

The formation of rSilC-titania microspheres was further investigated by polarized light microscopy. Polarized light microscopy experiments were conducted by MBD, Dr. Nicole Poulsen, and Dr. Gul Ahmad with the microscope facilities kindly provided by Matije Crne and Mohan Srinivasarao (Georgia Institute of Technology). Addition of rSilC to the titania

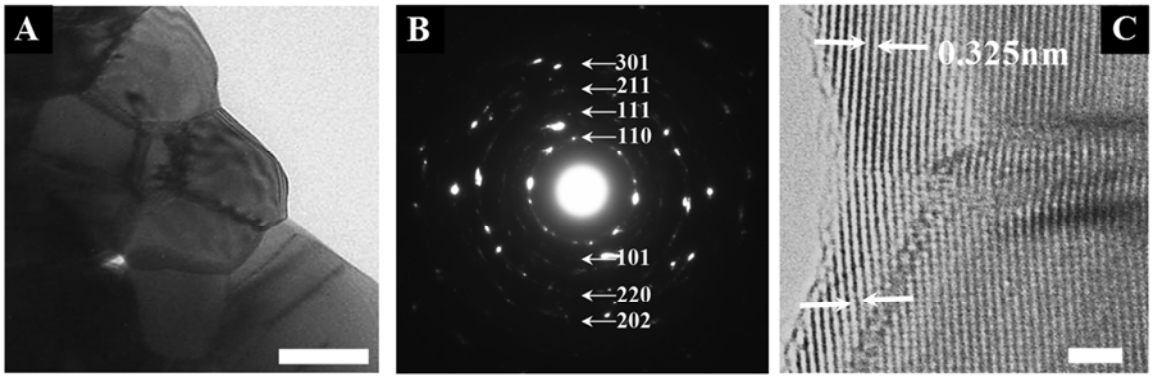

Figure 5.6: TEM characterization of rSilC-rutile titania. A) Bright field image depicting a cross-section of the rutile columns observed in Figure 5.5. B) Electron diffraction of this material with diffraction rings indexed to denoted rutile planes. C) High resolution bright field micrograph, with the spacing of lattice fringes noted. Images collected by Dr. Ye Cai (Georgia Institute of Technology).

precursor solution rapidly induced the formation of large, irregularly-shaped aggregates (Figure 5.7A). These structures were consistent with the masses of round hollow spheres observed by SEM analysis (see Figure 5.1D). The hollow spherical particles in Figure 5.7A were observed to remain unchanged in their morphology or crystallinity even after prolonged incubation times (up to 24 hours) in aqueous solution. In contrast, precipitates removed from the reaction solution after 10 min, rinsed thoroughly in water and subsequently dehydrated in methanol and *in vacuo,* were found to contain rutile microspheres (Figures 5.7 C and D). Additional experiments later indicated that methanol dehydration of rSilC-titania alone was sufficient to trigger the transformation of the hollow spheres of titania into the large rutile microspheres (Figure 5.7B). The rSilC-titania precipitate was found to contain almost exclusively crystalline microspheres after extended periods of drying *in vacuo* (≥24 hours) (Figure 5.7D). These observations suggest that rSilC caused the rapid deposition of amorphous titania in aqueous solution and induced conversion of the hydrated, amorphous aggregates into rutile only upon efficient removal of the associated H_2O. Interestingly, the application of methanolic or methanol/vacuum dehydration techniques to rSil1L-titania or poly-l-lysine-titania precipitates failed to elicit any changes in the morphology or crystalline character of these materials (see Figure 5.4).

The initial discovery of highly-ordered rutile microcrystals in the rSilC-titania precipitate was quite surprising, as this represents the first demonstration of the room temperature, near-neutral pH formation of rutile TiO_2. Conventional synthesis of rutile TiO_2 is typically conducted at high temperatures (600–1000°C), under extremely acidic

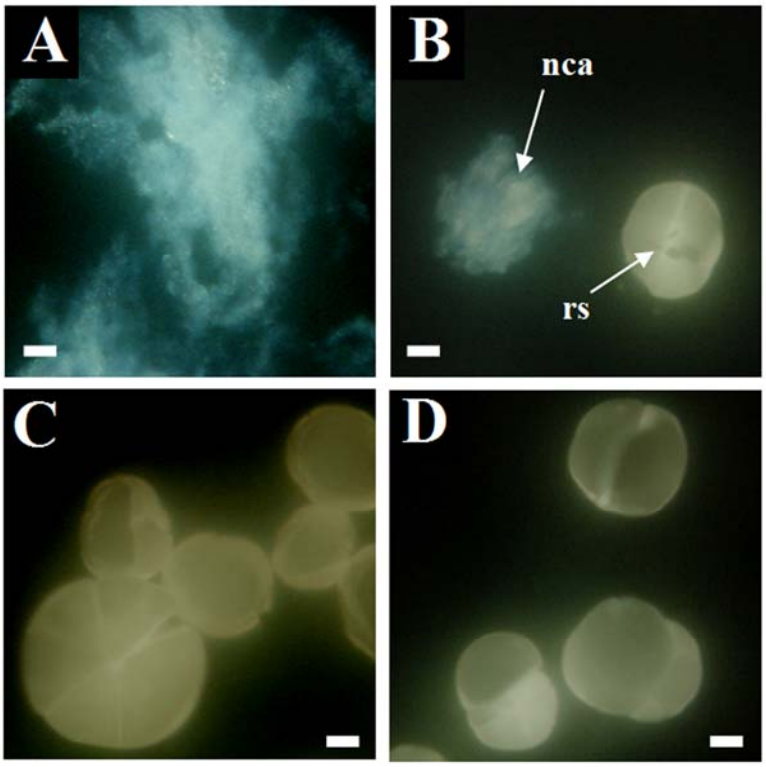

Figure 5.7: Polarized light microscope imaging of microsphere formation. The structures of rSilC-titania were documented at different processing stages: A) In the TiBALDH reaction solution after 10 minutes, B) following subsequent washing with water and methanol, and 30 min incubation in methanol, C) after washing (with H_2O and methanol) and drying for 30 min under vacuum, and D) after continued drying for 24 hours under vacuum Scale bars correspond to 10 μm in each image. In B) nano-crystalline agglomerates (nca) and rutile microspheres (rs) are denoted. This figure represents the contributions of several individuals, see experimental section for details.

conditions (i.e., pH<0), or hydrothermally at moderate temperatures and elevated pressures under extremely acidic solutions[26-39]. Until the recent publication of this work, such high temperatures or harsh environments were necessary to form rutile through the reorganization of the condensed TiO_6 octahedra. We hypothesize that following dehydration, the recombinant silaffin rSilC facilitates the crystallization of amorphous titania by: (i) acting as an acid base catalyst in the hydrolysis and condensation reactions between TiO_6 octahedra, and (ii) guiding the rearrangement of these units into a rutile

lattice structure. The numerous lysine-residues found in rSilC can donate and accept protons, and the highly-repetitive spacing of functional groups in this protein may lower the activation energy for the alignment of TiO_6 octahedra into a rutile lattice structure.

Much like rSilC, the recombinant silaffin rSil1L also contains lysine residues (although in a lower proportion), which should enable the protein to act as an acid-base catalyst. Unlike rSilC however, this particular recombinant silaffin contains only a short repetitive sequence domain. Taken together, these structural issues may inhibit rSil1L from guiding the formation of the rutile crystal lattice, even after extensive dehydration of the titania precipitate.

The transformation of amorphous mineral deposits into crystalline phases has also been observed in biological mineralization processes. Within the last decade, sea urchin and molluscan bivalves larvae have been found to utilize amorphous calcium carbonate (ACC) as a transient precursor which is later transformed into crystalline (i.e., calcite or aragonite) $CaCO_3$[40]. ACC is also widely found as a component of crustacean exoskeletal cuticle, where it presumably acts as a reinforcing phase[40]. The ACC common to these crustacean however, is maintained as an amorphous phase and does not devitrify[40]. ACC can thus be classified into two types, kinetically-stable ACC and transient ACC[40]. The most striking difference between these two classes of ACC is their water content; transient ACC is essentially anhydrous while kinetically-stable ACC has 1 mole of water associated with every mole of $CaCO_3$[40].

Exploiting this difference in hydration states, Aizenberg and coworkers have recently formed large patterned single crystals of $CaCO_3$ from a hydrated ACC precursor phase[41]. In Aizenberg's study, hydrated ACC was deposited on a patterned self-

assembled monolayer[41]. The crytallization of this ACC was found to be dependent upon the efficient removal of water associated with the transient amorphous phase[41]. The effective dehydration of the newly forming calcite in this previous work was achieved by introducing closely-spaced channels, which served as reservoirs into which H_2O and other impurities were expelled during the induced $CaCO_3$ crystallization process[41].

Analogously, the removal of H_2O could be an important factor in the transformation of the hydrated, partially amorphous titania, into rutile. Drawing on the example of ACC, the dehydration of titania may, in effect, transform this material from a stable hydrated form to an anhydrous transient material. We suggest that the numerous pores present within the transformed rutile microspheres may act as channels that allow for the removal of water from the structure and enable the crystallization process to occur. Although the mechanism of pore channel formation within the microspheres is currently unclear, the hollow nature of the initial titania aggregates may be an important prerequisite.

It is interesting to note that although methanol is likely acting to remove water from the initially rSilC-precipitated transient titania phase in this system, this alcohol is often used to induce β-sheet formation in silk proteins[14,42,43]. It is conceivable that methanol may be imposing a structural rearrangement of rSilC. Unfortunately, evidence that may support or refute this possibility has not been gathered at this time.

5.4 Summary and Outlook

The highly-cationic recombinant silaffins rSilC and rSil1L were found to initiate the precipitation of titania from buffered TiBALDH solutions, while the nearly zwitterionic rSil3 and acidic silaffin rSilN did not possess this activity. The synthesis of

rutile by the recombinant silaffin rSilC through a simple methanolic dehydration procedure is unprecedented and opens new possibilities for the synthesis of this functional materials. Numerous methods exist for the synthesis of nano- and micropatterned organic polymers, yet these structures perform poorly in photonic and electronic applications due to their inherent low refractive index and high electrical resistance. Attaching rSilC to nano- or micropatterned polymer surfaces would enable the *in situ* formation of rutile on these structures under gentle solution conditions. The resulting patterned polymer-ceramic materials could be attractive for photonic bandgap filters, diffraction gratings and optoelectronic devices.

To the author's knowledge, this study represents the first time that recombinant biomolecules have been observed to impose polymorph control on a "synthetic" material. Like many first discoveries, the observed transformation of rSilC-titania to rutile TiO_2 opens considerably more questions than have been answered in this initial study. We have designed and are currently expressing and purifying new recombinant silaffins which may aid in the elucidation of the interdependence of silaffin and TiO_2 structure. The possible induction of secondary structure upon rSilC by methanol treatment is an intriguing topic which requires further study. Additional characterization of the transformation of rSilC precursor titania to rutile, especially if done *in situ,* may better reveal the mechanisms involved in this phenomenon.

5.5 Contributions

Recombinant silaffin expression plasmids were prepared by N. Kröger and N. Poulsen (GT). Large scale expression and purification of rSilN, rSilC, rSil1L, and rSil3 were conducted by G. Ahmad and V. Sheppard (GT). Titania precipitation reactions

were conducted by GA. SEM, FIB-SEM, and limited XRD and TEM characterization of titania precipitates were conducted by MBD. XRD characterization of titania precipitates was also conducted by M. Haluska (GT). TEM characterization of recombinant silaffin-titania materials was conducted by Y. Cai (GT). Original manuscript prepared by N. Kröger with input from K. H. Sandhage (GT), myself, and G. Ahmad. Manuscript rewritten with additions for this dissertation by MBD.

5.6 References

1. Mann, S. *Biomineralization: Principles and Concepts in Bioinorganic Materials Chemistry*; Oxford University Press: Oxford, NY, **2001**.
2. Naik, R. R.; Stone, M. O.; *Mater. Today,* **2005**, *8*, 18.
3. Douglas, T. *Science*, **2003**, *299*, 1192.
4. Sarikaya, M., Tamerler, C.; Jen, A. K.; Schulten, K.; Baneyx, F. *Nat. Mater.* **2003**, *2*, 577.
5. Xu, A.; Ma, Y; Helmut, D. *J. Mater. Chem.* **2007**, *17*, 415.
6. Sanford, K.; Kumar, M. *Curr. Opin. Biotechnol.*, **2005**, *16*, 416.
7. Vendrely, C.; Scheibel, T. *Macromol. Biosci.*, **2007**, *7*, 401.
8. Wang, X.; Kim, H. J.; Wong, C.; Vepari, C.; Matsumoto, A.; Kaplan, D. L. *Mater. Today,* **2006**, *9*, 44.
9. Flynn, C. E.; Lee, S.; Peelle, B. R.; Belcher, A. M. *Acta Materialia*, **2003**, *51*, 5867.
10. Shimizu, K.; Cha, J.; Stucky, G. D.; Morse, D. E. *Proc. Natl. Acad. Sci. U.S.A.* **1998**, *95*, 6234.
11. Zhou, Y.; Shimizu, K.; Cha, J. N.; Stucky, G. D.; Morse, D. E. *Angew. Chem. Int. Ed.,* **1999**, *38*, 780.
12. Tahir, M. N.; Théato, P.; Müller, W. E. G.; Schröder, H. C.; Borejko, A.; Faiß, S.; Janshoff, A.; Huth, J.; Tremel, W. *Chem. Commun*. **2005**, *44*, 5533.
13. Schröder, H. C; Boreiko, A.; Korzhev, M.; Tahir, M. N.; Tremel, W.; Eckert, C.; Ushijima, H.; Müller, I. M.; Müller, W. E. G.; *J. Biol. Chem.* **2006**, *281*, 12001-9.

14. Foo, C. W. P.; Patwardhan, S. V.; Belton, D. J.; Kitchel, B.; Anastasiades, D.; Huang, J.; Naik, R. R.; Perry, C. C.; Kaplan, D. L. *Angew. Chem. Int. Ed.,* **2006**, *103*, 9428.

15. Kroger, N.; Deutzmann, R.; Sumper, M. *Science* **1999**, *286*, 1129.

16. Cole, K. E.; Ortiz, A. N.; Schoonen, M. A.; Valentine, A. M. *Chem. Mater.* **2006**, *18*, 4592.

17. Pender, M. J.; Sowards, L. A.; Hartgerink, J. D.; Stone, M. O.; Naik, R. R.; *Nano Lett.* **2006**, *6*, 40.

18. Sewell, S. L.; Wright, D. W. *Chem. Mater.* **2006**, *18*, 3108.

19. Cole, K. E.; Valentine, A. M.; *Biomacromol*. **2007**, *8*, 1641.

20. Poulsen, N.; Kröger, N. *J. Biol. Chem.,* **2004**, *279*, 42993.

21. Bartl, M. H.; Boettcher, S. W.; Frindell, K. L.; Stucky, G. D. *Acc. Chem. Res.* **2005**, *38*, 263.

22. Luckarift, H. R.; Dickerson, M. B.; Sandhage, K. H.; Spain, J. *Small* **2006**, *2*, 640.

23. Dickerson, M. B.; Jones, S. E.; Cai, Y.; Ahmad, G.; Naik, R. R.; Kröger, N.; Sandhage, K. H. *Chem. Mater.* **(submitted).**

24. Baes, C. F.; Mesmer, R. E. *The Hydrolysis of Cations;* Krieger Publishing Company: Florida, USA, **1986.**

25. Sumper, M.; Kröger, N. *J. Mater. Chem.* **2004**, *14*, 2059.

26. Gopal, M.; Chan, W. J. M.; DeJonghe, L. C. *J. Mater. Sci.* **1997,** *32*, 6001.

27. Ovenstone, J.; Yanagisawa, K. *Chem. Mater.* **1999**, *11*, 2770.

28. Wu, M.; Long, J.; Huang, A.; Luo, Y.; Feng, S.; Xu, R. *Langmuir* **1999**, *15*, 8822.

29. Aruna, S. T.; Tirosh, S.; Zaban, A. *J. Mater. Chem.* **2000**, *10*, 2388.

30. W. P. Huang, X. H. Tang, Y. Q. Wang, Y. Koltypin, A. Gedanken, *Chem. Comm.* **2000**, 1415-1416.

31. Wang, C.; Deng, Z. X.; Li, Y. D. *Inorg. Chem.* **2001**, *40*, 5210.

32. Yin, H.; Wada, Y.; Kitamura, T.; Kambe, S.; Murasawa, S.; Mori, H.; Sakata, T.; Yanagida, S. *J. Mater. Chem.* **2001**, *11*, 1694.

33. So, W. W.; Park, S. B.; Kim, K. J.; Shin, C. H.; Moon, S. J. *J. Mater. Sci.* **2001**, *36*, 4299.

34. Andersson, M.; Osterlund, L.; Ljungstrom, S.; Palmqvist, A.; *J. Phys. Chem. B* **2002**, *106*, 10674.

35. Zhang, D. B.; Qi, L. M.; Ma, J. M.; Cheng, H. M. *J. Mater. Chem.* **2002**, *12*, 3677.

36. Yin, S.; Li, R. X.; He, Q. L.; Sato, T. *Mater. Chem. Phys.* **2002**, *75*, 76.

37. Yang, S.; Liu, Y.; Guo, Y.; Zhao, J.; Xu, H.; Wang, Z.; *Mater. Chem. Phys.* **2003**, *77*, 501.

38. Tang, Z. L.; Zhang, J. Y.; Cheng, Z.; Zhang, Z. T. *Mater. Chem. Phys.* **2003**, *77*, 314.

39. Yang, J.; Mei, S.; Ferreira, J. M.; Norby, P.; Quaresma, S.; *J. Coll. Interf. Sci.* **2005**, *283*, 102.

40. Addadi, L.; Raz, S.; Weiner, S.; *Adv. Mater.* **2003**, *15*, 959.

41. Aizenberg, J.; Muller, D. A.; Grazul, J. L.; Hamann, D. R. *Science* **2003**, *299*, 1205.

42. Phillips, D. M.; Drummy, L. F.; Naik, R. R.; De Long, H. C.; Fox, D. M.; Trulovec, P. C.; Mantz, R. A. *Chem. Comm.* **2005**, 4206.

43. Kweon, H. Y.; Park, Y. H. *J. App. Pol. Sci.* **1999**, *73*, 2887.

CHAPTER 6: REACTIVE SURFACE GROUP AMPLIFICATION FOR THE IMMOBILIZATION OF MINERALIZING PROTEINS ON SYNTHETIC AND BIOGENIC SILICA

6.1 Introduction

The last few years have witnessed considerable advances in the bioenabled or biomimetic syntheses of inorganic materials[1-18]. Of particular interest has been the use of proteins to produce (*in vitro*) nonbiologically native material chemistries[1-14,16,18]. Proteins (termed silicateins) isolated from the glassy spicules of the sponge *Tethya aurantia* have been observed to initiate the synthesis of gallium oxide, titania, and $BaTiOF_4$[1-3]. Analogs of another class of silica precipitating proteins isolated from diatom frustules, the silaffins, have also proven effective in producing titania from aqueous, neutral pH solutions at room temperature[4-8]. Indeed, the recombinant silaffin, rSilC, was recently found to initiate the synthesis of rutile (a TiO_2 polymorph typically accessible only through high temperatures or extremely acidic conditions[8]). Peptides identified through the screening of phage-displayed libraries have likewise enabled the production of "synthetic" materials. Examples of such peptide-initiated syntheses include simple oxides (i.e., ZnO, TiO_2), II-VI semiconductors (i.e., ZnS, CdS), magnetic alloys (i.e., FePt, CoPt) and, recently, binary ceramic compounds (i.e., $CaMoO_4$, and $BaTiO_3$)[9-14]. Although these developments hint at the exciting future of this field, the full potential of bioenabled or biomimetic syntheses will not be realized until these materials can be produced in a manner conducive to their integration into devices.

The most direct route to the organization of such materials is likely through the pre-immobilization of the precipitating biomolecule on a surface. To date, only a handful

of studies have investigated this important topic[15-18]. Stone and colleagues have succeeded in producing ordered arrays of silica and silver particles on surfaces pre-patterned with peptides[15,16]. Surface bound recombinant silicateins have also been utilized to produce silica, as well as titania and zirconia[17,18]. Although pioneering, these works make use of expensive laser-based optical patterning, electrostatic surface binding, gold surfaces, and/or exotic chemicals which impose limitations on their applicability to other materials systems and devices[15-18].

In this dissertation chapter, a general, facile procedure that utilizes simple (i.e., typically off-the-shelf) reagents to functionalize surfaces with high loadings of (mineralizing) poly-peptides is demonstrated for the first time. Although similar chemistries have been applied to the surface conjugation of DNA or dispersion of carbon nanotubes with great effect, this technique has not been applied to bioenabled materials synthesis[19,20]. The dendritic amplification of the desired functional groups will likely prove beneficial in systems where the substrates possess low densities of reactive moieties. This newly-developed immobilization procedure was observed to make a positive impact on the extent of surface mineralization.

6.2 Experimental Procedure

6.2.1 Materials

Silica Stöber spheres of 1 μm average diameter were obtained from Fiber Optic Research Center, Inc. (New Bedford, MA). Starter cultures of diatoms were purchased from the Pravasoli-Guillard National Center for the Culturing of Marine Phytoplankton Bigelow Laboratory for Ocean Sciences (West Boothbay Harbor, Maine). Poly-ethylene glycol diacrylate (n=400) was obtained from Polysciences, Inc. (Warrington, PA). The

cross-linking reagent, p-(maleimido)phenyl isocyanate (PMPI) was synthesized as previously described (this reagent may also be purchased from Pierce Biotechnology, Inc.) under the guidance of Dr. Simon C. Jones (Georgia Institute of Technology)[21]. Amine-terminated nitrilotriacetic acid (NTA) was synthesized (also available from Sigma-Aldrich) and thiolated by Mr. Peter Hotchkiss (Georgia Institute of Technology) following procedures previously described in the literature[22]. All other reagents were purchased from Sigma-Aldrich and used without further purification. Proteins utilized in this study were expressed and purified from transformed *Escherichia coli* cells utilizing standard molecular biology techniques[7].

6.2.2 Silica Surface Functionalization

6.2.2.1 Cleaning and Silanization

The organic components of cultured diatoms were removed from the silica frustules by refluxing harvested cells in an aqueous 50% HNO_3 solution for 1 hour. Both the culturing and acid cleaning of these diatoms was conducted by Dr. Gul Ahmad (Georgia Institute of Technology). Frustules were collected by centrifugation and rinsed 3 times with 0.2 μm-filtered 18.2 MΩ water. Residual organic matter associated with the frustules was pyrolyzed at 500°C for 8 hours in air. The diatom frustules or silica Stöber spheres were prepared for functionalization by stirring in a 50 vol% solution of concentrated HCl in methanol for 1 hour[23,24]. The cleaned silica was collected by centrifugation and rinsed 3 times with 0.2 μm-filtered 18.2 MΩ water and 1 time with ethanol. The silica frustules (100 mg) or spheres (1 g) were silanized in a 20 vol% solution of 2-[2-(3-trimethoxysilyl-propylamino)-ethylamino]ethylamine (TATMS) dissolved in 80 mL of ethanol for 16 hours with stirring. The samples were collected by

centrifugation, rinsed twice with 40 mL of ethanol, 3 times with 5 mM acetic acid, and one additional time with ethanol. The silane coat was cured at 110°C for 2 hours. Where noted, samples were alternatively silanized with a 2 vol% solution of 3-aminopropyl-triethoxy silane (APTES) dissolved in ethanol. The samples were otherwise treated in accordance with the procedure outlined for samples silanized with TATMS.

6.2.2.2 Functional Group Amplification

The TATMS-silanized samples (100 mg) were reacted in an alternating fashion with excess (1.5 mL) poly-functional 50 wt% solutions of dipentaerythritol penta-/hexa-acrylate (5/6 poly-acrylate) and tris(2-aminoethyl)amine (TAEA) in ethanol to allow for dendritic growth of a multi-amine/acrylate film. Silica samples were incubated for at least 1 hour in each solution, collected by centrifugation (13k rpm for 3 minutes) and washed 5 times in an equal volume of ethanol. The iterative reaction of 5/6 poly-acrylate and TAEA for the amplification of surface groups was developed by Dr. Guojie Wang (Georgia Institute of Technology). All incubation reactions were conducted with the samples rotated at 30 rpm to prevent sedimentation. Addition of final acrylate layers (spacers) were conducted as described above utilizing a mixed solution of 0.55 M poly-ethylene glycol (PEG) diacrylate (MW = 508 g) and 0.44 M (5/6 poly-acrylate) in ethanol. This final acrylate layer was reacted with TAEA as previously described.

6.2.2.3 Protein Cross-Linker Addition

100 mg of the multi-amine/acrylate film functionalized diatom frustules or silica Stöber spheres were rinsed in 1 ml of anhydrous acetonitrile. The terminal amine groups of these samples were reacted with the hetero-bifunctional cross-linker PMPI (3 mg)

dissolved in 1 ml of anhydrous acetonitrile for 1 hour. The silica samples were recovered from solution by centrifugation and rinsed 5 times with anhydrous CH_3CN. The available maleimide groups resulting from this reaction were then reacted with a thiol-NTA-bearing solution. This solution consisted of 1.5 mg of thiol-NTA dissolved in 1 ml of pH 7.1, 100 mM HEPES buffer, containing 150 mM NaCl, 10 mM EDTA, and 5 mM of the reducing agent Tris(2-carboxyethyl)phosphine hydrochloride (TCEP). This thiol-NTA-containing solution was incubated with the silica substrates for 16 hours. The NTA-functionalized samples were collected by centrifugation and rinsed 1 time with 1.5 ml of 0.2 μm-filtered 18.2 MΩ water. Residual maleimide functionalities were capped by reaction with a 10 vol% solution of 2-mercaptoethanol in ethanol for 1 hour. The samples were recovered by centrifugation and rinsed seven times with ethanol. The carboxylic acid moieties of the surface bonded NTA ligand were deprotonated by a 10 minute incubation of the substrates in 1 ml of pH 9.5, 100 mM Tris-HCl buffer. The samples were collected by centrifugation and incubated in a solution of 200 mM $NiSO_4$ in pH 7.5, 100 mM Tris-HCl buffer for 1 hour. The samples were collected by centrifugation and subsequently rinsed 3 times with pH 8, 50 mM Tris-HCl buffer containing 1 M NaCl (binding buffer).

6.2.3 Protein Conjugation

Proteins to be immobilized, rSilC (7.5-12 mg/ml) or enhanced green fluorescent protein (eGFP-His_6) (0.5 mg/ml), were incubated in an excess amount with the derivitized silica samples in a pH 8, 50 mM Tris-HCl buffer containing 1 M NaCl for 16 hours at 4°C. Expression, purification and conjugation of eGFP-His_6 conducted by Dr. Nicole Poulsen (Georgia Institute of Technology). Expression, purification and

conjugation of rSilC conducted by MBD[7]. Samples were recovered by centrifugation and rinsed three times with 500 μl of binding buffer.

6.2.4 Quantification of Unbound/Bound eGFP-His_6

The quantification of unbound and bound eGFP-His_6 was conducted by Dr. Nicole Poulsen (Georgia Institute of Technology). Following incubation with eGFP-His_6, Dr. Poulsen pelleted the Stöber spheres by centrifugation and transferred the supernant (unbound fraction) to a fresh tube. The Stöber silica was then washed with 100 ul binding buffer, again pelleted by centrifugation and the resulting supernatant was combined with the unbound fraction. 25 ul of the unbound fraction was diluted into 75 ul binding buffer and the fluorescence was measured by Dr. Poulsen using a Spectra Max Gemini Microplate Spectrofluorometer (Ex: 485 nm; Em: 510 nm, cutoff 495nm). At least 2 independent samples were measured 3 times, with error bars representing one standard deviation.

6.2.5 Mineralization of Immobilized Proteins

Silica substrates with conjugated proteins, and control specimens which lacked the PMPI and NTA cross-linkers, were suspended in 900 μl of pH 7, 55 mM phosphate-citrate buffer solution, to which was added 100 μl of titanium-bis-ammonium-lactato-dihydroxide (TiBALDH) (final concentration 200 mM). The samples were incubated in this solution for 30 minutes, then collected by centrifugation and rinsed 3 times with water and once with methanol.

6.2.6 Materials Characterization

Scanning electron microscopy was conducted with a field emission gun microscope (Leo 1530 FEG SEM, Carl Zeiss SMT Ltd., Cambridge, UK) equipped with an energy dispersive x-ray spectrometer (INCA EDS, Oxford Instruments, Bucks, UK). Transmission electron microscopy was conducted by Dr. Ye Cai (Georgia Institute of Technology) with a JEOL 4000 EX instrument.

6.3 Results and Discussion

6.3.1 Protein Binding Efficacy of the Dendritic Growth Technique

Silica substrates (e.g., microscope slides, silica beads, oxidized Si wafers) are common surfaces used for the immobilization of proteins[25]. Unfortunately, the relative abundance of reactive surface groups (i.e., silanols) on these substrates is often poor[23,26]. As the number of available reactive surface groups is directly proportional to the amount of protein that may be covalently immobilized on a surface, a barren silica surface will not yield optimal protein loadings. Addressing this issue, a facile and flexible reaction scheme capable of amplifying the number of available reactive moieties present on silica surfaces has been developed[27,28]. Expanding upon previous demonstrations that this dendritic growth technique can improve the quality of surface sol-gel coatings or number of amine groups available to reactive dyes, this reaction scheme has been explored for the immobilization of proteins on synthetic and biogenic silica surfaces[27,28].

A number of established protein cross-linking reagents and immobilization strategies rely upon surfaces coated with amines[25,29]. Therefore, amine terminated Stöber silica spheres were prepared by a dendritic functional-group amplification (DFGA) process in order to evaluate the efficacy of this procedure for protein immobilization.

Table 6.1 and Figure 6.1 outline the series of chemical reactions, developed by Dr. G. Wang, Prof. Nils Kröger, and MBD (Georgia Institute of Technology), to increase the number of amine groups available for reaction with the hetero-bifunctional cross-linker p-(maleimido)-phenyl isocyanate (PMPI)[21,30,31]. In order to determine how many iterations of the DFGA process were required to reach maximal protein loading, Stöber spheres were coated by 1, 3, and 5 poly-acrylate/amine layers (see protocols for G1, G3, and G5 in Table 6.1). Stöber silica spheres were also amine functionalized with a common silanizing reagent (APTES) as a comparison to the DFGA samples[25]. The amine terminated Stöber silica spheres (i.e., APTES or TATMS+DFGA samples) were then reacted with PMPI to generate maleimide functionalized surfaces (Figure 6.1). This maleimide moiety was then utilized to bind thiolated nitrilotriacetic acid (NTA) to the silica spheres. Once charged with a divalent metal ion (e.g., Ni^{2+}, Co^{2+}), NTA selectively binds proteins or peptides containing six contiguous histidine residues (His_6)[32].

In order to quantify the binding capacity of the Ni^{2+}-NTA functionalized Stöber silica, DFGA or APTES processed substrates were incubated with an excess amount of hexahistidine-tagged enhanced green fluorescent protein (eGFP-His_6). The quantity of eGFP-His_6 bound by the substrates was taken obtained from the amount of eGFP-His_6 remaining in solution (i.e., as determined by Dr. N. Poulsen by fluorescence spectroscopy) following the incubation period (Figure 6.2). Inspection of Figure 6.2 reveals that the DFGA prepared substrates quantitatively bound up to 41% more eGFP-His_6 than did silica spheres pre-functionalized with APTES. Stöber spheres functionalized by DFGA or APTES processing alone (i.e., no PMPI and Ni^{2+}-NTA reaction steps) were observed to bind low levels of eGFP-His_6. This indicated that the

Table 6.1: Description of the chemical modification steps applied to Stöber spheres.

Sample name	Processing history
APTES	• APTES silanization • PMPI • thiolated-NTA, Ni^{2+} • protein incubation (eGFP-His_6 or rSilC)
G1	• TATMS silanization • 1 iteration of 5/6 poly-acrylate and TAEA • 1 iteration of PEG diacrylate, 5/6 poly-acrylate layer and TAEA • PMPI • thiolated-NTA, Ni^{2+} • protein incubation (eGFP-His_6 or rSilC)
G3	As G1, with 3 iterations of 5/6 poly-acrylate and TAEA
G5	As G1, with 5 iterations of 5/6 poly-acrylate and TAEA
APTES (-)	• APTES silanization • protein incubation (eGFP-His_6 or rSilC)
G1(-)	• TATMS silanization • 1 iteration of 5/6 poly-acrylate and TAEA • 1 iteration of PEG diacrylate, 5/6 poly-acrylate layer and TAEA • protein incubation (eGFP-His_6 or rSilC)
G3(-)	As G1(-), with 3 iterations of 5/6 poly-acrylate and TAEA
G5(-)	As G1(-), with 5 iterations of 5/6 poly-acrylate and TAEA

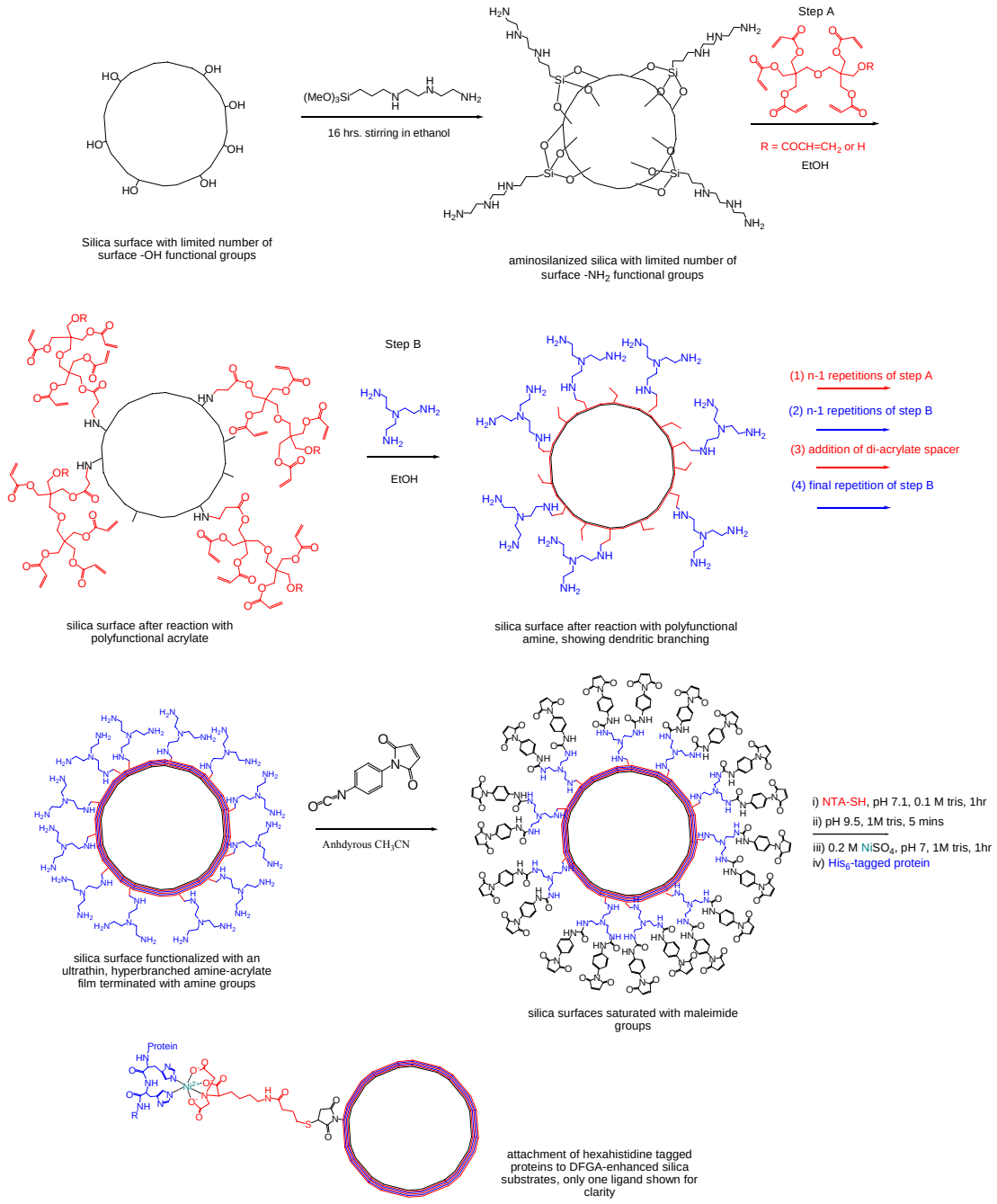

Figure 6.1: Scheme of the chemical reactions involved in the dendritic functional-group amplification process and addition of protein cross-linking reagents to silica surfaces. Scheme based on a figure originally created by Dr. Simon C. Jones (Georgia Institute of Technology).

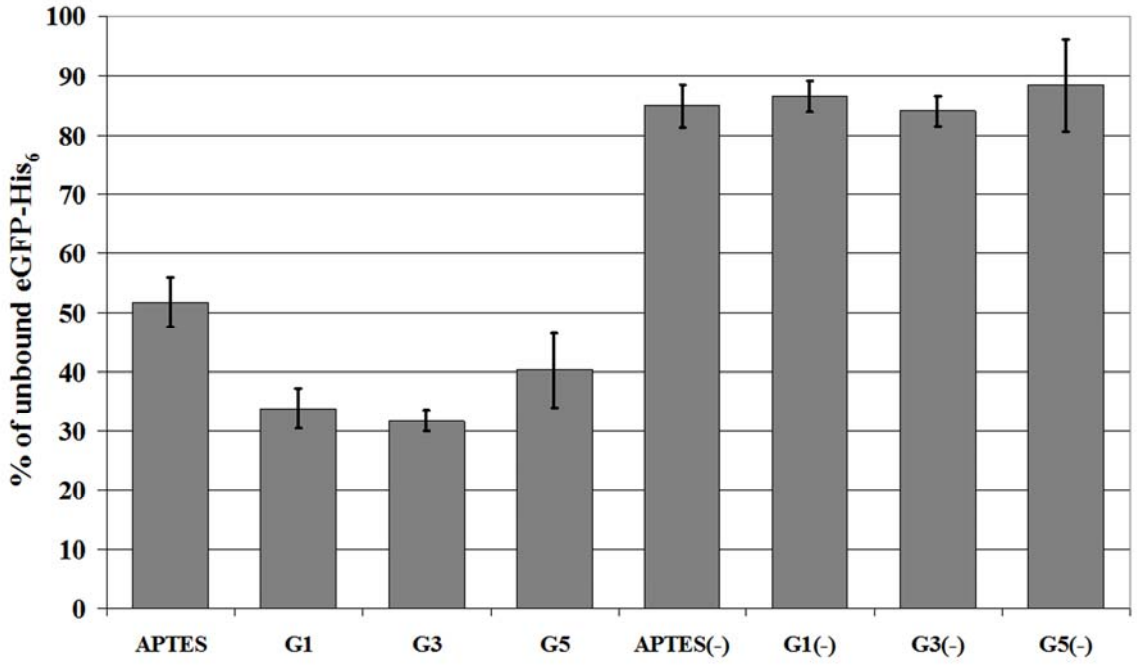

Figure 6.2: Percentage of eGFP-His6 remaining in solution after incubation with APTES or DAFG-enhance silica spheres. Negative control samples, not possessing the NTA ligand, are designated with a minus sign (-). Data collected by Dr. Nicole Poulsen (Georgia Institute of Technology).

binding of eGFP-His_6 to the Ni^{2+}-NTA functionalized silica substrates was largely occurring through the expected specific interaction of the hexahistidine domain of the protein and the NTA-chelated nickel ion. Figure 6.2 also reveals that the gains afforded by the DFGA process occurred quite quickly, as the G1 sample was observed to bind essentially the same level of eGFP-His_6 as the G3 or G5 substrates.

6.3.2 Mineralization of Surface Immobilized Proteins

6.3.2.1 Stöber Spheres Substrates

Having confirmed that the DFGA/Ni^{2+}-NTA functionalized Stöber spheres were capable of binding substantial amounts of His_6 tagged proteins, the use of these substrates to immobilize mineralizing proteins was then explored. Specifically, rSilC, a

recombinant silaffin possessing a C-terminal hexahistidine tag and titania precipitation activity was utilized in this study[7]. In order to determine if the mineralization activity of this protein was preserved following immobilization, silica Stöber spheres loaded with rSilC were exposed to a near neutral pH titania precursor (TiBALDH) solution. The scanning electron microscope (SEM) characterization of rSilC functionalized APTES, DFGA G1, G3, and G5 substrates following exposure to these mineralizing conditions are presented in Figure 6.3. All substrates functionalized with Ni^{2+}-NTA and incubated with rSilC were found to be covered with fine particles not native to the otherwise smooth surface of the silica spheres. Negative control samples, processed by the DFGA method and incubated with rSilC, but lacking the Ni^{2+}-NTA ligand necessary to conjugate this protein, were not observed to have developed any such patches of new precipitate (Figure 6.3D, F, and H). APTES control substrates however, were decorated with small amounts of precipitate, though to a lesser extent than their Ni^{2+}-NTA functionalized counterpart. Energy dispersive x-ray spectroscopy (EDS) indicated that the newly formed rough patches of material noted in SEM contained titanium and oxygen (Figure 6.4A). The silicon, and to some extent, oxygen and carbon signals additionally observed in this spectrum (Figure 6.4A), may be attributed to the silica Stöber spheres and their organic coatings. Elemental analysis of the DFGA processed negative control substrates (Figure 6.4B) yielded EDS spectra of only silicon, oxygen, and carbon (i.e, no titanium).

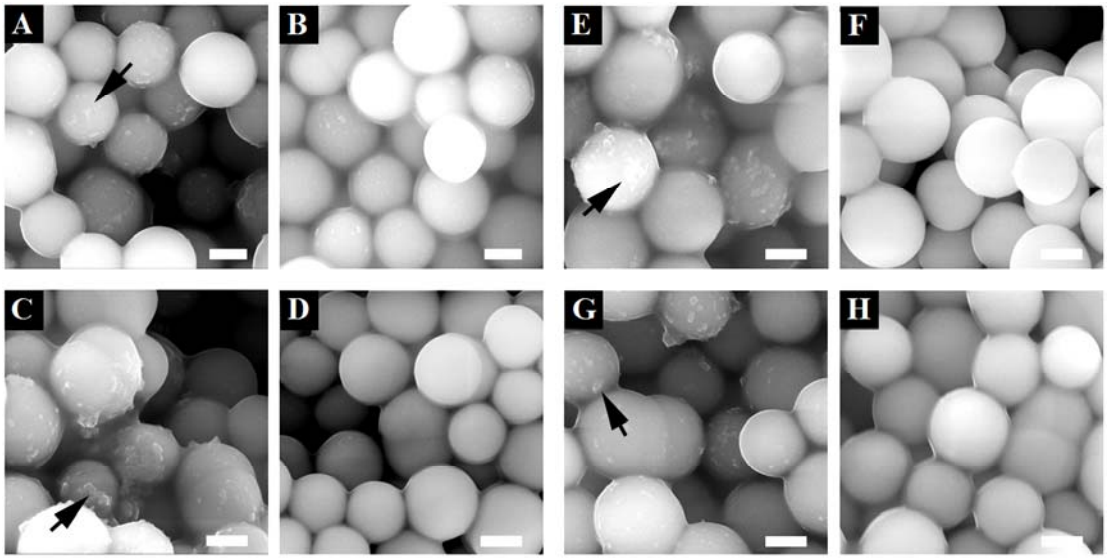

Figure 6.3: SEM characterization of functionalized silica spheres following exposure to titania mineralizing conditions. Silica treated by APTES silanization A) with and B) without the NTA cross-linker; DAFG-enhanced G1 silica C) with and D) without NTA; DAFG-enhanced G3 silica E) with and F)without the NTA; DAFG-enhanced G5 spheres G) with and H) without NTA. Scale bars represent 250 nm. Black arrows designate titania deposits.

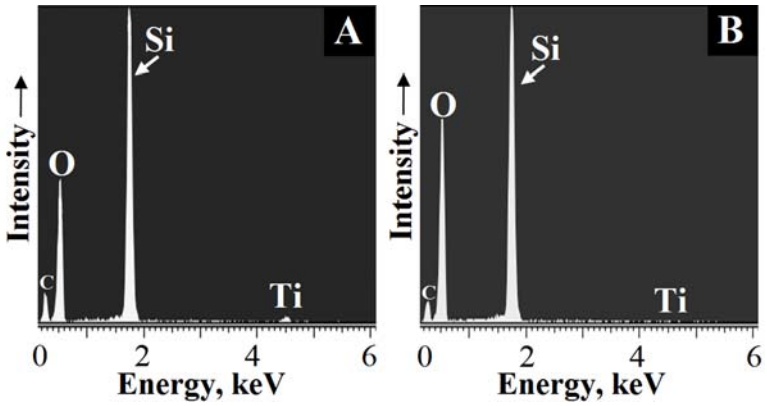

Figure 6.4: Energy dispersive x-ray spectroscopy analysis typical of the spectra gathered from functionalized Stöber silica. A)APTES, APTES (-), G1, G3, and G5 samples, B) G1(-), G3(-), and G5(-) samples. Where (-) designates those samples lacking the NTA cross-linking reagent.

6.3.2.2 Diatom Silica Substrates

In order to evaluate the applicability of DFGA-enhanced immobilization to silica substrates of complex morphology, the procedure outlined for G5 Stöber spheres was repeated on diatom frustules. The diatom frustule (i.e., silica cell wall) is an attractive substrate for study as such a structure possesses intricately detailed features on both the micro- and nanoscales (i.e., wall thicknesses, pore sizes, and spines)[33]. Following exposure to mineralizing conditions, rSilC-loaded diatom frustules were observed to be covered with a large amount of granular material (Figure 6.5). Diatoms similarly functionalized by the DFGA processes and displaying Ni^{2+}-NTA, but lacking rSilC, were not noted to develop such coatings (Figure 6.6). The EDS spectra of the rSilC functionalized frustules indicated that the encrusting material contained a large proportion of titanium (Figure 6.5D). Drawing on the previous reported activity of rSilC, the granular coating present on these diatoms is ikely to be titania[7]. Indeed, high resolution TEM analysis, conducted by Dr. Ye Cai (Georgia Institute of Technology), of the suspected titania coating revealed the presence of small (i.e., >5 nm) crystallites which possessed lattice fringe spacings corresponding to either the anatase or monoclinic polymorphs of TiO_2 (Figure 6.7). Consistent with the prior SEM characterization of the same materials, TEM observations of diatom frustules functionalized with NTA, but lacking rSilC, did not reveal the presence of any titania based materials (Figure 6.7c).

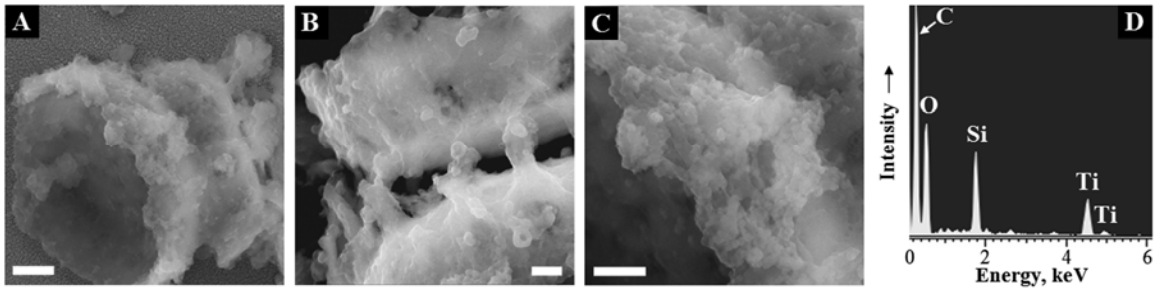

Figure 6.5: A, B, C) SEM and D) EDS characterization of diatom frustules encrusted with immobilized rSilC precipitated titania. Scale bars represent 250 nm in each image.

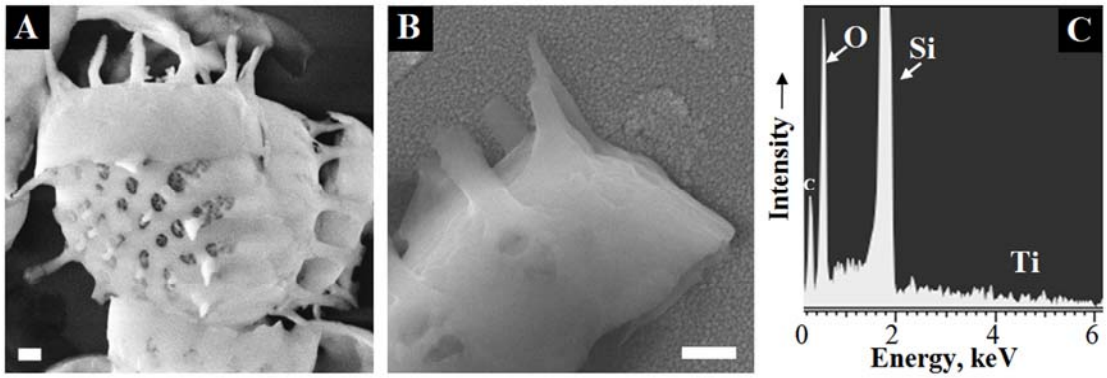

Figure 6.6: A and B) SEM and C) EDS characterization of diatom frustules functionalized by the DAFG-enhanced immobilization procedure but, lacking rSilC. Titania deposits were not observed on these samples. Scale bars represent 250 nm in each image.

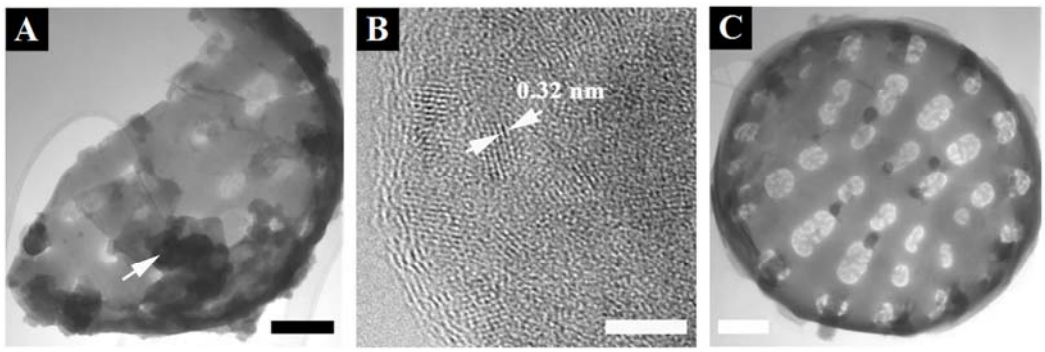

Figure 6.7: TEM characterization of diatom frustules functionalized with the DAFG-enhanced immobilization procedure and exposed to mineralizing conditions. Frustules with and without rSilC depicted in A) and C), respectively. High resolution TEM characterization of the titania coating of the frustule depicted A) presented in B). Scale bars correspond to 5 nm in B) and 200nm in A) and C). White arrow in A) designates an area of rSilC-titania. Lattice fringe spacings in B) is denoted in image. Images taken by Dr. Ye Cai (Georgia Institute of Technology).

6.4 Summary and Outlook

A highly facile and flexible strategy for the enhancement of surface chemistry has been presented and newly applied to protein conjugation in this study. The dendritic functional-group amplification process was demonstrated to increase the loading of hexahisitidine tagged proteins on silica surfaces by more than 40%, as compared to traditional immobilization procedures. These poly-functional acrylate/amine based films were also found to be effective in conjugating the mineralizing recombinant silaffin, rSilC, to silica surfaces in its active form. Immobilized rSilC was utilized to deposit titania on intricately detailed biogenic silica substrates under gentle reaction conditions (i.e., aqueous solutions, near neutral pH, ambient temperature).

Extensions of the methods outlined in this study may facilitate the bioenabled synthesis of materials on surfaces which previously lacked sufficient functional groups to support efficient immobilization. In a manner previously demonstrated for NTA-functionalized agarose beads, the surface conjugation of silica precipitating proteins may be used to encapsulate enzymes inside of glass capillary tubes or other appropriate silica substrates for use in analytical devices or enzymatic bioreactors[34]. Coupled with current and future advances in the protein and peptide mediated synthesis of functional inorganic materials, the DFGA-enhanced protein immobilization processes will surely allow for the greater integration of bioenabled synthesis into functional micro and nano-devices[9-14].

6.5 Contributions

Research initiated by MBD and Prof. Kenneth Sandhage (Georgia Institute of Technology). Advances in this project were made with the collaboration of Prof. Nils Kröger (Georgia Institute of Technology), and Prof. Seth Marder (Georgia Institute of

Technology). Acrylate/amine reaction chemistry of the DFGA process developed by G. Wang (Georgia Institute of Technology) and modified to include PEG reagents by MBD. Cross-linking strategy by MBD and Prof. Nils Kröger. PMPI synthesized by MBD under the direction of Dr. Simon C. Jones (Georgia Institute of Technology). Thiolated NTA synthesized and provided by Mr. P. Hotchkiss (Georgia Institute of Technology). Large scale expression and purification of rSilC and eGFP-His_6 conducted by MBD and Dr. N. Poulsen (Georgia Institute of Technology), respectively. Diatom frustules grown and provided by G. Ahmad (Georgia Institute of Technology). Substrate preparation and titania precipitation reactions by MBD. SEM, XRD, and EDS characterization of titania precipitates was conducted by MBD. Quantification of substrate protein loading conducted by Dr. N. Poulsen. TEM characterization of materials conducted by Dr. Y. Cai (Dr. N. Poulsen (Georgia Institute of Technology)). Manuscript prepared by MBD.

6.6 References

1. Sumerel, J. L.; Yang, W.; Kisailus, D.; Weaver, J. C.; Choi J. H.; Morse D. E.; *Chem. Mater*. **2003**, *15*, 4804.
2. Kisailus, D.; Najarian, M.; Weaver, J. C.; Morse, D. E. *Adv. Mater*. **2005**, *17*, 1234.
3. Brutchey, R. L.; Yoo, E. S; Morse, D. E. *J. Am. Chem. Soc.* **2006**, *128*, 10288.
4. Cole, K. E.; Ortiz, A. N.; Schoonen, M. A.; Valentine, A. M. *Chem. Mater.* **2006**, *18*, 4592.
5. Pender, M. J.; Sowards, L. A.; Hartgerink, J. D.; Stone, M. O.; Naik, R. R.; *Nano Lett.* **2006**, *6*, 40.
6. Sewell, S. L.; Wright, D. W. *Chem. Mater.* **2006**, *18*, 3108.
7. Kröger, N; Dickerson, M. B.; Ahmad, G.; Cai, Y.; Haluska, M. S.; Sandhage, K. H.; Poulsen, N.; Sheppard, V. C. *Angew. Chem. Int. Ed*. **2006**, *45*, 7239.

8. Umetsu, M.; Mizuta, M.; Tsumoto, K.; Ohara, S.; Takami, S.; Watanabe, H.; Kumagai, I.; Adschiri, T. *Adv.. Mater.* **2005**, *17*, 2571.

9. Dickerson, M. B.; Jones, S. E.; Cai, Y.; Ahmad, G.; Naik, R. R.; Kröger, N.; Sandhage, K. H. *Chem. Mater.,* **2007,** (submitted).

10. Flynn, C. E.; Mao, C.; Hayhurst, A.; Williams, J. L.; Georgiou, G.; Iversona, B.; Belcher, A.M. *J. Mater. Chem.,* **2003**, *13*, 2414.

11. Reiss, B. D.; Mao, C.; Solis, D. J.; Ryan, K. S.; Thomson, T.; Belcher, A. M., *Nano Lett.* **2004**, *4*, 1127.

12. Naik, R.R.; Jones, S.E.; Murray, C. J.; McAuliffe, J.C.; Vaia, R.A.; Stone, M. O. *Adv. Funct. Mater.* **2004**, *14*, 25.

13. Ahmad, G.; Dickerson, M. B.; Church, B.C.; Cai, Y.; Jones, S. E.; Naik, R. R.; King, J. S.; Summers, C. J.; Kröger, N.; Sandhage, K. H. *Adv. Mater.* **2006**, *18*, 1759.

14. Ahmad, G.; Dickerson, M. B.; Cai, Y.; Jones, S. E.; Ernst, E.M.; Haluska, M. S.; Campbell, A. L.; Naik, R. R.; Kröger, N.; Sandhage, K. H. *J. Am. Chem. Soc.,***2007** (Submitted).

15. Brott, L. L.; Naik, R. R.; Pikas, D. J.; Kirkpatrick, S. M.; Tomlin, D. W.; Whitlock, P. W.; Clarson, S. J.; Stone, M. O. *Nature*, **2001**, *413*, 291.

16. Naik, R. R.; Stringer, S. J.; Agarwal, G.; Jones, S. E.; Stone, M. O. *Nat. Mater.,* **2002,** *1*, 169.

17. Tahir, M. N.; Théato, P.; Müller, W. E. G., Schröder, H. C.; Janshoff, A.; Zhang, J.; Huthe, J.; Tremel, W. *Chem. Commun.,* **2004**, 2848.

18. Tahir, M. N.; Théato, P.; Müller, W. E. G., Schröder, H. C.; Borejko, A.; Faiß, S.; Janshoff, A.; Huthe, J.; Tremel, W. *Chem. Commun.,* **2005**, 5533.

19. Beier, M.; Hoheisel, J. D.; *Nuc. Acids Res.,***1999,** *27*, 1970.

20. Pan, B.; Cui, D.; Gao, F.; He, R. *Nanotechnol.,* **2006,** *17*, 2483.

21. Annunziato, M. E.; Patel, U. S.; Ranade, M.; Palumbo, P. S.; *Bioconjugate Chem.,* **1993**, *4*, 212.

22. Du Roure, O.; Debiemme-Chouvy, C.; Malthete, J.; Silberzan, P. *Langmuir*, **2003**, *19*, 4138.

23. Han, Y.; Mayer, D.; Offenhäusser, A.; Ingebrandt, S. *Thin Solid Films*, **2006**, *510*, 175.

24. Cras, J.J.; Rowe-Taitt, C.A.; Nivens, D.A.; Ligler, F.S. *Biosen. Bioelectron.*, **1999**, *14*, 683.

25. Cass, T.; Ligler, F.S. *Immobilized Biomolecules in Analysis*, Oxford University Press, Oxford, **1998**.

26. Lochmüller, C. H.; Kersey, M. T. *Langmuir*, **1988**, *4*, 572.

27. Weatherspoon, M. R.; Dickerson, M. B.; Wang, G.; Cai, Y.; Shian, S.; Jones, S. C.; Marder, S. R.; Sandhage, K. H. *Angew. Chem. Int. Ed*., **2007**, (in press).

28. Wang, G.; Hayek, A.; Jones, S.C.; Marder, S. R. *Chem. Commun.,* **2007**, (submitted).

29. Wong, S.S. *Chemistry of Protein Conjugation and Cross-Linking,* CRC Press, Boca Raton, FL, **1991**.

30. Jin, L.; Horgan, A.; Levicky, R., *Langmuir*, **2003**, *19*, 6968.

31. Chen, G.; Horgan, A.; Levicky, R. *Colloids Surf., B: Biointerfaces,* **2004**, *35*, 59.

32. Crowe, J.; Dobeli, H.; Gentz, R.; Hochuli, E.; Stuber, D.; Henco, K. *Methods Mol. Biol.,* **1994**, *31*, 371.

33. Round, F. E.; Crawford, R. M.; Mann, D. G. *The Diatoms: Biology and Morphology of the Genera*, Cambridge University Press, Cambridge, **1990.**

34. Luckarift, H. R.; Johnson, G.R.; Spain, J. C. *J. Chromatogr. B Analyt. Technol. Biomed. Life Sci.*, **2006**, *843*, 310.

CHAPTER 7: OBSERVATIONS AND OUTLOOK

The aspiration of this doctoral research was to couple the attractive features of protein mediated inorganic materials biosynthesis with the highly functional properties of advanced inorganic oxides not natively produced in the biological world. This objective was accomplished through the identification of peptides from a phage-displayed peptide library that initiated the synthesis of germania or titania. Investigations utilizing the recombinant silaffins rSilC and rSil1L, as well as hen egg white lysozyme, to produce titania from aqueous, near-neutral pH solutions also proved to be extremely successful. Lysozyme was additionally found to direct the formation of zirconia, a technologically important and non-biologically produced ceramic. The procedure for the immobilization of mineralizing biomolecules presented in this dissertation was observed to produce a marked improvement in the extent of surface mineralization noted on silica substrates.

7.1 The Bio-Enabled Formation of Titania

7.1.1 Titania Precipitation Activity

Much of the research summarized in this dissertation has focused upon the peptide or protein initiated synthesis of titania from the aqueous precursor titanium(IV) bis-(ammonium lactato)-dihydroxide (TiBALDH). While the mechanism by which biomolecules destabilize this complex, and condense titania, remains unknown, insights have been made into the requirements of biomolecules to initiate titania synthesis. Utilizing peptides identified by the biopanning of TiO_2, as well as designed peptides, it was found that the titania precipitation activity of a given peptide correlated with the number of positive charges carried by the peptide (i.e., increased positive charge resulted

in increased activity). This result was also noted in collaborative work with recombinant proteins, where only the most positively charged silaffins, rSilC and rSil1L were observed to precipitate titania from TiBALDH. It was also noted in this recombinant silaffin study that the lysine-enriched but only slightly positively charged (i.e., +3), protein rSil3 did not initiate titania precipitation. This implied that biomolecules must not only be enriched in positively charged moieties but possess an overall positive charge in order to facilitate the hydrolysis of the TiBALDH molecule. Unfortunately, zwitterionic peptides enriched in both acidic and basic residues were not identified during the biopanning of TiO_2. Investigating the titania precipitation activity of such peptides would solidify this initial recombinant silaffin observation.

7.1.2 Bio-Enabled Titania Crystal Structure

The majority of the titania precipitating biomolecules utilized in this dissertation research induced the formation of nano-crystalline anatase and/or monoclinic TiO_2. While these precipitates often contained an amorphous component, only the titania formed by hen egg white lysozyme was noted to be completely amorphous. Lysozyme's synthesis of amorphous, rather than crystalline, titania may be attributed to the intentionally high protein content of the titania precipitates, as the entrapped enzyme may have interrupted the long range ordering of the inorganic phase. It is also conceivable that the charge density of lysozyme may have played a role in the formation of amorphous titania. Lysozyme's low positive charge density may have resulted in the incomplete hydrolysis of the TiBALDH complex, leaving the Ti partially chelated and interrupting crystal formation.

Reviewing the x-ray diffraction (XRD) patterns presented in Figure 3.6 of this dissertation, it is notable that the diffraction patterns of the titania formed by peptides of low titania precipitation activity (i.e., Ti-4 and Ti-2) tend to have a more defined peak (or shoulder) at 28.5° than the patterns of the titania formed by peptides with high activity (i.e., Ti-1 or dTi-1-RKK). The titania precipitation activity of these peptides was found to correlate to their enrichment in positive charges. This trend in 28.5° peak intensity also appears to extend to titania generated by other biomolecules. The XRD pattern of titania produced by rSil1L, the least cationic of the titania precipitating recombinant silaffin, possesses a strong 28.5° peak (see Figure 5.4). The XRD pattern of the titania generated by the highly-positively-charged molecule poly-l-lysine, also presented in Figure 5.4, exhibits only a slight shoulder at this angle. The 28.5° diffraction peak observed in these patterns is best matched to the diffraction of the (002) plane of β-TiO_2. Given these observations, it appears that there is a trend in the amount of β-TiO_2 produced by a biomolecule and the positive charge density of that biomolecule. Stated concisely, less cationic peptides and proteins appear to produce a greater proportion of β-TiO_2 than their highly cationic counterparts. Further research is required however, to verify and explain this phenomenon.

No discussion of the titania crystal structures produced by biomolecules would be complete without considering the incredible transformation of the titania initially precipitated by rSilC into highly organized microspheres of rutile. Summarizing the findings presented in Chapter 5 of this dissertation, the highly repetitive primary structure of rSilC appears to have some bearing on the appearance of rutile TiO_2. This hypothesis has been drawn from observations that, rutile titania was not formed in the presence of

rSil1L, poly-l-lysine, or any of the other biomolecules explored within this dissertation. It should be noted that conditions identical to those utilized to generate rutile TiO_2 in the presence of rSilC, failed to produce this crystalline phase of titania in the presence of rSil1L, poly-l-lysine, or the peptide Ti-1. New recombinant silaffins have been designed and are currently being expressed and purified which may aid in the elucidation of the interdependence of protein and TiO_2 structure.

Beyond the use of newly designed silaffins, future investigations should include a more detailed examination of the role of methanol in the transformation of rSilC-titania to rutile TiO_2. Specifically, determining the constituents (e.g., water, lactic acid, unconsumed TiBALDH, or protein) which are removed from the titania precipitate by methanol rinsing would be beneficial. Based upon these results, alternative solvents which may surpass the action of methanol in this system could possibly be identified. The potential induction or modification of the secondary structure of rSilC by methanol may also be a possible driving force in the emergence of rutile TiO_2 and should be investigated. Ultimately, the information gathered in the initial and future investigations of the formation of rutile TiO_2 by rSilC, may be extended to the production of highly crystalline ceramics of other chemistries.

7.2 Mineralization with Immobilized Biomolecules

The mineralization of proteins or peptides conjugated to surfaces represents the most challenging research summarized in this dissertation. Given the relative success of the dendritic amplification of surface functionality, it is unlikely that substantially more protein will be able to be loaded onto planar substrates. Advances in the quality of peptide or protein synthesized inorganic material coatings will likely come through either

the use of higher surface area substrates or biomolecules which precipitate relatively greater amounts of material. In particular, the use of slightly oxidized, high surface area Si replicas of diatom frustules may provide greater protein loading and thus better mineralized coatings than the silica diatom cell walls utilized in my dissertation research[1]. A specific example of a biomolecule which may be conjugated to surfaces in place of rSilC is the peptide BT2. In solution, this peptide produces 4.2 mg of the functional ceramic $BaTiO_3$ per mg of peptide, which represents more than a ten-fold increase in the amount of inorganic formed as compared to rSilC (0.3 mg titania/mg protein)[2].

7.3 Outlook of the Field

The studies presented in this dissertation represent mere bricks in the grand tower that the bio-enabled formation of materials will become. The current trend in the peptide-induced synthesis of increasingly sophisticated ceramic compounds (e.g., $CaMoO_4$ and $BaTiO_3$) should rapidly open new possibilities in the production of highly-functional materials under gentle solution conditions[2,3]. Such biomolecule initiated and mediated reactions may, for the first time, allow for the integration of these inorganics with sensitive soft materials (e.g., drugs or enzymes) to produce unique multi-functional composites. It is likely that within the next decade that we will witness the *in vitro* or possibly even *in vivo* production of compounds foreign to biomineralization which possess hierarchical structures and properties exceeding the rutile TiO_2 produced by rSilC.

7.4 References

1. Bao, Z.; Weatherspoon, M.; Cai, Y.; Ahmad, G.; Allan, S. M.; Graham, P. D.; Dickerson, M. B.; Church, B.; Kang, Z.; Summers, C.; Abernathy, H.; Meilin, L.; Sandhage, K. H. *Nature*, **2007**, *446*, 172.

2. Ahmad, G.; Dickerson, M. B.; Cai, Y.; Jones, S. E.; Ernst, E. M.; Haluska, M. S.; Campbell, A. L.; Naik, R. R.; Kröger, N.; Sandhage, K. H. *J. Am. Chem. Soc.*,**2007** (Submitted).

3. Ahmad, G.; Dickerson, M. B.; Church, B. C.; Cai, Y.; Jones, S. E.; Naik, R. R.; King, J. S.; Summers, C. J.; Kröger, N.; Sandhage, K. H. *Adv. Mater.* **2006**, *18*, 1759.

APPENDIX A: ADDITIONAL SEQUENCE DATA FROM THE BIOPANNING OF TiO_2

Table A.1: Peptides identified through the screening of a (001) rutile TiO_2 substrate with a phage displayed library.

Peptide Name	Sequence	pI	(D+E)	H	(K+R)	(S+T+Y)
iR001a	AL A V V Y D Y S A P A	3.1	1	0	0	3
iR001b	I E P V T N K T F P E T	4.3	2	0	1	3
iR001c	W V K V D G M H D L P A	5.1	2	1	1	0
iR001d	S P S M L T S M W P N T	6.0	0	0	0	5
iR001e	S P T P L Q M F Q A S P	6.0	0	0	0	3
iR001f	L D A F G I T P M Q L K	6.8	1	0	1	0
iR001g	K I P F E R M E L N L S	7.1	2	0	2	1
iR001h	A L K H M D E P R S G S	7.8	2	1	2	2
iR001i	T M Y K R D P Q L A L W	9.8	2	0	2	2
iR001j	T F M P G S T G L K I P	10.1	0	0	1	3
iR001k	T I Y L P S R H L P T S	9.8	0	1	1	5
iR001l	S L E A K P T G H R P P	10.1	1	1	2	2
iR001m	V P L Q N N L S T T K L	10.1	0	0	1	3
iR001n	Y P P R E S R T L S T A	9.8	1	0	2	5
iR001o	G G S L V A K A T A P N	10.1	0	0	1	2
iR001p	S T N V Y N Y R A T K L	10.0	0	0	2	5
iR001q	I T S R L A P T S L P F	11.0	0	0	1	4
iR001r	Q H A N H Q A W N N L R	11.0	0	2	1	0
iR001s	Q H F G K T P A R Y Q P	10.3	0	1	2	2
Averages		8.3	0.7	0.4	1.2	2.6

Table A.2: Peptides identified through the screening of a (100) rutile TiO_2 substrate with a phage displayed library.

Peptide Name	Sequence	pI	(D+E)	H	(K+R)	(S+T+Y)
ir100a	T S L C S G D Y C P S A	3.1	1	0	0	5
ir100b	V D A S F K P A S L P T	6.8	2	0	1	3
ir100c	G H T L E T H T I P N T	6.0	1	2	0	4
ir100d	N V T T M T N H L V Y S	7.8	0	1	0	5
ir100e	Q S P S I R D N H G I A	7.8	1	1	1	2
ir100f	K A A D T M K A Y Y H T	9.7	1	1	2	4
*ir100g	Q K H E H T Q W L S A V	8.0	1	2	1	2
ir100h	S G S Y L N S K M T P L	9.8	0	0	1	5
ir100i	M S P A N K T A A P S P	10.1	0	0	1	3
*ir100j	L K M N P S I S S S L K	10.5	0	0	2	4
ir100k	D R P I L A Y P T S P R	9.8	1	0	2	3
ir100l	H S H I R P T P S T S F	11.0	0	2	1	5
ir100m	R H L A H L P F H G S V	11.0	0	3	1	1
ir100n	I S D R I N P A Q Y K R	10.3	1	0	3	2
ir100o	L T A K S I P E S R S R	11.3	1	0	3	4
ir100p	T P K P M N W P P R V L	11.5	0	0	2	1
Averages		9.1	0.6	0.8	1.3	3.3

*These peptide identified twice.

Table A.3: Peptides identified through the screening of a (110) rutile TiO_2 substrate with a phage displayed library.

Peptide Name	Sequence	pI	(D+E)	H	(K+R)	(S+T+Y)
ir110a	T P T P I S S P P Q E L	3.3	1	0	0	4
ir110b	W E A R S L D M E F L T	3.9	3	0	1	2
ir110c	M P A V M S S A Q V P R	11.0	0	0	1	2
ir110d	T V Q L I P P S V Q F P	6.0	0	0	0	2
ir110e	T Y S W K N N D H S Q D	5.1	2	1	1	4
ir110f	M N L K E H N L S P P F	7.8	1	1	1	1
ir110g	N M T T Y P M H N N T V	7.8	0	1	0	4
ir110h	Y H P F R I G M Q G P A	9.8	0	1	1	1
ir110i	N T T H K S H E M N T V	8.0	0	2	1	4
ir110j	V L P P K P M R Q P V A	11.5	0	0	2	0
ir110k	H P W Y V E R A V R S I	9.8	1	1	2	2
ir110l	H S L S K P H P T S S V	10.1	0	2	1	5
ir110m	S N V A N M Q R W P S Q	11.0	0	0	1	2
ir110n	F L P H S I P P H L S R	11.0	0	2	1	2
ir110o	V L P P K P M R Q P V A	11.5	0	0	2	0
ir110p	A L P M L K P A R L T H	11.5	0	1	2	1
ir110q	S N V A N M Q R W P S R	12.4	0	0	2	2
Averages		8.9	0.7	0.7	1.1	2.2

APPENDIX B: ADDITIONAL SEQUENCE DATA FROM THE PCR-DRIVEN BIOPANNING OF TiO_2

B.1 PCR-Driven Peptide Library Screening Results.

In order to identify peptides which may have resisted glycine-HCl elution due to their high TiO_2 affinity, rutile substrates incubated with a phage-displayed peptide library were subjected to a PCR-based screening method[1]. While no additional clones were isolated from the (100) or (110) rutile substrates post glycine-HCl elution, 11 clones were identified from the (001) sample (Figure AI.1). The sequences of these peptides are displayed in Table AI.2. Overall, these PCR-isolated (001) rutile peptides are more acidic in nature (7.0 average pI) than the peptides identified during higher stringency biopanning and possess amino acid residue compositions very similar to those peptides identified in the initial panning procedure. It should be noted that the PCR (001) peptides also lack any neighboring histidine, lysine, or arginine residues as was observed for the peptides identified during the additional rounds of high stringency biopanning. The possible mechanism for the high affinity binding of these peptides to the TiO_2 substrates is unclear as they lack any specific enrichment in amino acids, as such; it is possible that these sequences originated as contaminants. Two of these PCR identified peptides, PCR-9 and PCR-10, were tested for titania precipitation activity and found to produce 0.07 and 0.00 mg of titania/mg of peptide, respectively. The low precipitation activities of these peptides further precluded these sequences from continued study.

Table B.1: The characteristics and sequences of the peptides identified during PCR driven biopanning of rutile crystal substrates. Additional peptides were only identified from the (001) substrate. The amino acid residues histidine (H), arginine (R) and lysine (K) thought to be associated with TiO_2 binding and precipitation activities are bolded. An asterisk (*) denotes those peptides selected for TiO_2 precipitation assay testing.

Peptide Name	sequence	pI	H	(K+R)	(D+E)	(S+Y+T)
PCR001-1	A D T W P E G L Y S L I G	3.1	0	0	2	3
PCR001-2	F P Q A W **R** D D P G P S	3.9	0	1	2	1
PCR001-3	N S E M A **K** P P G G A N	7.0	0	1	1	1
PCR001-4	V Q S A I P E G **H** L T	5.1	1	0	1	2
PCR001-5	M G L S S **K** I D S V N N	6.8	0	1	1	3
PCR001-6	**K** A L G P D P A T P P L	6.8	0	1	1	1
PCR001-7	V A L E I T **H** L V P F **R**	7.8	1	2	1	0
PCR001-8	A T W L P T T N I **H** P M	7.8	1	1	0	3
*PCR001-9	T S T Q W **H** P **H** W L P P	8.0	1	2	0	3
*PCR001-10	**K** L T S P Y V L P T N	9.7	0	1	0	5
PCR001-11	I I G T P S V F **R** S P M	11.0	0	1	0	3
Average		7.0	0.4	1.0	0.8	2.3

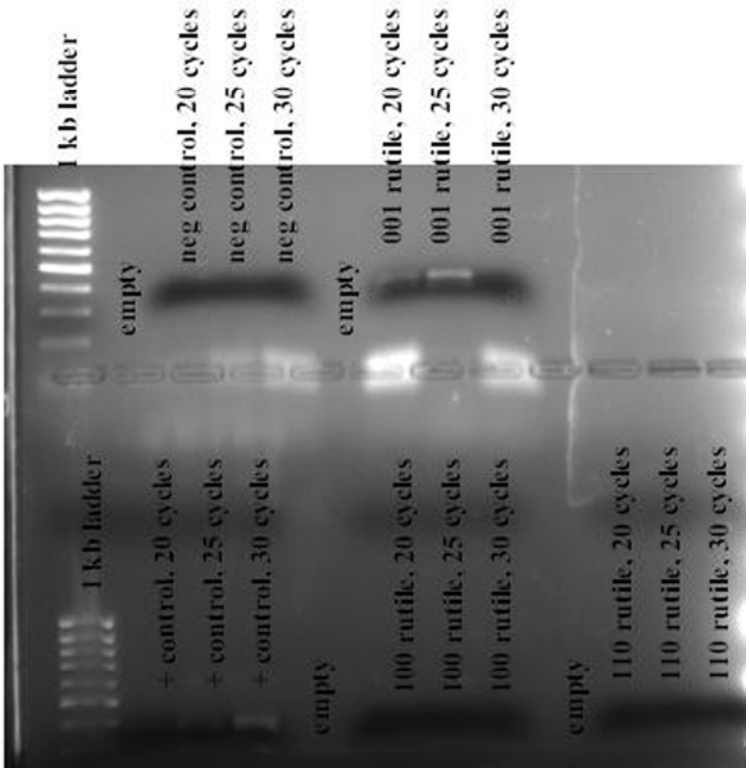

Figure B.1: Image of an agarose gel containing the PCR products produced through the PCR-based biopanning of several rutile substrates. Sample identities and number of PCR cycles are listed on the image.

B.2 PCR-Driven Peptide Library Screening Method

The Polymerase Chain Reaction (PCR) method was performed as previously described with minor modifications[1]. The phage library was bound with the rutile substrates in 0.5%TBST buffer for 1 hour. The substrates were washed 5 times with 0.5% TBST, transferred to fresh microcentrifuge tubes and washed an additional 5 times with 0.8% TBST. Phage were then eluted with the glycine-HCl procedure described above. The substrates were transferred to fresh microcentrifuge tubes and washed an additional 3 times with 0.8% TBST. The rutile substrates were incubated in 100 µl of phage lysis buffer (10mM Tris-HCl pH 8.3, 10mM EDTA, 1% Triton X-100) for 10 minutes at 95°C. An aliquot (10 µl) of the phage lysis solutions were mixed into a 40 µl PCR master mix solution containing Taq polymerase, and placed into a 94°C thermocycler block and held for 2 minutes. PCR amplification was performed using 20, 25, or 30 cycles of denaturation at 94°C for 30 seconds, annealing at 60°C for 30 seconds, and extension at 72°C for 30 seconds, followed by a final extension cycle of 72°C for 2 minutes. This PCR procedure was conducted with the assistance of Dr. Nicole Poulsen (Georgia Institute of Technology). The PCR products were separated on a 1.2% agarose gel by DNA electrophoresis. The PCR products were extracted from the gel utilizing a Qiaex II extraction kit (Qiagen Inc., Valencia, CA) and cloned into a TOPO vector (Invitrogen, San Diego, Ca) according to the manufacturers' instructions with the assistance of Dr. Gul Ahmad (Georgia Institute of Technology). DNA was extracted from the TOPO clones utilizing a QiAprep Spin Miniprep kit (Qiagen Inc., Valencia, CA) and sequenced using an ABI 310 (PE Applied Biosystems, Ca) automated sequencer. DNA sequencing was conducted on my behalf by Sharon E. Jones (Air Force Research Laboratory).

B.3 Reference

1. Naik, R.R.; Jones, S.E.; Murray, C.J.; McAuliffe, J.C.; Vaia, R.A.; Stone, M.O. *Adv. Func. Mater.* **2004**, *14*, 25.

VITA

Matthew Benjamin Dickerson was born in Columbus, Ohio at The Ohio State University hospital on February 25, 1977, the son of Connie Graham and Ronald Benjamin Dickerson. After graduating from Westerville North High School in Westerville, Ohio in 1995, he attended The Ohio State University in Columbus, Ohio. There, he initially studied molecular genetics and received a Bachelor's of Science degree in Materials Science and Engineering in 2000. Matthew was awarded a National Collegiate Inventors Award by the Inventor's Hall of Fame for his senior undergraduate research project on the low-temperature production of W/ZrC composites. Matthew continued this research at The Ohio State University, earning a Master's of Science degree in June 2002 for his thesis entitled "The Fabrication of Dense, Near Net-Shaped, Very-High-Melting, Tungsten/Non-Oxide Ceramic Composites at Low Temperatures by the PRIMA-DCP Process". In July of 2006, Matthew married Miranda Bertie. Matthew continued his graduate education at The Ohio State University working in collaboration with the Air Force Research Laboratory. In January 2004, Matthew transferred to the Georgia Institute of Technology where he earned the degree Doctor of Philosophy in Materials Science in August 2007.